UCGE Reports
Number 20268

Department of Geomatics Engineering

GPS L5 Software Receiver Development for High-Accuracy Applications
(URL: http://www.geomatics.ucalgary.ca/research/publications/GradTheses.html)

by

Cécile Mongrédien

May 2008

UNIVERSITY OF CALGARY

GPS L5 Software Receiver Development for High-Accuracy Applications

by

Cécile Mongrédien

A THESIS

SUBMITTED TO THE FACULTY OF GRADUATE STUDIES

IN PARTIAL FULFILMENT OF THE REQUIREMENTS FOR THE

DEGREE OF DOCTOR OF PHILOSOPHY

DEPARTMENT OF GEOMATICS ENGINEERING

CALGARY, ALBERTA

MAY, 2008

Abstract

The GPS L5 signal, part of the effort to modernize GPS, was designed to increase performance for civilian users. In order to fully exploit the structural innovations brought by this signal, new receiver architectures are needed. This dissertation proposes novel acquisition and tracking algorithms that can maximize the L5 signal performance in terms of acquisition robustness, tracking sensitivity and measurement accuracy.

A cascaded algorithm is shown to enable robust and direct acquisition of the signal. A coarse acquisition step that coherently combines the data and pilot channel is first used to acquire the PRN code delay. An intermediate 1-ms FLL-based tracking is then introduced to remove the residual Doppler error and a pilot-only fine acquisition step is implemented to simultaneously acquire the NH code delay and perform bit synchronization.

Different data- and pilot-only constant bandwidth tracking strategies are investigated to assess their relative performance in terms of sensitivity and accuracy in the presence of white noise, oscillator phase noise and receiver dynamics. Results show that the L5 dataless channel can increase phase and frequency tracking sensitivity by approximately 5 dB in addition to increasing accuracy. The superiority of phase tracking is also demonstrated since, in addition to enabling navigation message decoding, it is also shown to provide greater accuracy and better sensitivity than frequency tracking. Code tracking accuracy is also shown to greatly benefit from the dataless channel through the use of long coherent integration times. Further measurement accuracy can be achieved through

an innovative technique that coherently combines the data and pilot channel at the correlator level.

Although shown to greatly benefit from the presence of a dataless channel, the constant bandwidth tracking is outperformed by the Kalman filter-based tracking in all areas investigated. The difference between the two tracking strategies is the most significant for carrier tracking where the Kalman filter-based strategy improves the tracking accuracy by approximately one order of magnitude and lowers the tracking threshold by approximately 3 dB. These two tracking strategies are also compared in the position and velocity domains. Results confirm the superiority of the Kalman filter-based strategy, especially in terms of velocity estimation.

Acknowledgements

There are some people that mean very much to me, and I would like to thank them for their support throughout my graduate studies. I am thankful to:

- **Ma famille.** Je pense en particulier a mes parents et a mes soeurs qui, malgré les nombreux kilomètres qui nous ont separés ces dernieres années, n' ont jamais cessé de m' apporter leur amour et de croire en moi. Sans votre soutien je n' aurais jamais pu aller aussi loin.

- **Gérard Lachapelle and M. Elizabeth Cannon.** Thanks for welcoming me as an internship student in winter 2004 and for to hiring me as a graduate student afterwards. Since then your continuous guidance and support have made my work in the PLAN group a wonderful learning experience.

- **Wouter.** Because you mean so much to me. Thanks for helping me keep things in perspective, time after time, and for giving me a reason to succeed.

- All my friends in Calgary. You have made my stay in Canada a fantastic life experience. I would particularly like to thank **Anne and Eric** who have been there for me since the beginning and **Lorraine, Melanie and Niklas** for the numerous and unforgettable trips we shared all across Canada.

- All the members, past and present, of the **PLAN Group** for providing me with such a comfortable working environment and, in particular, **Olivier, Oleg, Diep, Cyrille, Florence, Aiden and Daniele**.

Table of Contents

List of Tables

List of Figures and Illustrations

List of Symbols and Abbreviations

Acronyms

ARNS	…	Aeronautical Radio Navigation Service
AWGN	…	Additive White Gaussian Noise
BER	…	Bit Error Rate
BOC	…	Binary Offset Carrier
BPSK	…	Binary Phase Shift Keying
C/A	…	Coarse Acquisition
CB	…	Constant Bandwidth
CDP	…	Composite Dot-Product discriminator
C/N_0	…	Carrier to Noise density ratio
C-NAV	…	Modernized GPS navigation message format
CDMA	…	Code Division Multiple Access
DC	…	Deflection Coefficient
DD	…	Decision Directed discriminator
DP	…	Dot-Product discriminator
DLL	…	Delay Lock Loop
DS-SS	…	Direct Sequence Spread Spectrum
ELS	…	Early-Late Spacing
Eb/N_0	…	Energy per bit to Noise density ratio
FE	…	Frontend filter bandwidth
FEC	…	Forward Error Correction
FFT	…	Fast Fourier Transform
FLL	…	Frequency Lock Loop
FTS	…	Frequency and Time Standard
GLONASS	…	Global Navigation Satellite System
GNSS	…	Global Navigation Satellite System
GPS	…	Global Positioning System
I&D	…	Integrate and Dump
IF	…	Intermediate Frequency
I5	…	GPS L5 data channel
KF	…	Kalman Filter
LFSR	…	Linear Feedback Registers
LOS	…	Line-Of-Sight
LSA	…	Least-Squares Adjustment
L1	…	L1 frequency band centred at 1575.42 MHz
L2	…	L2 frequency band centred at 1227.60 MHz
L2C	…	GPS L2 Civil signal
L5	…	L5 frequency band centred at 1176.45 MHz
NAV	…	Legacy GPS navigation message format
NC	…	Narrow Correlator
NCO	…	Numerically Controlled Oscillator

NH	…	Neuman-Hofman
NLOS	…	Non Line-Of-Sight
NP	…	Neyman-Pearson
NRZ	…	Non-Return to Zero
PDF	…	Probability Density Function
OCXO	…	Oven Controlled Crystal Oscillator
P	…	Precise
PLL	…	Phase Lock Loop
PVT	…	Position, Velocity and Time
PRN	…	Pseudo-Random Noise
PSD	…	Power Spectrum Density
PSNR	…	Post-correlation SNR
Q5	…	GPS L5 pilot channel
QPSK	…	Quadrature Phase Shift Keying
RF	…	Radio Frequency
RMS	…	Root Mean Square
ROC	…	Receiver Operating Characteristics
RHCP	…	Right Hand Circularly Polarized
RV	…	Random Variable
RW	…	Random Walk
STD	…	Standard Deviation
SMR	…	Signal-to-Multipath Ratio
SNR	…	Signal-to-Noise Ratio
SV	…	Space Vehicle
SoL	…	Safety-of-Life
TCXO	…	Temperature Controlled Crystal Oscillator
XO	…	Crystal Oscillator
bps	…	bit per second
sps	…	symbol per second

Symbols

$(\tilde{\bullet})$	…	Quantity $(\bullet)$ filtered by the receiver frontend filter
$(\hat{\bullet})$	…	Estimate of the quantity $(\bullet)$
$(\bullet)_k$	…	Quantity $(\bullet)$ at epoch k
$(\bullet)^+$	…	Quantity $(\bullet)$ after a measurement update
$(\bullet)^-$	…	Quantity $(\bullet)$ before a measurement update
A	…	Signal amplitude
B_L	…	One-sided loop filter bandwidth

D_{NH}	… NH bit sign
D_{NH}^2	… Product of consecutive NH bit sign
D_d	… Symbol bit sign
D_d^2	… Product of consecutive symbol bit sign
$D_{(\bullet)}$	… Discriminator of type $(\bullet)$
D_0	… Decide the signal is absent
D_1	… Decide the signal is present
F	… Dynamic matrix
G	… Shaping matrix
G	… Correlation gain
$\overline{G}_{C/A}$	… Normalized power density spectrum of the C/A code
$\overline{G}_{L5}$	… Normalized power density spectrum of the L5 PRN code
H	… Fourier transform of the frontend filter impulse response
H	… Design matrix
H_0	… Null hypothesis, the signal is absent
H_1	… Alternate hypothesis, the signal is present
H	… Design matrix
J	… Least-Squares cost function
K	… Kalman gain
K_B	… Boltzman constant
LR_I	… Receiver in-phase local replica
LR_Q	… Receiver in-quadrature local replica
L_f	… Two-sided pull-in range of the frequency discriminator
L_ϕ	… Two- pull-in range of the phase discriminator
NH_{10}	… NRZ materialization of the HN_{10} sequence
NH_{20}	… NRZ materialization of the HN_{20} sequence
NBP	… Narrow-band power
NP	… Normalized power
P	… Signal power
P_D	… Probability of detection
P_{FA}	… Probability of false alarm
P_M	… Probability of missed detection
P_R	… Probability of correct rejection
Q_K	… Marcum Q-function of order K
$\overline{R}_{C/A}$	… Normalized auto-correlation function of the C/A code
$\overline{R}_{L5}$	… Normalized auto-correlation function of L5 PRN code
$\tilde{R}_{L5}$	… Correlation of the local code with the filtered incoming signal
SNR_{pre}	… Pre-correlation SNR

SNR_{post}	…	Post-correlation SNR
T	…	Coherent integration time
T	…	Test Statistic
T_R	…	Receiver oscillator time
T^S	…	Satellite oscillator time
T_C	…	Spreading code chip duration
T_R	…	Receiver noise temperature
T_{Sky}	…	Sky noise temperature
T_{Sys}	…	System noise temperature
W	…	Weighting function
WBP	…	Wide-band power
c	…	NRZ materialization of the spreading code
c_l	…	Speed of light
d	…	NRZ materialization of the navigation message
f_C	…	Spreading code rate
f_D	…	Doppler shift
f_{L1}	…	L1 carrier frequency
f_{L5}	…	L5 carrier frequency
f_e	…	FLL tracking error variance due to receiver dynamics
h	…	Frontend filter impulse response
n_I	…	In-phase correlation noise (assumed Gaussian)
n_Q	…	In-quadrature correlation noise (assumed Gaussian)
r	…	Residual vector
t	…	GPS time
v	…	Measurement noise vector
x	…	State vector
z	…	Observation vector
Δ	…	Early-Late spacing
Δt_{Atmo}	…	Delay due to the propagation through the atmosphere
α	…	Probability of false alarm
β	…	Probability of missed detection
β_{RMS}	…	RMS bandwidth of the signal
β_{rect}	…	Effective rectangular bandwidth of the signal
γ	…	Detection threshold
δt_R	…	Time varying receiver clock bias
δt^S	…	Time varying satellite clock bias
$\delta\tau$	…	Estimated code phase error

$\delta\!f$	…	Estimated Doppler frequency error
$\delta\!x$	…	Perturbation of the state vector
$\delta\!z$	…	Misclosure vector
$\delta\phi$	…	Estimated carrier phase error
θ	…	Parameter vector that characterize the received signal
$\hat{\theta}$	…	Estimate of the parameter vector
θ_e	…	PLL tracking error variance due to receiver dynamics
λ	…	Non centrality parameter
ϕ	…	Initial carrier phase offset
η	…	Doppler Dilatation coefficient
υ	…	Innovation sequence
ρ	…	True satellite-receiver range
σ_A	…	Allan standard deviation
σ_{LB}	…	Cramer-Rao lower bound tracking standard deviation
$\sigma_{(\bullet)}^2$	…	Variance of the quantity $(\bullet)$
τ	…	Time delay
χ^2	…	Chi-square

CHAPTER ONE: INTRODUCTION

The *Global Positioning System* (GPS) was designed to provide position, velocity and timing information to users worldwide, 24 hours a day, regardless of the weather conditions. As a military system, GPS was originally intended to offer civilian users a limited accuracy. This had the effect of initially limiting civilian interest for GPS operations. However, innovative techniques, such as measurement differencing or semi-codeless tracking of the military signals (Lachapelle 2004), gradually improved civilian accuracy and made GPS the main positioning and navigation tool for an increasing number of professional activities (e.g. surveying, ship and aircraft navigation). Simultaneously, miniaturization of electronic components and progress in power management have allowed the integration of GPS chips on autonomous devices such as handheld GPS receivers or cellular phones and have increased its adoption by the general public (e.g. for pedestrian or car navigation). However, this unexpected rise of product development and increasing user demand for location services presents a wide range of challenges, and has highlighted the inherent limitations of the legacy civilian GPS system.

1.1 Background

Efforts to overcome the weaknesses of the legacy civilian GPS system and satisfy the increasing demand for higher performance *Global Navigation Satellite Systems* (GNSSs) have led to the launch of four major global initiatives:

- Modernization of the GPS (Phases II and III)

- Restoration and modernization of the Russian *GLObal Navigation Satellite System* (GLONASS)

- Development of the European Galileo system

- Development of the Chinese Compass system

All four initiatives benefit from the experience gained during the design and exploitation of GPS I and GLONASS. Through innovative design of their respective space and control segments, they all aim at offering enhanced positioning accuracy and reliability as well as improved measurement accuracy, tracking robustness and tracking sensitivity. The focus of these improvements is three-fold: 1) improved satellite availability and/or frequency diversity, 2) increased signal power and 3) signal structure innovations.

Among these initiatives, GPS modernization is of major interest for the GNSS community owing to the emerging availability of GPS Phase II. This modernization was launched under the joint initiative of the U.S. Departments of Defence and Transportation. It began with the introduction of new military and civilian signals to enhance the performance of the legacy GPS system. For the military, the existing P(Y) encrypted signal, transmitted on the L1 and L2 frequencies, is being augmented by a new spectrally split Military signal (M code). The civilian community, on the other hand, is benefiting from the addition of two new civil signals at the L2 and L5 frequencies. The implementation of the L2 civil signal (L2C) started in September 2005 with the successful launch of the first IIR-M satellite. As of February 2008, five such satellites have been placed in orbit and are successfully transmitting L2C; and a full L2C-enabled constellation is expected to be operational by 2010. The L5 signal, broadcast in the protected *Aeronautical Radio Navigation Service* (ARNS) band centred at 1176.45 MHz,

is intended to support *Safety-of-Life* (SoL) applications such as aviation navigation. Its implementation was originally scheduled to start with the launch of the next generation of GPS satellites, namely the II-F satellites, in early 2008. However, delays in the IIR-M satellites launch schedule have deferred the first II-F satellite launch to 2009. In the meantime, the U.S. Air Force is having a IIR-M satellite reconfigured to include an L5 demonstration payload. Upon successful review, this IIR-M satellite, planned for launch in June 2008, would temporarily transmit the third civil signal. This, in turn, would provide an on-orbit demonstration capability for the L5 signal and would secure the L5 frequency filing (GPS World 2008). It would also enable the Air Force to conduct some early signal testing prior to any II-F satellite launches.

While it is understood that the major improvement for civilian users will be achieved through direct access (that is, without having to rely on codeless or semi-codeless acquisition and tracking techniques) to signals broadcast at three different frequencies, it is important to bear in mind that the accuracy of the navigation solution will also depend on measurement accuracy. Assuming that ranging biases due to atmospheric and orbital errors can be efficiently mitigated, it can be considered that measurement accuracy is ultimately conditioned by tracking performance. Since GPS signals' synchronization enables tracking aiding from one frequency to another (Cannon 2004), it is straightforward to understand that the overall positioning accuracy will ultimately be driven by the signal that offers the highest tracking performance. In this regard, both modernized civil signals should benefit from their improved structure (e.g. dataless channel, improved spreading sequence properties or enhanced navigation message format) and should outperform L1 C/A. Furthermore, to ensure its spectral compatibility

with the two military GPS signals broadcast in the same frequency band, many trade-offs were made in designing the L2C signal structure. In particular, the transmitted power and chipping rate had to be set lower for the L2C signal than for its L5 counterpart (Fontana et al 2001). It is therefore anticipated that the L5 signal should offer the highest performance.

In light of the above, it is important to confirm that the key L5 structural innovations do indeed help overcome the inherent weaknesses of the legacy C/A signal in terms of acquisition, tracking and data demodulation. Three innovations in the L5 signal are of central interest for signal performance as they are expected to lead to substantial improvements in tracking sensitivity and measurement accuracy: 1) the presence of a pilot channel broadcast in quadrature from the traditional data bearing channel, 2) the use of new spreading sequences that are broadcast at a higher chipping rate, and 3) the introduction of a *Forward Error Correction* (FEC) scheme applied to the navigation message. It is expected that the presence of a pilot channel will enhance phase tracking sensitivity and accuracy. Combined with the FEC encoding of the navigation message, this should result in greater data demodulation sensitivity and reliability. Similarly, it is assumed that the increased L5 chipping rate will provide superior noise and multipath mitigation capacities. Additionally, the introduction of secondary codes, referred to as *Neuman-Hofman* (NH) codes, will reduce the susceptibility to narrow-band interferences. However, to fulfill the aforementioned expectations and effectively provide a superior navigation solution, innovative L5 receiver architectures are needed. It is therefore critical to identify any challenge inherent to L5 receiver design, and to confirm, in light of these challenges, the effective performance of the L5 signal.

1.2 Limitations of Previous Work

The recent development of GPS software receivers has brought a new perspective to receiver design. Such receivers can provide cost-effective and versatile testbeds for innovative receiver design (e.g. for acquisition or tracking algorithms). They have therefore been extensively used to further improve L1 C/A acquisition and tracking sensitivity (Psiaki & Jung 2002, Shanmugam 2008, Yu 2007). Additionally, in the context of GNSS modernization, they can facilitate research on the performance of the new GNSS signals (Julien 2005, Gernot 2007).

In this perspective, the development of GPS L5 software receivers has, thus far, remained fairly limited. Despite the significant amount of interest initially raised by the L5 signal structure design (Hegarty 1999, Spilker & Van Dierendonck 1999), subsequent research has resulted in limited investigation into the various L5 receiver architectures and their associated performances. In terms of receiver architecture, Ries et al (2002) and Macabiau et al (2003) cover a wide range of L5 receiver functions (e.g. acquisition, tracking, data demodulation and ionospheric correction implementation). They address the data/pilot combining issue for acquisition and tracking; and compare single versus dual frequency ionospheric correction implementations in light of expected L1 and L5 pseudorange accuracy. However, the performance evaluations are mostly theoretical and few simulation results are shown. Further research on L5 receiver architecture has focused mainly on acquisition implementations and, more specifically on L5 secondary codes acquisition and on data/pilot combining. Hegarty & Tran (2003) and Zheng & Lachapelle (2004) proposed acquisition schemes that aim at minimizing the

computational burden while maximizing PRN code detection performance. Yang et al (2004) and Hegarty (2006) discussed optimal ways of re-combining the data and pilot channels' power in light of both PRN and NH code acquisition. These investigations mostly focused on spreading code acquisition and did not consider the effects of frequency errors. In terms of L5 performance analysis, Bastide (2004) offers the most comprehensive overview. This investigation, however, focuses more on analyzing the degradation of L5 navigation performance in the presence of interference, and is placed in the context of civil aviation requirements. Acquisition, tracking and data demodulation sensitivity thresholds are derived but the receiver architectures under consideration focus on robustness and reliability over accuracy. While ideal for aviation navigation applications, such implementations leave room for significant accuracy improvements.

The relative scarcity of research on the L5 signal is probably a consequence of the absence of real field data at the L5 frequency combined with the high cost of hardware simulators. This implies that, to date, most of the L5 software development endeavours have relied on software signal simulators. While software simulators offer numerous advantages (e.g. controllability, repeatability and ease of configuration), they suffer two major drawbacks: 1) integrity and 2) accuracy. When research groups develop software signal simulators to test their software receivers, the integrity of their findings can be threatened by the inter-dependence of their simulation tools and software receivers. Besides, faithfully modelling GNSS signal propagation paths can be very challenging. Specifically, it requires a deep understanding of various GNSS error sources and of the physical processes that create them. In an effort to alleviate the latter problem, research groups tend to use "specialized" L5 software signal simulators. Such tools limit the

number of errors simulated to those relevant to their research. While enabling more faithful simulation, this approach, has mostly limited the extent of previous research to acquisition and tracking, offering little perspective into the measurements and position domains.

Finally, L5 research efforts have remained focused on classical GPS receiver architectures. While it is important to confirm the advantages of the L5 signal modulation in this context, it is important to bear in mind that superior tracking architectures have been proposed to enhance L1 C/A performance. In particular, Kalman filter-based tracking (and acquisition) techniques have been shown to result in significant sensitivity gain over various constant loop bandwidth implementations (Psiaki & Jung 2002, Humphreys et al 2005, Yu et al 2006). While originally introduced for high sensitivity capabilities, later research demonstrated that these techniques could also produce high quality carrier phase measurements (Petovello & Lachapelle 2006). Adapting these techniques to the L5 signal could therefore create the opportunity to further improve L5 tracking and measurement accuracy. Ziedan (2005) uses similar techniques but focuses on very weak signal power and does not compare the results to constant bandwidth tracking techniques.

1.3 Objectives and Contribution

The aim of this dissertation is 1) to identify receiver architectures that are most suited to accommodate the major structural innovation inherent to the L5 signal and to maximize its acquisition, tracking and positioning performance and 2) to implement them in a full

GPS L5 software receiver. To reach these objectives, the following research goals have been identified:

1. **To understand all the important parameters in the design of an L5 acquisition algorithm.** The focus here is to assess how the secondary codes and the pilot channel impact the acquisition process; and to find innovative solutions that minimize the computational burden and maximize detection performance.

2. **To analyze the L5 constant bandwidth code and carrier tracking performance**. The aim is to confirm that the L5 signal structure improves tracking accuracy. The advantages of pilot-channel tracking and a fast chipping rate are highlighted in terms of carrier tracking sensitivity and code tracking accuracy, respectively.

3. **To compare constant bandwidth and Kalman filter-based tracking for L5.** Kalman filter-based tracking has proven to be successful in improving L1 C/A tracking sensitivity and accuracy. Recognizing that the L5 constant bandwidth tracking performance is superior to that of L1 C/A, it becomes critical to verify whether Kalman filter-based tracking can provide further improvements to the L5 tracking sensitivity and accuracy.

4. **To use representative simulation and analysis tools with a high degree of fidelity.** It is important to ensure that the results presented are meaningful. In the absence of available real GPS L5 data, it was necessary to use simulation tools. The goal is to obtain two versatile, independent and complementary tools:

    a) **A Spirent GPS L5 hardware simulator** is used in combination with a NovAtel Euro-L5 card to produce high-fidelity L5 IF samples; and

b) A full GPS L5 software receiver is developed to confirm, in post-mission, tracking performance at the measurement and position levels.

In light of these objectives, the major contributions of this thesis can be summarized as follows:

1. *Characterization of the benefits and limitations of GPS L5*. Such a characterization is important given the key role of the L5 signal in the overall GPS positioning accuracy. Included in this characterization is a thorough assessment of:

   a) L5 acquisition implementation issues and resulting performance

   b) L5 tracking performance using constant bandwidth and Kalman filter-based algorithms

2. *Confirmation of tracking performance results at the measurement and position levels*. Typically, performance evaluation of the various tracking implementations is conducted at the tracking level. Useful information can be gathered by comparing the impact of various errors on different code and carrier discriminators. However, significant insight can be gained if the impact of these errors can be further propagated. Given this, the various tracking implementations are compared at the measurement and position levels.

3. *Use of independent simulation and analysis tools*. In the absence of real GPS L5 data, performance analysis must be conducted using simulation tools such as a signal simulator and a software receiver. To ensure the integrity of the findings presented herein, high-fidelity L5 IF samples obtained from a hardware receiver were used.

1.4 Dissertation Outline

This dissertation focuses on the development of a GPS L5 software receiver. In order to provide a comprehensive view of the research realized, the subsequent chapters are structured in the following way.

Chapter 2 reviews the GPS L1 C/A and L5 signal structures. The improvements expected from the latter are presented in light of the weaknesses of the former. Such an evaluation is performed in terms of acquisition, tracking and data demodulation.

Chapter 3 introduces the simulation and analysis tools used throughout this dissertation. The Spirent GSS 7700 hardware is presented with particular emphasis on its error modeling capabilities. The architecture of the L5 software receiver developed in the frame of this research is then outlined. Finally, the derivation of the truth measurements is briefly discussed.

Chapter 4 is an in-depth investigation of the challenges brought by the L5 signal structure in terms of acquisition. The general goal and architecture of a GPS acquisition module are reviewed. The impact of the new L5 spreading sequence and data/pilot implementations are thoroughly discussed and ways of implementing efficient and robust L5 acquisition are proposed and compared.

Chapter 5 is a thorough study of the GPS L5 constant bandwidth tracking loops. The architecture and error sources of the carrier and code tracking loops are presented. The L5 tracking performance is assessed in the presence of noise, oscillator phase noise, multipath and dynamics. The benefits of pilot tracking over data tracking are demonstrated in terms of accuracy, sensitivity and robustness. An innovative correlator level data/pilot combining scheme is proposed and tested.

In Chapter 6, an L5 Kalman filter-based tracking architecture is proposed and evaluated. Its advantages in terms of code and carrier tracking are demonstrated in the presence of noise, oscillator phase noise and dynamics.

Chapter 7 summarizes the major findings of this research and makes recommendations for future work.

CHAPTER TWO: GPS C/A AND L5 SIGNAL STRUCTURES

After a brief review of GPS principles, this chapter presents the structures of two GPS civil signals, namely the *Coarse Acquisition* (C/A) and L5 signals. It is important to understand that these signals were designed to fulfill very different requirements. The GPS C/A code was a pioneer signal that was designed in the 1970s to facilitate the acquisition of the military signals and that was left freely available to civilian users. The range of applications that rely on it is much wider than anticipated and presents a variety of challenges that had not been forecasted. The C/A signal structure is therefore presented in light of the initial requirements it was meant to fulfill, and its limitations discussed in the context of the challenges it is currently facing. In contrast, the L5 signal was introduced to overcome some weaknesses in the C/A signal and to support *Safety-of-Life* (SoL) applications such as aviation navigation. The L5 signal structure is therefore described to highlight how it differs from the C/A structure and why it is expected to outperform it in terms of tracking robustness, measurement accuracy and interference protection.

2.1 GPS Overview

The fundamental principles of GPS operation are well described in Parkinson (1997a), Misra & Enge (2006) or Kaplan et al (2006). In essence, GPS operates on the principles of measuring the distance between the user and satellites with known location, where the user position can then be retrieved by multi-lateration. Despite the simplicity of this concept, some complexity arises in its implementation since the following key

requirements need to be met: 1) the user must have accurate information about the location of all satellites used in its multi-lateration computations, and 2) the user must be able to accurately estimate its range to each of the satellites in view (i.e. to each of the satellites from which a signal is received).

In GPS, these requirements are fulfilled through careful design of the broadcast signals. The electromagnetic signals broadcast from the satellite in the *Radio Frequency* (RF) band use a two-layer *Direct Sequence Spread Spectrum* (DS-SS) modulation technique to carry the GPS data and are based on *Code Division Multiple Access* (CDMA) principles to distinguish signals coming from different satellites. The first layer of the modulation consists of a sequence of bits that conveys all the information necessary for precise positioning (e.g. satellites location or ionospheric corrections), and is referred to as the navigation message. The second layer consists of a repeating pseudo-random sequence of bits that spread the signal across a wide bandwidth and is therefore referred to as the spreading code. The purpose of the spreading code is two-fold: 1) to allow determination of the signal propagation time or, equivalently, the distance between the receiver and the satellite, and 2) to spread the signal across a wide bandwidth and therefore provide a satisfactory level of tolerance against intentional or unintentional interference (including other GNSS signals).

In GPS I, three signals were designed to meet the aforementioned specifications. Two high-performance signals were designed for military users, and one lower performance signal was left available to civilian users. The military signals, broadcast in the L1 (1575.42 MHz) and L2 (1127.60 MHz) frequency bands, use long spreading codes and high chipping rates. These codes, referred to as *Precise* (P) spreading codes, are further

encrypted by a classified code to form secure versions of the published P codes. The resulting precise encrypted codes, referred to as P(Y) codes, are therefore restricted to authorized users. The third signal, transmitted on the L1 frequency only, was mainly intended to facilitate the acquisition of the two military signals (hence its name, C/A for *Coarse Acquisition*). To this end, the spreading code it uses is much shorter and has a slower chipping rate than the precise encrypted P(Y) spreading codes. Since all the GPS signals broadcast by one satellite are synchronized, military users can use the timing information provided by the C/A signal to lock onto both precise military signals. While shorter spreading codes and slower chipping rates can make acquisition faster, they also provide lower tracking accuracy and reliability. Consequently, the accuracy available to most civilian users is limited by the shortcomings of the C/A signal in terms of tracking accuracy, sensitivity and reliability.

In GPS II, four additional signals are being introduced: two new military signals broadcast in the L1 and L2 frequency bands, and two new civilian signals transmitted on the L2 and L5 (1176.45 MHz) frequencies. Designed to meet the same fundamental system requirements, these signals are also expected to increase the accuracy available to both military and civil users. From a civilian perspective, the advantage of broadcasting civil signals at the L2 and L5 frequencies is two-fold. First it brings the advantages of frequency diversity to civilian users. This, in turns, greatly enhances the civilian system reliability (to counter possible jamming in individual frequency bands) and ionospheric mitigation capabilities (since ionosphere is a dispersive medium, as will be explained in chapter 3). Second, these signals exhibit key structural innovations that improve measurement accuracy, tracking sensitivity and tracking robustness. In particular, the L5

signal, intended to support SoL applications, is expected to offer the highest accuracy amongst GPS civil signals. More specifically, the L5 signal was designed to provide the following (Spilker & Van Dierendonck 2001): enhanced cross-correlation side-peaks protection, improved narrow-band interference mitigation, instantaneous carrier phase ambiguity resolution for cm-level positioning, and improved multipath performance. Furthermore, and contrary to the high-performance military signals, the L5 signal was designed to enable direct code acquisition without the C/A code.

Despite its inherent limitations, the GPS C/A signal has shaped the field of satellite navigation. Similarly, thanks to its high-accuracy profile, the GPS L5 has the potential to revolutionize the scope of civilian GPS operations. A summary of the GPS L1 C/A and L5 signals' characteristics are given in and a thorough description of their structure is given in the following sections.

2.2 C/A Signal Structure

The C/A signal is *Right Hand Circularly Polarized* (RHCP) and use a *Binary Phase Shift Keying* (BPSK) modulation. As mentioned previously, the L1 carrier is modulated by a navigation message and a spreading code. These sequences both use rectangular *Non-Return to Zero* (NRZ) materialization. The L1 frequency is centred at 1575.42 MHz, resulting in a wavelength of approximately 19 cm.

The navigation message contains information relevant to precise positioning (Spilker 1997a). In particular, it includes: 1) a set of precise orbital parameters, called ephemeris parameters, from which the current position, velocity and clock error of the satellite can be derived, 2) a set of coarser orbital parameters, called almanac parameters, from which

the location of all the GPS satellites can be approximated over a period of 14 days, and 3)

a set of ionospheric correction parameters, that can be used by single frequency users to

remove (on average) about 50% of the ranging error due to signal propagation through

the ionosphere (Klobuchar 1997).

Table 2.1 - GPS C/A and L5 Signals Characteristics

Properties	GPS L1 C/A	GPS L5	
		I5	Q5
Frequency [MHz]	1176.45	1575.42	1575.42
Transmitted Power [dBW]	- 157	- 154	- 154
Code Length [Chips]	1023	10230	10230
Code Chipping Rate [Mcps]	1.023	10.23	10.23
Modulation	BPSK	QPSK	
Navigation Data	Yes	Yes	No
Data Rate [sps]	50	50	-
Data Encoding	No	FEC (7, 1/2)	-
Secondary Code	No	Yes	Yes
Secondary Code Length [Chips]	-	10	20

The navigation message repeats every 12.5 min and has a data rate of 50 Hz. This

relatively low data rate was selected to enable low *Bit Error Rates* (BER) for common

Signal-to-Noise Ratios (SNRs) (Van Dierendonck 1997).

To spread the signal over a wide frequency, the C/A signal uses 1023-bit PRN codes broadcast with a 1.023 MHz chipping rate; the C/A spreading codes repetition period is therefore one millisecond. These spreading codes are part of the 1023-bit Gold code family described in Gold (1967) and Spilker (1997b). They are obtained as the modulo-2 addition of two maximum length sequences generated by two *Linear Feedback Registers* (LFSR) of 10 stages each. Maximum length sequences offer better auto-correlation side peaks protection than Gold codes; the latter were however selected for the superior cross-correlation (with code from other satellites) side peaks protection they offer. The degradation they suffer in terms of auto-correlation side-peaks protection is minimal since the Gold codes provide, in the absence of any Doppler effects, a minimum auto- and cross-correlation side peaks isolation of 23.9 dB.

Figure 2-1 shows the normalized auto-correlation plot for PRN 23 C/A code materialization. It can be seen that the main auto-correlation peak is a perfect triangle. In fact, in the context of tracking, it is common to neglect the auto-correlation side peaks and therefore to model the auto-correlation function as

$$\overline{R}_{C/A}(x) = \begin{cases} 1 - |x| & if \quad |x| \le 1 chip \\ 0 & if \quad |x| > 1 chip \end{cases} \tag{2-1}$$

where $\overline{R}_{C/A}$ is the normalized auto-correlation function of the C/A spreading code materialization.

This approximation, however, cannot be made in the context of signal acquisition, where auto- or cross-correlation side-peaks must be taken into account.
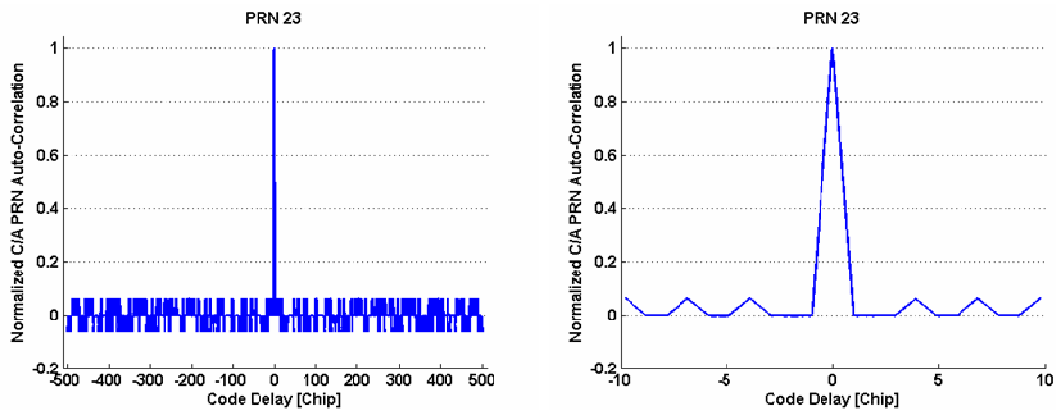
Figure 2-1 – Example of GPS C/A Code Normalized Auto-Correlation (Left) and Zoomed-in View About ± 10 chips (Right)

Since the *Power Spectral Density* (PSD) and the auto-correlation of a wide-sense stationary signal form a Fourier pair (Brown & Hwang 1992), the PSD of the C/A signal can be obtained by applying a Fourier transform to its auto-correlation function. As demonstrated by Macabiau (2003), and confirmed by Figure 2-2, the resulting PSD is a peak spectrum that can be approximated by its sinc envelope. The spectral lines result from the spreading sequence periodicity and are separated by an increment of 1 kHz (since the PRN code has a repetition period of 1 ms). The sinc shape corresponds to the PSD of the rectangular materialization used for the spreading code chips. Finally, the normalized PSD of the GPS C/A signal can be approximated as

$$\overline{G}_{C/A}(f) = T_C \left(\frac{\sin\left(\frac{\pi f}{f_C}\right)}{\frac{\pi f}{f_C}} \right)^2 \tag{2-2}$$

where $\overline{G}_{C/A}$ is the normalized PSD of the C/A spreading code, and $T_C = 1/f_C$ is the C/A spreading code chip duration.

The C/A signal is broadcast with a minimum specified received power of -158.5 dBW when using a 0 dBic antenna RHCP (ICD-GPS-200D). This very low signal power, combined with the spreading of the navigation message over a very large bandwidth brings the signal PSD under the thermal noise floor and effectively limits interferences between GPS and other existing communications systems.
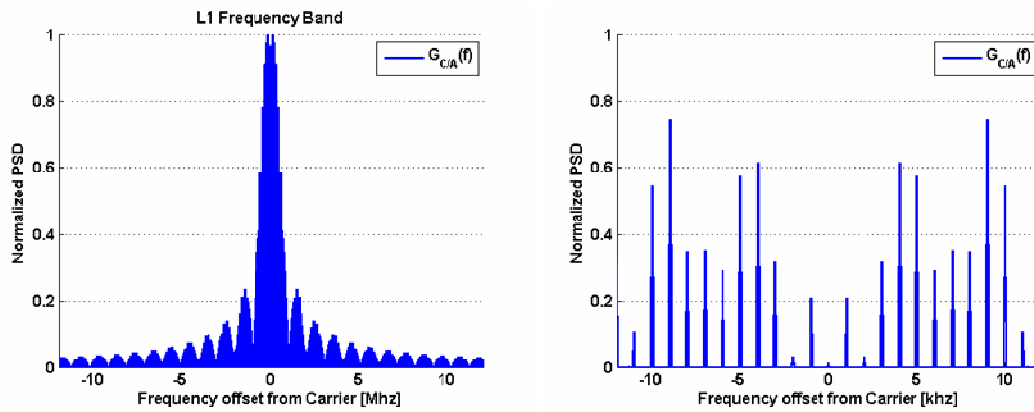
Figure 2-2 – Example of GPS C/A Signal Normalized Power Spectral Density Spectrum (Left) and Zoomed-in View about ± 10 kHz (Right)

Finally, considering all the above and taking the propagation time into account, the C/A signal received from a particular satellite can be modeled, at the receiver antenna, as

$$s_{C/A}(t) = \sqrt{2P_{C/A}(t)}d(t_{C/A}(t))c_{C/A}(t_{C/A}(t))\cos(2\pi f_{L1}t_{C/A}(t) + \phi_{C/A}) + n(t) \qquad \textbf{(2-3)}$$

where $P_{C/A}(t)$ is the instantaneous power of the received C/A signal, and $P_{C/A}(t) = A_{C/A}^2(t)/2$, with $A_{C/A}(t)$ the instantaneous amplitude of the signal, $d(t)$ is the NRZ materialization of the navigation data bit, $c_{C/A}(t)$ is the NRZ materialization of the C/A spreading code, f_{L1} is the L1 frequency, $\phi_{C/A}$ is the initial carrier phase offset, $n(t)$

is the noise on the received signal, and $t_{C/A}(t)$ is a function incorporating the effects of propagation delay and Doppler shift on the received C/A signal.

In the framework of this dissertation, the noise is assumed to be a zero-mean *Additive White Gaussian Noise* (AWGN) process. In reality, the noise is neither white nor Gaussian. The Gaussian assumption, however, is justified by the central limit theorem (Walpole et al 1998), and is found to work well in practice. Similarly, the noise bandwidth limitation due to frontend filtering and the correlation introduced in consecutive noise samples by the sampling processes are ignored. However, the whiteness approximation was found to work well in practice. Under normal conditions, the L1 C/A thermal noise floor, which is based on the Boltzman constant and the system temperature, can be approximated at about -205 dBW/Hz (Van Dierendonck 1997).

In general, $t_{C/A}(t)$ is an arbitrary function of t, where t denotes the GPS time, that depends on the conditions encountered by the signal on its propagation path between the satellite and the user; a simple first order approximation can however be given by (O'Driscoll 2007)

$$t_{C/A}(t) = (1 + \eta)t - \tau_{C/A} \qquad\qquad \textbf{(2-4)}$$

where η is the time dilation coefficient due to the Doppler effect and $\tau_{C/A}$ is the time delay introduced on the L1 C/A signal during the satellite-receiver propagation time.

The Doppler effect is a time contraction (or dilatation) due to the relative satellite-user motion along the propagation path of the radio wave and can be expressed as (Axelrad & Brown 1997)

$$\eta = \frac{v_{Sat} - v_{Rx}}{c} \cdot u \tag{2-5}$$

where v_{Sat}, v_{Rx} are the velocity vectors for the satellite and receiver respectively, c is the speed of light, u is unit vector along the *Line Of Sight* (LOS) between the satellite and the receiver, and $x \cdot y$ is the dot-product of the vector x and y.

Thus, if two events are separated by T seconds in the transmitted signal, they will be separated by $T \times (1+\eta)$ seconds when the signal reaches the receiver. This effect is commonly associated with the frequency shift it creates on the signal carrier

$$\cos(2\pi f_{L1}(1+\eta)t) = \cos(2\pi(f_{L1} + f_D)t) \tag{2-6}$$

where $f_D = \eta f_{L1}$ is known as the Doppler shift.

However, it is important to note that this effect impacts all components of the transmitted signal. Therefore the signal effectively suffers two additional Doppler effects: one on the navigation message (data Doppler) and one on the spreading code (code Doppler). The time delay can be expressed as

$$\tau_{C/A} = \frac{\rho}{c_l} + \Delta t_{C/A,Atmo} \tag{2-7}$$

where ρ is the true distance between the satellite and the receiver, c_l is the speed of light, and $\Delta t_{C/A,Atmo}$ is the delay due to propagation of the radio wave through the atmosphere. From a GPS standpoint, the atmosphere reduces to two layers: the ionosphere and the troposphere. Their respective effects on radio wave propagation will be further discussed in Chapter 3.

Now that the C/A signal structure has been reviewed, it is instructive to look at the L5 signal structure to understand how it is expected to outperform the C/A signal.

2.3 GPS L5 Signal Structure

The L5 signal is broadcast using a *Quadrature Phase Shift Keying* (QPSK) modulation with a minimum specified received power of -154.9 dBW (IS-GPS-705). The L5 frequency is centred at 1176.45 MHz, resulting in a wavelength of approximately 25 cm. The L5 signal is composed of two channels: 1) a data channel (I5) that carries the navigation message, and 2) a pilot channel (Q5) that does not possess a navigation message. The I5 and Q5 channels are synchronized and orthogonal. In addition, they equally share the total L5 signal power. Consequently, taken separately, I5 and Q5 will have a minimum received power 0.6 dB higher than currently specified for the GPS C/A signal.

The presence of a dataless channel, broadcast in quadrature from the conventional data channel, allows significant phase tracking sensitivity, accuracy and robustness gain. The absence of unknown data bit transitions on the Q5 channel enables the use of pure Phase Lock Loop (PLL) discriminators (instead of the traditional Costas discriminator used for data bearing channel such as GPS L2-P(Y) or GPS L1-C/A) that possess wider linear tracking ranges and were shown (e.g. Julien 2005) to improve the phase tracking sensitivity, to remove the risk of half cycle slips and to reduce that of full cycle slips. It also allows the use of longer coherent integration times which can enhance thermal noise mitigation on the correlator output values and improve tracking accuracy. Longer coherent integrations also play a critical role in the re-acquisition of weak signals.

Another consequence of this channel separation is that several implementations can be envisioned for the acquisition and tracking of the L5 signals since some trade-offs must be made in terms of complexity, computational burden, accuracy and reliability.

The L5 data bit rate has been set to 50 *bits per second* (bps). However, to compensate for the fact that the QPSK modulation induces a 3 dB degradation in the energy allocated for the transmission of the navigation data bit, the original navigation data bit stream is coded with a rate-$1/2$, $K = 7$ *Forward Error Correction* (FEC) convolutional code. The effect of this encoding is to offer more reliable recovery of the data bit train. Spilker (1977) demonstrated that a receiver using soft decision Viterbi decoding can decode, with the same error rate, a 50 bps data stream and its corresponding FEC ($1/2,7$) encoded stream transmitted with 5 dB less signal-to-noise ratio. Another consequence of this encoding is that the data channel will have to effectively transmit the encoded symbols at 100 *symbols per second* (sps) to maintain an effective navigation message rate at 50 bps. Besides, the C-NAV navigation message format used for the L5 signal differs from the NAV navigation message format used for the C/A signals. In particular, the rigid frame and superframe sequencing order adopted for the NAV message (Spilker 1997a) is replaced by a more flexible sequencing scheme where the control segment can modify the L5 subframe broadcasting order as it sees fit. The C-NAV message also includes new ephemeris parameters that improve the accuracy of the satellite position determination.

The PRN codes used on each channel are 10230 chips long and are broadcast with a 10.23 MHz chipping rate; the L5 PRN codes repetition period is therefore one millisecond. These codes are generated from two different maximum length sequence generators, XA and XB_i, of 13 stages each. XA generates a truncated sequence of 8190

chips and XB_i a sequence of 8191 chips. Both sequences are modulo-2 added to generate the 10230-chip PRN codes. Note that, due to their desired length, the L5 PRN codes are not Gold Codes. As such, their auto- and cross-correlation properties are not optimal. However, owing to their increased length, and to a careful selection of initial stages, they provide a minimum isolation 2.5 dB better than the current GPS C/A code, as illustrated in Table 2.2.

Table 2.2 - GPS L5 Code Isolation Properties (Ries et al 2002)

Minimum Side Peaks Protection [dB]		Minimum Cross-Correlation Peaks Correction [dB]		
R(I,I)	**R(Q,Q)**	**C(I)**	**C(Q)**	**C(I,Q)**
Without NH code				
-29.2	-29.0	-26.4	-26.5	-62.1
With NH code				
-29.8	-29.4	-28.1	-28.5	-33.3
R(I,I) = auto-correlation of all I5 codes, R(Q,Q)= auto-correlation of all Q5 codes, C(I)= cross-correlation of all I5 codes vs. all I5 and Q5 codes, C(Q)= cross-correlation of all Q5 codes vs. all I5 and Q5 codes, C(I,Q) = cross-correlation of (I,Q) pair.				

The I5 and Q5 channels are further modulated by *Neuman-Hofman* (NH) codes. The NH-modulated PRN codes are referred to as tiered sequences. For the I5 component, the PRN code is further modulated by a 10-bit NH sequence ($NH_{10} = 0000110101$). For the Q5 component, the PRN code is further modulated by a 20-bit NH sequence ($NH_{20} = 00000100110101001110$). Each bit of the NH codes is 1 ms, and the NH bit transitions are fully aligned with the PRN code roll-over. This results in 10 and 20 ms

tiered sequences on the data and pilot channel respectively. Besides, the NH_{10} and NH_{20} sequences are fully synchronized with the 10 ms symbol bit and the 20 ms data bit respectively.

Figure 2-3 shows the normalized tiered sequence auto-correlation plot for PRN 23 on the L5 data and pilot channels. It is interesting to note that the NH codes create several secondary peaks on the tiered sequence auto-correlation. As underlined in Ries et al (2002) and Macabiau et al (2003), these peaks create a risk for biased acquisition. This issue will be addressed in detail in Chapter 4.

As for the C/A signal, the L5 signal PSD is a peak spectrum that can be approximated by its sinc envelope. Since the tiered sequences have repetition periods of 10 and 20 ms, the code spectral line separation is reduced from 1 kHz to 100 Hz and 50 Hz on the data and pilot channel, respectively. Besides, since the L5 spreading code chips are broadcast at a 10.23 MHz chipping rate, the main lobe of the sinc envelope is increased from approximately 2 MHz to 20 MHz, as shown in Figure 2-4. The normalized PSD of the GPS L5 signal can therefore be approximated as

$$\overline{G}_{L5}(f) = T_C \left(\frac{\sin\left(\frac{\pi f}{f_C}\right)}{\frac{\pi f}{f_C}} \right)^2 \tag{2-8}$$

where $\overline{G}_{L5}$ is the normalized PSD of the L5 spreading code, and $T_C = 1/f_C$ is the L5 spreading code chip duration.
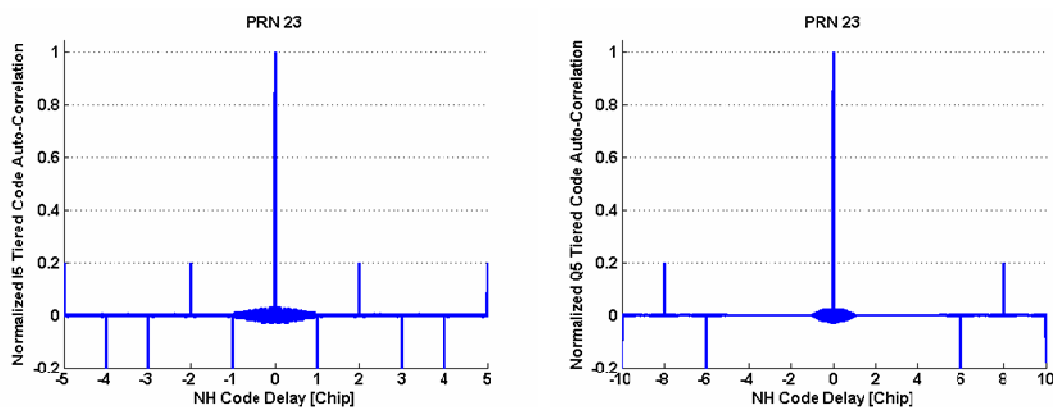
Figure 2-3 – Example of GPS I5 Code (Left) and GPS Q5 Code (Right) Normalized Auto-Correlation

The purpose of the NH sequences is three-fold. First, due to their periodicity, they narrow the code spectral line separation from 1 kHz to 100 Hz and 50 Hz on the data and pilot channels respectively. As illustrated in Figure 2-4, it has the effect of reducing the power carried in each spectral line and therefore, to enhance the L5 signal inherent mitigation capacities against narrow-band interference.
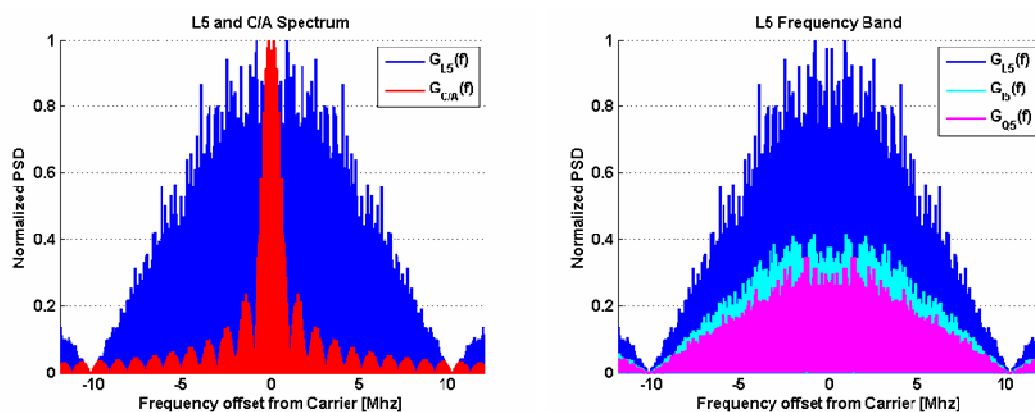
Figure 2-4 – GPS L5 and C/A Normalized Power Spectral Density Spectrum (Left) and GPS L5, I5 and Q5 Normalized Power Spectral Density Spectrum (Right)

As shown in Table 2.2, the NH codes also improve the cross-correlation properties amongst spreading codes. Finally, as they are aligned with the navigation data and symbol bits, data synchronization can be performed by correlating the received NH sequences with the locally generated ones. This method provides better reliability compared to classical techniques such as the histogram process (van Dierendonck 1997). From the above, and taking the propagation time into account, the L5 signal received from a particular satellite at the receiver antenna can be represented as

$$s_{L5}(t) = \sqrt{P_{L5}(t)} \begin{pmatrix} d(t_{L5}(t))NH_{10}(t_{L5}(t))c_{I5}(t_{L5}(t))\cos(2\pi f_{L5}t_{L5}(t) + \phi_{L5}) \\ + NH_{20}(t_{L5}(t))c_{Q5}(t_{L5}(t))\sin(2\pi f_{L5}t_{L5}(t) + \phi_{L5}) \end{pmatrix} + n(t) \qquad \textbf{(2-9)}$$

where $P_{L5}(t)$ is the instantaneous power of the received L5 signal, $d(t)$ is the NRZ materialization of the navigation data bit, $c_{I5}(t)$ and $c_{Q5}(t)$ are the NRZ materializations of the L5 PRN codes on the data and pilot channels respectively, $NH_{10}(t)$ and $NH_{20}(t)$ are the NRZ materializations of the L5 NH codes on the data and pilot channels respectively, f_{L5} is the L5 frequency, ϕ_{L5} is the initial carrier phase offset, $n(t)$ is the noise on the received signal, and $t_{L5}(t)$ is a function incorporating the effects of propagation delay and Doppler shift on the received L5 signal.

The noise is again assumed to be a zero-mean AWGN process. However, to account for the larger filter insertion loss expected due to more stringent filtering requirements, a larger L5 noise figure has been suggested by Hegarty (2006). The -200 dBW/Hz noise floor value he proposed has been widely accepted and is therefore used herein.

In general, $t_{L5}(t)$ will differ from $t_{C/A}(t)$; this is due to the presence of a dispersive medium on the satellite-to-receiver propagation path.

Now that the structures of the C/A and L5 signals have been discussed, it is interesting to review the limitations of the C/A signals and how the L5 signal is expected to improve on these.

2.4 GPS C/A Signal Limitations and Improvements Brought by GPS L5

The desire to use GPS under ever more challenging conditions has shed light on some limitations of the legacy GPS system and its unique civilian signal, the L1 C/A code. GPS modernization and, in particular the L5 signal, were intended to overcome these limitations. From a signal perspective, these limitations can be summarized in three main points: sensitivity, reliability and accuracy. The C/A signal limitations and improvements brought by the L5 signal will be discussed in light of all the signal processing operations which include acquisition, tracking and data demodulation.

2.4.1 Acquisition Reliability

Acquisition reliability refers here to the receiver's ability to acquire the signal spreading code autocorrelation main peak. In this respect, the two main sources of unreliable acquisition are the auto- and cross-correlation side peaks. The C/A signal provides a minimum isolation of 23.9 dB against both. Although offering a very reasonable margin in open-sky environments, this value may appear very limited in more challenging environments where signals suffer from severe attenuation and multipath conditions. The main challenge arises when the signals reach the receiver with very different power. This is often the case in urban canyons where some signals arrive at the receiver after passing through materials (e.g. concrete buildings) while other arrive unobstructed. The power

difference can easily reach the C/A cross-correlation protection level. As demonstrated in MacGougan (2003), such occurrence can lead to the acquisition and tracking (over short periods) of cross-correlation peaks. The easiest way to provide higher reliability is to design codes that exhibit better correlation properties. This can be achieved using longer codes. In this perspective the L5 PRN codes offer, as a truncated Gold family, correlation properties close to the theoretical bound (Ries et al 2002). In particular, as shown in Table 2.2, the L5 auto-correlation and cross-correlation side peak protections are increased by 5.1 and 2.5 dB respectively with respect to the C/A code. As explained earlier, the most significant gain is the 2.5 dB improvement in cross-correlation peak isolation.

Furthermore, the presence of secondary codes modifies the correlation properties of the L5 spreading sequences. As shown in Table 2.2, when the correlation is taken over a PRN code period, the NH codes improve the L5 codes auto- and cross-correlation side peak protections by an additional 0.4 and 1.7 dB respectively, which is particularly interesting in terms of cross-correlation side peak protection.

 However, as illustrated in Figure 2-3, they create secondary auto-correlation side peaks when the correlation is taken over the full I5 or Q5 tiered codes. This implies that the L5 tiered codes auto-correlation side peaks protection is reduced to 14 dB on both data and pilot channel. As underlined in (Ries et al 2002), these peaks create a risk for biased acquisition. Furthermore, Macabiau et al (2003) demonstrated that, due to their short length, the NH code correlation properties are greatly affected by residual Doppler errors. In the presence of frequency errors as small as 30 Hz, the auto-correlation side peaks

protection could drop to 6.8 dB (ibid). This particular issue will be further discussed in Chapter 4.

2.4.2 Tracking Sensitivity

Tracking Sensitivity is defined here as the minimum pre-correlation *Signal-to-Noise Ratio* (SNR) that ensures the correct tracking of the signal. Equivalently, the tracking sensitivity of a receiver will determine the maximum amount of attenuation GPS signals can undergo without compromising the receiver's ability to remain locked onto the incoming signal. Designing signals that would lower the receiver tracking threshold would greatly enhance satellite navigation in degraded environments such as urban canyons or indoors where attenuations of 20 dB or more are common.

In principle, the easiest method to increase the maximum level of permissible attenuation is to increase the signal power at the satellite end. The specified minimum receiver powers are -158.5 dBW and -154.9 dBW for the C/A and L5 signals respectively. However, according to Hudnut et al (2004), the actual C/A received power seems to be varying more between -154 dBW and -157 dBW. If a similar trend were to occur for the L5 received power, the overall gain in received power would be 3.6 dB. This gain, however, would be counterbalanced by the fact that the L5 noise floor is about 5 dB higher than the C/A noise floor.

The easiest way to increase tracking sensitivity is to improve the correlation gain or, equivalently, the post-correlation SNR. To this end, increasing the coherent integration time is the most efficient strategy. The coherent integration process, however, is limited by two mechanisms: 1) unknown data bit transition due to the presence of a navigation

message, and 2) susceptibility to frequency errors. Provided frequency errors can be constrained, the presence of a dataless channel can provide significant sensitivity gains. (Watson 2005) demonstrated that for a stand-alone receiver, coherent integrations in excess of one second remain extremely challenging. Increasing the coherent integration time from 20 ms (symbol bit duration on the C/A signal) up to one second can provide an additional 20 dB gain in post-correlation SNR (ibid), which, in principle, would be feasible for static applications and using a highly stable receiver oscillator. An alternate strategy consists in using non-coherent integrations. This technique is based on the summation of successive squared coherent correlations. Assuming that the coherent integrations are aligned with the data bit train, this technique presents the double advantage of being less sensitive to frequency error and data bit transition than the coherent integration strategy but the squaring of the successive correlation outputs has the disadvantages of removing the information about the data bit sign and squaring the noise components. The latter translates into squaring losses (Lachapelle 2004) that reduce the gain of the non-coherent integration technique. Moreover, the lower the post-correlation SNR after the coherent integration time, the higher the losses (ibid).

The receiver tracking sensitivity is also a function of the individual code and carrier tracking loops implementations. In this regard, the carrier tracking loop is known to offer the worst performance (Ray 2005). In particular, the L1 C/A carrier sensitivity is limited by the occurrence of a 180 degree phase shift, due to a data bit transition, that requires the use of a Costas loop for phase tracking. The presence of a pilot channel (that does not exhibit these sudden phase shift) enables the use of pure *Phase Lock Loop* (PLL)

discriminators. Julien (2005) demonstrated that, thanks to their wider linear region, these discriminators could improve phase tracking sensitivity by approximately 6 dB.

2.4.3 Tracking Accuracy

The accuracy of a tracking loop is characterized by its resistance to the following tracking error sources: 1) thermal noise, 2) multipath, 3) interference, and 4) receiver dynamics. Noise and multipath will more severely affect the code tracking loop than the carrier tracking loop, whereas interference may greatly affect both (Ray 2005). The impact of these errors on code tracking accuracy depends primarily on the spreading sequence used to modulate the signal. To that end, higher chipping rate provides superior inherent mitigation capacities.

For a given signal, a lower bound on code tracking accuracy due to white noise can be obtained using its *Root Mean Square* (RMS) bandwidth (Betz 2002). This lower bound, based on the performance of a maximum likelihood estimator of the time of arrival driving a *Delay Lock Loop* (DLL), is given, in units of seconds, by

$$\sigma_{LB} = \frac{1}{2\pi\beta_{RMS}} \sqrt{\frac{B_L}{\lambda \frac{C}{N_0}}} \qquad \textbf{(2-10)}$$

with

$$\beta_{RMS} = \sqrt{\int_{-B}^{B} f^2 \overline{G}(f) df} \qquad \textbf{(2-11)}$$

where β_{RMS} is the RMS bandwidth of the signal, B_L is the DLL filter one-sided noise bandwidth, $\lambda = \int_{-B}^{B} G(f) df$ is the fraction of power remaining after bandlimiting the signal

to $\pm B$ Hz, C/N_0 is the carrier-to-noise PSD ratio (over the $\pm B$ Hz bandwidth) and

$\overline{G}(f) = \dfrac{G(f)}{\lambda}$ is the normalized signal PSD.

It can be seen from Equations 2.11 that a signal that carries more power away from the carrier frequency will have a greater RMS bandwidth, and therefore will be better able to mitigate white noise. As confirmed by , signals using a 10.23 MHz chipping rate (including the GPS P(Y) and L5) possess an RMS bandwidth approximately three times greater than signals using a 1.023 MHz chipping rate (including the GPS C/A and L2C) and, accordingly, are expected to provide a more accurate code tracking accuracy in the presence of white noise. It is interesting to note that a tenfold chipping rate increase only translates in a three fold code tracking accuracy improvement. This limited enhancement can be explained by frontend filtering effects that limit the effective signal power received by the receiver. It is also a consequence of the spectral shape of the PSK-modulated signals. Indeed, as outlined in Betz (2002) and Julien (2005), modulations that carry the main part of their power around the central frequency are not optimal in terms of noise mitigation. In fact, *Binary Offset Carrier* (BOC) modulations, that possess a split spectrum, provide greater resistance to white noise.

Similarly, the resistance of a signal to narrow-band interferences can be assessed through its effective rectangular bandwidth β_{rect}. The effective rectangular bandwidth of a signal's PSD is defined in Betz (2002) as the bandwidth of a rectangular spectrum having both the same maximum and the same area. It can therefore be written as:

$$\beta_{rect} = \frac{\int\limits_{-B}^{B} G(f)\,df}{G(f_{max})} \tag{2-12}$$

where $G(f_{max})$ is the maximum value of the signal's PSD.

Greater values of β_{rect} provide better resistance to interference. This is understandable since the wider the effective rectangular bandwidth, the smaller the amount of energy carried in a given small frequency band and, therefore, the less the narrow-band interference is likely to affect a significant part of the useful signal.

Table 2.3 – Signal Modulation Spectral Characteristics (Betz 2002)

Signal Modulation	RMS Bandwidth	Effective Rectangular Bandwidth
BPSK (1)	1.1	1.0
BPSK (10)	3.5	9.3
Computed with a receive bandwidth of 24 MHz		

As shown in , signals using a 10.23 MHz chipping rate possess an effective rectangular bandwidth approximately nine times greater than signals using a 1.023 MHz chipping rate. Therefore, the L5 signal is expected to be less affected by narrow-band interferences than its L1 counterpart. It is important to note that the values shown in do not account for the effect of secondary codes. As underlined in Ries et al (2002) and confirmed by Figure 2-4, the NH sequences lower the amount of energy carried in individual spectral lines by 10 and 13 dB on the data and pilot channels, respectively. This effectively reduces the

maximum value of the L5 signal PSD and further increases its effective rectangular bandwidth.

In terms of multipath, a general rule of thumb is that reflected signals with a delay greater than one chip will not have a significant impact on tracking (Ray 2005). Accordingly, signals using a faster chipping rate (or, equivalently, signals with shorter code chip durations) will exhibit lower susceptibility to long multipath. Numerous publications comparing the impact of multipath on code tracking for the GPS C/A and P(Y) signals and other signals have confirmed this statement and demonstrated that, in terms of inherent resistance to long specular multipath, the L5 signal will significantly outperform its L1 counterpart (e.g. Braasch 1997, Betz 2002, Tran 2004). However, as underlined in Hegarty et al (2004a), true specular multipath rarely occurs in typical multipath environments. In these environments, short-delay multipaths are usually dominant and multiple multipaths frequently co-exist and interact. Under these conditions, Hegarty et al (2004a) showed that the performance of wide bandwidth signals (such as the L5 signal) do not provide significant improvements over narrow bandwidth signals (such as the C/A signal).

The impact of noise and multipath on carrier tracking accuracy depends primarily on the carrier wavelength (Ray 2005). To that end, a shorter wavelength improves the signal inherent mitigation capacity against noise and multipath. As previously mentioned, the L5 and L1 signals' wavelengths are 25 cm and 19 cm respectively. This implies that in terms of carrier tracking the C/A signal is more resistant to noise and multipath than its L5 counterpart.

The impact of dynamics on carrier tracking depends primarily on the order of the tracking loop used. In this regard, a tracking loop of order n is resistant to receiver to satellite LOS dynamics of order $n-1$ (Ward et al 2006).

2.4.4 Data Demodulation Sensitivity and Reliability

It is necessary to properly decode the navigation message in order to derive pseudorange measurements and calculate navigation solutions. Data demodulation performance is affected by: 1) post-correlation SNR, 2) carrier phase tracking sensitivity and reliability, and 3) navigation message encoding. As previously mentioned, the C/A navigation message has a data rate of 50 Hz. This relatively low rate, compared to a typical communication device, allows an acceptable *Bit Error Rate (*BER) for common SNR (Van Dierendonck 1997). However, the simple parity check algorithm implemented on the GPS C/A navigation message offers limited demodulation performance (Spilker 1997a).

Considering that the L5 and C/A navigation messages are broadcast with the same 50 Hz data rate, the L5 post-correlation SNR is reduced by approximately 6 dB when compared to its C/A code counterpart. This degradation results from a 3 dB loss entailed by the QPSK modulation (since the data channel is only allocated half of the total power) and another 3 dB loss due to the convolutional encoding (since the symbol bits only last 10 ms and therefore carry half the amount of power contained in a full data bit). However, the convolutional encoding can improve the BER by approximately 5 dB (Spilker & Van Dierendonck 2001) and therefore mostly compensate for this degradation.

Furthermore, pure PLL tracking is expected to improve the L5 carrier tracking sensitivity by approximately 6 dB; this improvement will translate in a direct increase of the L5 data demodulation sensitivity. Besides, Julien (2006) demonstrated that pure PLL tracking also reduces the occurrences of half and full cycle slips which significantly enhance the data demodulation reliability.

CHAPTER THREE: SIMULATION TOOLS

This chapter introduces the tools that will be used in the subsequent chapters to evaluate the L5 signal performance. Since this signal is not yet transmitted by GPS satellites, an L5 signal simulator is required. Similarly, few off-the-shelf GPS L5 receivers are currently available. In addition, the performance analysis enabled by commercial receivers is limited by two factors: 1) the algorithms they implement for signal processing (e.g. acquisition and tracking) and navigation solution condition their performance but are not typically available to users; and 2) their outputs are typically limited to the measurement and position domains. In light of the above, an L5 receiver is also needed. The goal is therefore to develop complimentary simulation tools that accurately model the generation and processing of the L5 signals at the *Intermediate Frequency* (IF) level. This chapter starts with a description of the various error sources involved in GPS positioning with particular emphasis on their impact on the signal processing functions of the receiver. The L5 hardware simulator is then introduced and its ability to model the various error sources previously described is thoroughly explored. Following this, the global architecture of the L5 software receiver developed in this thesis is discussed. Specifically, the operation which is at the core of signal processing, namely signal correlation, is discussed in details. Finally, the derivation of the necessary truth information is described and its accuracy assessed.

3.1 GPS Error Sources

Several errors play a role in GPS positioning. Each of these error sources is briefly discussed here. A more comprehensive overview of the GPS error budget can be found in Parkinson (1997b), Misra and Enge (2006) or Conley et al (2006).

3.1.1 Satellite Ephemeris Errors

Satellite ephemeris errors occur because the satellite position broadcast in the navigation message does not match the actual location of the satellite. The navigation message contains a set of ephemeris parameters that are used to predict the position of GPS satellites. To this end, the GPS orbits are modelled as purely elliptical Kepler orbits perturbed by various forces including non-spherical Earth gravitational harmonics, lunar and solar gravitational attraction and solar flux (Spilker 1997c). To provide a better fit, the parameters for this model are updated regularly, based on measurements made by several ground stations. In normal operation, the fit interval is four hours and the range errors resulting from ephemeris inaccuracy have a standard deviation of approximately 2.6 m (Lachapelle 2004), although this level of performance is improving on a continuous basis.

This accuracy quote is valid for current satellites broadcasting the legacy navigation message (NAV format); however, the new generations of GPS satellites (including the IIR-M satellites) will broadcast the modernized GPS civil signals and, therefore, the modernized navigation message (C-NAV format). This new message includes additional ephemeris parameters that should further improve the accuracy of the broadcast satellite positions. Unfortunately this message is not yet transmitted by any GPS satellites. The

IIR-M satellites currently in orbits are capable of modulating either navigation message on the L2C signal they transmit (IS-GPS-200D). However, as shown in (Muthuraman et al 2007), the L2C signal is currently broadcast without any navigation message. This implies that the accuracy of the modernized set of ephemeris parameters has not yet been assessed.

It is important to bear in mind that this kind of error will be seen by the receiver as a slowly varying bias in the LOS signals' propagation time. Olynik (2003) showed that the satellite orbital errors were strongly correlated (greater than 90%) over time intervals shorter than five minutes. However, in terms of signal processing, the main concern is a change in the signal characteristics during coherent integration times; or, in the case of tracking, during a period of time smaller than the tracking loop response. These time intervals typically range from a few milliseconds to less than one second. This implies that the ranging bias induced by a satellite ephemeris error will be estimated and tracked without error in the acquisition and tracking module respectively.

3.1.2 Satellite Clock Error

The satellite clock error is the difference between the true GPS time and the time maintained in a GPS satellite. The satellites use highly stable atomic clocks (e.g. rubidium or caesium). These clocks, however, are not perfect and drift with time. A typical value for this drift is 1 part in 10^{13} over a day, which is equivalent to approximately 10^{-8} s or 3.5 m. This drift, originating from a deviation of the oscillator from its nominal frequency, is often called the oscillator frequency noise. The ground stations closely monitor and estimate this deviation; in turn, a set of clock parameters is

included in the navigation message and can be used at the receiver end to correct the satellite time in the following way (Spilker 1997a)

$$
\begin{aligned}
T^{S}(t) &= t + \delta t^{S}(t) \\
\delta t^{S}(t) &= a_{f0} + a_{f1}(t - t_{oc}) + a_{f2}(t - t_{oc})^2 + \Delta t_r - T_{GD}
\end{aligned}
\tag{3-1}
$$

where t is the GPS time, $T^{S}(t)$ is the time maintained by the satellite and $\delta t^{S}(t)$ is the satellite clock error, a_{f0}, a_{f1}, a_{f2} are the zero, first and second order clock correction coefficients referred to time t_{oc} and expressed in s, s^{-1} and s^{-2} respectively, Δt_r is the relativistic correction term expressed in s and T_{GD} is the group delay expressed in s.

After corrections, the current range biases due to satellite clock errors have a standard deviation of approximately 7 ns, or equivalently 2.1 m (Lachapelle 2004).

It is interesting to note that satellite clock errors will again be seen by the receiver as slowly varying biases. Olynik (2003) showed that the satellite clock errors were strongly correlated (greater than 90%) over time intervals shorter than one minute. As mentioned before, this implies that ranging biases induced by satellite clock errors will be estimated and tracked without error.

3.1.3 Tropospheric Errors

Tropospheric errors occur when signals propagate through the layer of the atmosphere called troposphere. This neutral layer of the atmosphere extends up to about 70 km above the earth's surface and perturbs the signal's propagations by slowing the signals and bending their paths. The typical measurement error due to the tropospheric effect is around 2.4 m for a zenith satellite and can increase by a factor of about 10 for low elevation satellites (Skone 2005). The troposphere error is composed of a wet and dry

(hydrostatic) component. The dry component accounts for 80-90 % to the total error but can be predicted with an accuracy of about 1% at the zenith using meteorological data. The wet component accounts for only 10-20 % to the total error but can only be predicted with an accuracy of about 10-20 % using meteorological data.

Olynik (2003) showed that the tropospheric delay remains highly correlated (greater than 90 %) for time periods shorter than ten minutes. Unless exceptionally high tropospheric activity is encountered, the slow changes in tropospheric delay will be easily estimated and tracked in the receiver without bias.

3.1.4 Ionospheric Errors

Ionospheric errors occur when signals propagate through the layer of the atmosphere called ionosphere. This layer of the atmosphere extends approximately from 70 to 1000 km above the earth's surface and is composed of charged elements (i.e. ions and free electrons). These electrons directly impact the propagation of the GPS signals. They have an opposite effect on the code and carrier portion of the signal, namely they delay the code (i.e. the navigation message and the PRN sequence used to spread it) and advance the carrier by an equal amount. The presence of free electrons is closely related to solar radiation. Consequently, the magnitude of the ionospheric error is influenced by solar cycles and shows diurnal variations with maximum effects typically occurring at 1400 local time (Skone 2005). Another interesting characteristic of the ionosphere is that it is a dispersive medium that impacts signals differently based on their transmission frequency. More specifically, the range error induced by the ionosphere is proportional to

the squared inverse of the transmission frequency. This implies that the L2 and L5 signals are more adversely affected by ionospheric errors than the L1 signal.

Although large variations can be observed depending on receiver location and solar cycle, the typical measurement error due to the ionospheric effect is approximately 5 m for a zenith satellite broadcasting a signal at the L1 frequency and can increase by a factor of about 3 for low elevation satellites (Skone 2005). This translates to approximately 9 m for a zenith satellite broadcasting a signal at the L5 frequency.

Using its dispersive property, dual frequency users are able to correct the first order ionospheric error which comprises 99 % of the total delay (Skone 2005). In contrast, single frequency users can only correct for approximately half of the ionospheric error using the broadcast ionospheric correction parameters (Klobuchar 1997). For these users, the ionospheric error typically remains, even after correction, the dominant error. In light of the above, the interest of GPS modernization for civilian users becomes obvious.

In general, the ionospheric delay varies pretty smoothly; Olynik (2003) showed that, even during periods of high ionospheric activities, this delay remains highly correlated (greater than 90 %) for time periods shorter than five minutes. This again implies that the ionospheric delays will be interpreted as part of the propagation path during signal acquisition and tracking, and therefore will not induce additional errors at these stages. It is important to note however that sudden changes in ionospheric delays do occur. These sudden variations can happen during ionospheric storms or ionospheric scintillations and usually translate into sudden phase jumps and deep power fades (Skone 2005, Psiaki et al 2007). These very abrupt changes in the phase of the received signal can be assimilated to high dynamics and can potentially lead to loss of phase lock (Yu 2006).

3.1.5 Receiver Clock Error

Accurate time keeping is one of the fundamental principle and key requirement that GPS relies on to provide accurate measurements and positions. As previously mentioned this requirement is fulfilled, at the satellite end, by using highly stable atomic clocks and by providing corrections to GPS users when deviations from the nominal frequency are observed. At the receiver end, cost, size and power consumption restrictions generally prohibit the use of atomic clocks. The common approach is therefore to use a lower grade oscillator and to estimate its timing errors (e.g. bias and drift) as part of the navigation solution. Interestingly, the receiver's oscillator imperfections will also result in phase errors that may impair the proper processing, and in particular tracking, of the received signal.

The oscillator frequency noise can usually be modelled through three main components: namely *Random Walk* (RW), flicker and white frequency noise. The resulting noise PSD can be written as (Winkel 2003)

$$S_{Osc\_Noise}(f) = \frac{1}{2}\left(\frac{h_{-2}}{f^2} + \frac{h_{-1}}{f} + h_0\right) \tag{3-2}$$

where h_{-2}, h_{-1} and h_0 represent the random walk, flicker and white components of the frequency noise.

The associated timing error is usually characterized through its Allan variance. A detailed treatment of this characterization can be found in Allan et al (1997). In brief, the Allan variance represents half of the root mean square of the change in frequency error between two adjacent samples (Petovello & Lachapelle 2000). Winkel (2003) shows that the three

components of the oscillator frequency noise will have different impacts on the Allan variance of the oscillator

$$\sigma_A^2(\delta) = \frac{h_0}{2\delta} + 2\ln(2)h_{-1} + \frac{2\pi^2}{3}\delta h_{-2} \qquad \text{(3-3)}$$

where δ is the true time interval between the two adjacent samples.

Oscillators can be broadly categorized into two families: the quartz crystal and the atomic oscillators (Raquet 2004). In the former, the nominal oscillating frequency is obtained by stimulating a quartz disc with an electric field; as a result, this reference frequency is sensitive to temperature. In addition, three types of quartz oscillators can be defined depending on the level of protection they offer against frequency variations due to temperature changes: the pure *Crystal Oscillators* (XO) offer no mitigation against these frequency variations, the *Temperature Compensated Crystal Oscillators* (TCXO) use a sensor to determine the temperature and to compensate the oscillating frequency accordingly, and the *Oven Controlled Crystal Oscillators* (OCXO) keep the temperature-sensitive components in a stable oven at a temperature that does not affect the oscillator frequency. The atomic oscillators, on the other hand, use quantum physics properties to define their nominal oscillating frequency. Caesium and rubidium clocks are well known examples of atomic oscillators. Winkel (2003) gives a set of h_{-2}, h_{-1} and h_0 values to represent the five aforementioned types of oscillator. These values are shown in Table 3.1, and their corresponding Allan variances are plotted in Figure 3-1.

It is important to bear in mind that each oscillator is unique in its own category; the parameters shown here are just meant to convey the importance of oscillator quality and to illustrate their expected stability behaviour over various time intervals.

Table 3.1 – Parameters for a Set of Oscillators

	Oscillator Parameters		
	h_0 [s]	h_{-1}	h_{-2} [Hz]
Quartz	$2e^{-19}$	$7e^{-21}$	$2e^{-20}$
OCXO	$1e^{-21}$	$1e^{-20}$	$2e^{-20}$
TCXO	$8e^{-20}$	$2e^{-21}$	$4e^{-23}$
Caesium	$2e^{-20}$	$7e^{-24}$	$1e^{-29}$
Rubidium	$1e^{-19}$	$1e^{-25}$	$2e^{-23}$
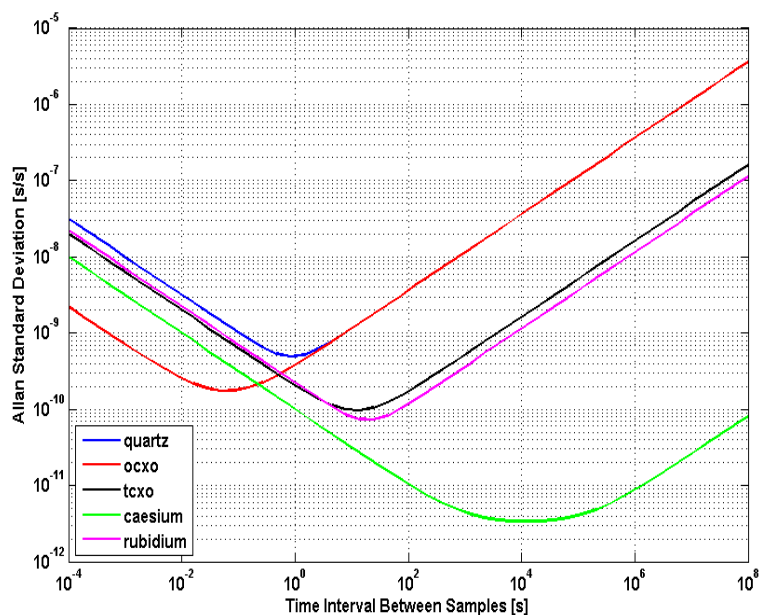
Figure 3-1 – Allan Standard Deviation for Quartz, TCXO, OCXO, Rubidium and Caesium Oscillators

As underlined in Raquet (2004), each type of oscillator comes with its specific tradeoffs (e.g. in terms of size, cost, power consumption and stability). Atomic clocks offer the best long term stability but are usually expensive, heavy and have high power

consumption. They are therefore well suited for GPS satellites where they can extend the interval over which the broadcast oscillator bias, drift and drift rate corrections are valid, and thereby limit the number of required uploads for these parameters. However, as illustrated in Julien (2005) and Watson (2005), atomic clocks are not necessarily ideal for receiver operations where short and medium term stabilities are of major interest (as they condition the efficiency of the coherent integration process); and low cost, weight and power consumption are often preferred.

Additional oscillator phase noise may arise due to vibrations caused by receiver motion. The vibration-induced phase errors are strongly related to the g-sensitivity of the oscillator. They are often referred to as external phase error, as opposed to internal phase error caused by inherent oscillator instabilities.

3.1.6 Thermal Noise and Interferences

Noise and interferences that spectrally overlap (and therefore obscure) the GPS signals will degrade the performance of GPS receivers. As opposed to noise, which is always present, interferences are generally intermittent. Being a spread spectrum system, GPS offers some inherent level of protection against interferences. Additionally, the impact of interferences on GPS signals will remain largely conditioned by their spectral characteristics. To this end, intentional and unintentional interferences are generally classified as either narrowband or wideband depending on the ratio of the interfering signal bandwidth to that of the GPS signals. Common interferences and their negative effects on GPS operations are reviewed hereafter.

Thermal Noise

Thermal noise corresponds to the ambient noise present at the receiver antenna. It is assumed to be AWGN, with a PSD equal to

$$N_0 = K_B . T_{Sys} \qquad\qquad\qquad (3\text{-}4)$$

with the system noise temperature given by

$$T_{Sys} = T_{Sky} + T_R \qquad\qquad\qquad (3\text{-}5)$$

where K_B is the Boltzman constant with value $1.38e^{-23} W/K/Hz$, T_{Sky} is the sky noise temperature with value $100K$ (for aviation applications), and T_R is the receiver temperature defined through the Friis formula as a function of frontend architecture and ambient temperature (Van Dierendonck 1997).

As previously mentioned -205 dBW/Hz and -200 dBW/Hz are typical values for N_0 at the L1 and L5 frequencies respectively and are used throughout this dissertation.

Narrowband Interference

Narrowband interference is generally a man-made RF signal with some narrower bandwidth than the GPS signal of interest. It is largely rejected by GPS processing as the signal is spread across a wide bandwidth, making it appear as a weak near-white noise. The spreading operation also reduces the power carried by each spectral line. For the C/A signal, this reduction is at least 18.3 dB, with the average reduction close to 30 dB (Spilker 1997b). As previously mentioned, the use of a secondary code enhances the inherent narrowband interference mitigation capacities of the L5 signal by 10 dB and

13 dB on the data and pilot channels, respectively. Besides, owing to its fast chipping rate, the L5 PSD is ten times wider than its L1 C/A counterpart further reducing the impact of narrowband interferences of the L5 signal.

However the narrowband interference environment is more severe on L5 than on L1 as aeronautical signals such as the DME/TACAN or JTIDS/MIDS are transmitted in the L5 band. Their impact on the L5 signal is thoroughly studied in Bastide (2004).

Wideband Interference

One common source of wideband interference is other GNSS signals transmitted at the same frequency. In this regard, intra-system interference refers to GNSS signals transmitted from a different GPS *Space Vehicle* (SV), while inter-system interference refers to GNSS signals broadcasted from satellite pertaining to a different GNSS constellation (e.g. Galileo or GLONASS). To limit the impact of intra- and inter-system interference, efforts are made to carefully select the GNSS signals' spreading codes and modulation. In particular, Ries et al (2002) highlights the importance of carefully designing the Galileo E5a spreading codes to ensure good interference protection against the GPS L5 signals. Similarly Betz (2002) underlines the interesting spectral separation properties of BOC modulated signals.

3.1.7 Multipath

Multipath is the phenomenon whereby a GPS signal is reflected or diffracted from various objects and therefore arrives at the receiver antenna via multiple paths (Braasch 1997). It can be either diffuse or specular. Specular multipath originates from reflection

over large and smooth surface. Specular multipath is usually stable and relatively easy to model using the Snell's laws of reflection (Snellius 1621). An example of such multipath is given in Figure 3-2.
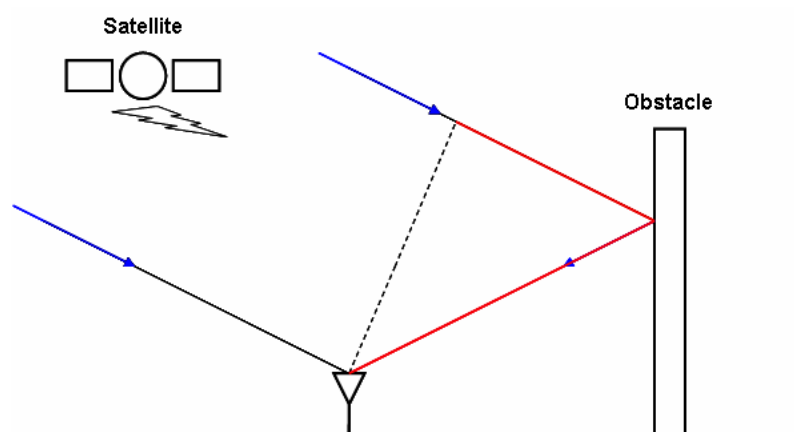
Figure 3-2 – Excess Propagation Length on Non Line-of-Sight (NLOS) Paths

Diffuse multipath, on the other hand, happens when the incoming signal is reflected in many directions by a rough surface. The roughness of a surface can be determined using the Rayleigh criterion (which compares the mean size of the surface's irregularities with the signal wavelength). Generally, diffuse multipath is less stable and more difficult to model than its specular counterpart.

In general, the nature of the reflective surface will greatly impact the multipath delay, phase and amplitude. This, in turns, will condition the overall effect of the multipath as it recombines with the LOS signal and/or other multipath signals. The effect of multipath on the incoming signal's code, carrier and amplitude is thoroughly described in Ray (1998), while its effect on the incoming signal's Doppler is discussed in Watson (2005).

At the signal processing level, the correlation is a linear process and as a consequence, the correlation between the incoming signals (direct and reflected) and the local code and carrier replicas will be the sum of the individual correlations. The superposition of the direct and reflected signals' correlation with the local code replicas is illustrated in Figure 3-3 for various delays and various *Signal to Multipath power Ratios* (SMRs).
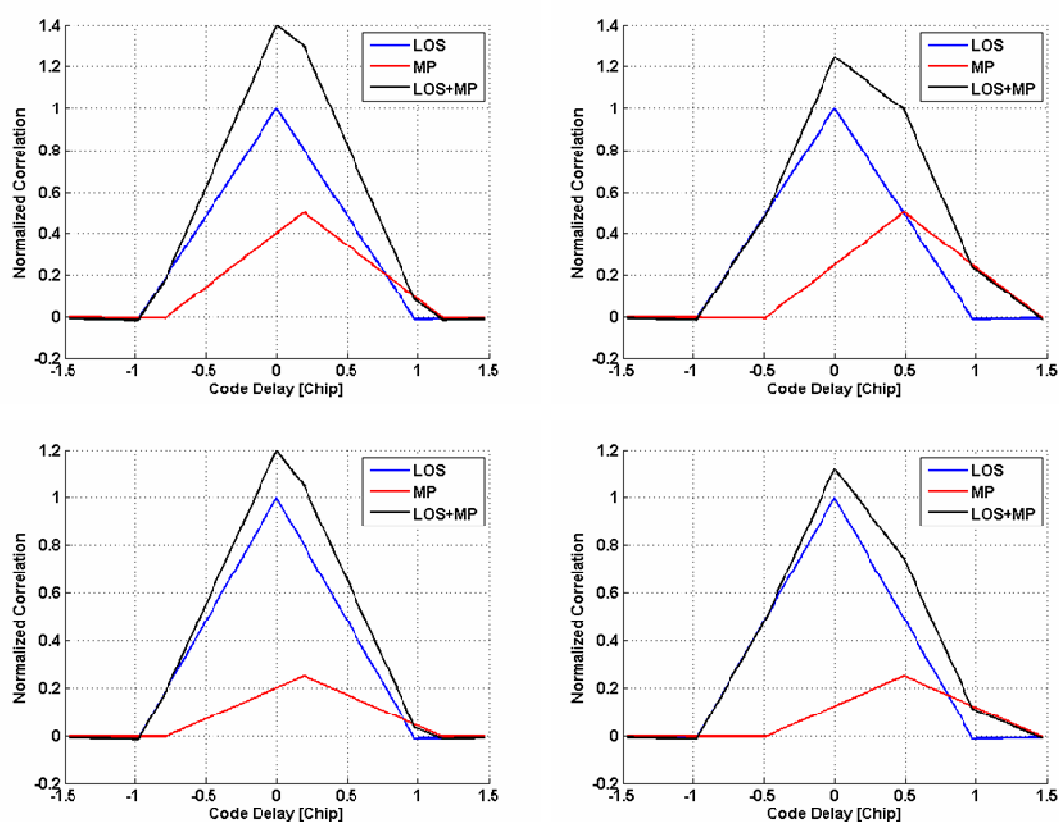
Figure 3-3 – Impact on the Normalized L5 Correlation Function of In-phase Multipaths with 0.2 (Left) and 0.5 (Right) chip delay and for a 6 dB (Top) and 12 dB (Bottom) SMR

This figure shows that the distortion of the resulting correlation peak depends upon 1) the width of the correlation function, 2) the multipath delay, 3) the multipath amplitude and 4) the relative phase of the direct and reflected signals. These distortions can translate in a

displacement of the correlation main peak and/or a modification of the correlation slopes. As will be seen in Chapter 5, these distortions will impact the code tracking accuracy. Similarly, the phasor of the direct, reflected and composite signals after correlation with the local carrier replicas is illustrated in Figure 3-4. This figure shows that the phase error is bounded to a quarter of a wavelength.
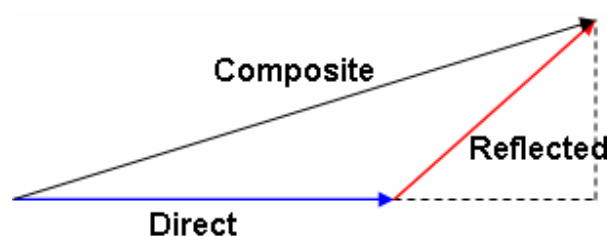
Figure 3-4 – Phasor Diagram of Direct, Reflected and Composite Signals

Now that the major GPS error sources have been presented, their implementation in the Spirent hardware simulator (and, more generally, in the L5 IF samples data collection set-up) can be discussed.

3.2 GPS L5 Hardware Simulator Realization

A Spirent GSS 7700 hardware simulator is used herein. Although this simulator is capable of outputting L1, L2C and L5 signals at the RF level, only the L5 data is simulated here. The L5 RF signal is simulated based on the input simulation parameters (e.g. location, time and atmospheric conditions) chosen by the user. It is computed as the sum of the signals broadcast by all the satellites in view plus some thermal noise. The

next subsections describe how the satellite constellation is obtained, and how individual L5 signals are modeled.

3.2.1 Satellite Constellation

The GPS constellation can be based on either a broadcast ephemeris or a broadcast almanac file. These files can be downloaded, for example, from the *Crustal Dynamics Data Information System* (CDDIS) institute website. Using this information, the true GPS satellite location can be determined at any given time. Based on the specified receiver location and simulation time, satellites situated below the user's horizon are discarded. Additionally, the user can decide to reject more satellites (e.g. include the effect of an elevation mask or to exclude a particular satellite) to study the impact of satellite geometry on position reliability and accuracy. It is also possible to simulate a kinematic receiver; to this end, a wide range of dynamics can be simulated to mimic various types of motion including that of cars, boats or planes. Once the satellites in view are selected and their position relative to the receiver computed, the transmitted signals have to be modeled for each satellite.

3.2.2 GPS L5 Signals Modeling

The L5 RF signals are modulated following the L5 signal interface control document (IS-GPS-705). The structure of the received L5 signals is therefore similar to Equation 2.9. However, the user can vary some parameters including the broadcast signal power and navigation message as well as the propagation delays and Doppler effects.

Signal Power

The signal power for individual satellites is user selectable. It can be chosen to reflect physical phenomenon (e.g. power attenuation over the propagation path or specific antenna gain pattern) or set arbitrarily to quantify the effect of various SNRs on receiver performance.

Navigation Message

The navigation message is reconstructed based on the input ephemeris file. Unless otherwise specified by the user, the broadcast ephemeris message perfectly matches the simulated GPS constellation. As discussed in the previous section the satellite-induced errors (including ephemeris and clock errors) result in a slowly varying ranging bias that does not have a significant impact on the signal processing functions of the receiver. Consequently, these errors are not simulated herein.

Propagation Delay and Doppler Effects

The propagation delay and Doppler effects are computed to include the effect of user-satellite geometry (i.e. the true geometric range and range rate) plus any other error sources specified by the user. In particular, it is possible to include the effect of atmospheric errors. As with the satellite-induced errors, the atmospheric errors result in a slowly varying ranging bias that does not have a significant impact on the signal processing functions of the receiver. Consequently atmospheric errors are not simulated herein.

It was previously mentioned that ionospheric scintillations can affect signal acquisition and tracking. However, ionospheric scintillation being a particularly difficult phenomenon to model, the Spirent simulator does not offer the option to model it.

Multipath

Many attempts have been made to characterize multipath in different environments (Jahn et al 1996, Brenner et al 1998, Dottling et al 2001, Lachapelle et al 2004, Hu et al 2007). They tend to show that the impact of multipath in the GPS propagation channel can be divided into near and far echoes; the former represent diffuse multipath and the later correspond to specular multipath. The Spirent simulator offers several options to model both.

In terms of specular multipath, it is possible to simulate signals reflected from the ground or from a vertical object with user selectable attenuation coefficient. Since the hardware simulator can only generate twelve RF signals (including LOS and reflected signals) at the L5 frequency, the user must specify, in both cases, which satellites will be affected by such reflections.

In terms of diffuse multipath, it is possible to use a more complex model based on an elevation-azimuth category mask editor. In this model, arrival angle is resolved into satellite elevation and azimuth in 5-degree increments for positive elevation only; and each bin is defined as belonging to one of the four categories: 1) obstruction, 2) LOS only, 3) LOS + echoes, and 4) echoes only. While obstructed signals are not simulated, LOS and echoes signals suffer Rician and modified Rayleigh fading respectively (Klukas et al 2003). The default elevation-azimuth category mask editor for urban environments

is shown in Figure 3-5. Models are also available for suburban environments and forest canopies.
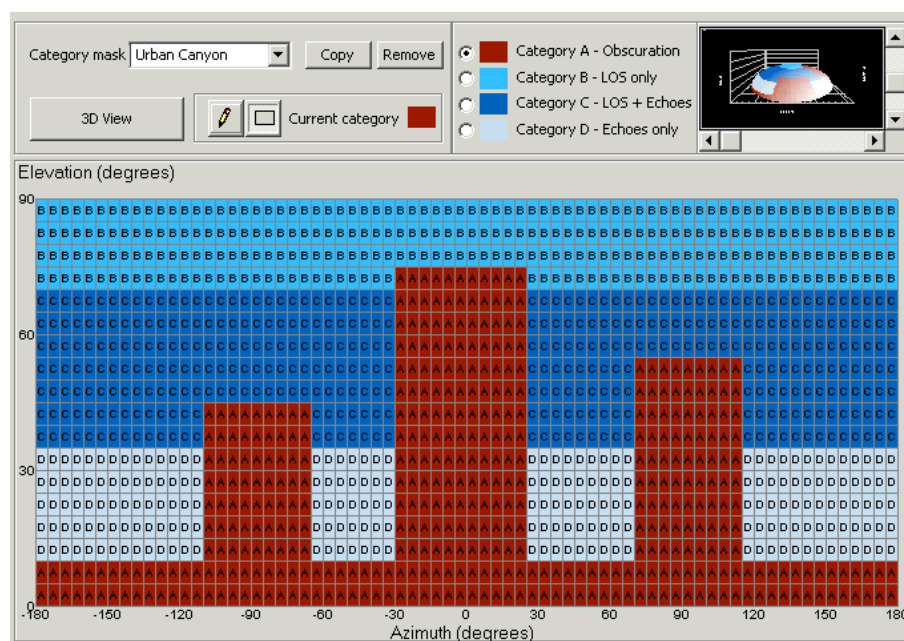
Figure 3-5 – Default Elevation-Azimuth Category Mask Editor for Urban Environments

Examples of Rician distribution are shown in Figure 3-6. The Rician and modified Rayleigh models used to describe the delay and power spread characteristics of multipath signals are based on some key assumptions (Watson 2005). For both models, a large number of NLOS components are presumed to be received with unknown amplitude and random phases. Using the central limit theorem (Walpole et al 1998), the NLOS components can be assumed to recombine into a composite signal with normally distributed amplitude and uniformly distributed phase. This condition should be valid for GPS signals as long as multiple NLOS signals do exist and NLOS conditions are not changing quickly over time. The second key assumption behind the Rician model is that

the LOS signal power is strong and constant. This assumption should be valid for GPS signals as long as they originate from high elevation satellites and do not propagate through building materials.
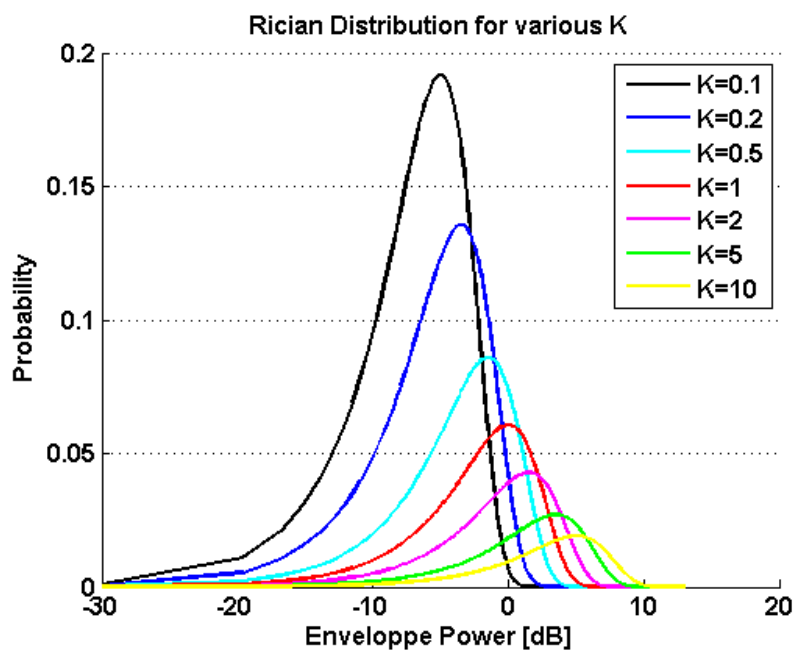
Figure 3-6 – Rician Power Probability Envelopes

Finally, the Spirent simulator also offers a means of introducing controlled multipath errors into the simulation using pseudorange ramps. Using such ramps, the user can artificially increase the simulated geometric range from the receiver to any given satellite thereby creating a perfect echo-only signal.

3.2.3 Data Collection System

As previously stated, the goal was to develop a tool that would accurately simulate the L5 signal generation at the IF level. The Spirent simulator however provides RF signals at

the L5 frequency. These signals are down-converted (and sampled) using the data collection setup shown in Figure 3-7.
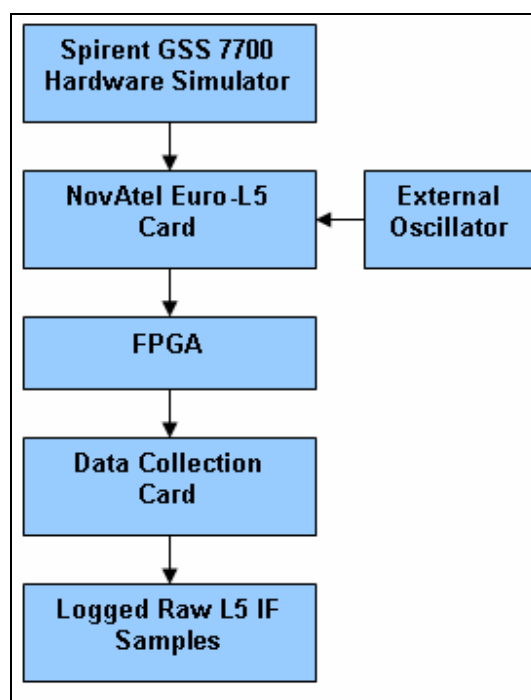
Figure 3-7 – Data Collection Set-Up

The RF signal from the simulator is passed to a NovAtel Euro-L5 card that acts as the frontend to the software receiver (the NovAtel card is also a four-channel GPS L5 receiver). L5 samples are tapped at a rate of 56 MHz using 2-bit quantization. These samples are then repackaged into a more compact format using an FPGA card before being passed to the data acquisition card. This card then stores the samples into files for later processing. In addition, an external oscillator can be used to drive the NovAtel card. This, in turn, can be used to assess the impact of various oscillator grades on receiver performance.

The IF samples thereby obtained can then be processed, in post-mission, by the IF software receiver described hereinafter.

3.3 GPS L5 IF Software Receiver

The L5 IF software receiver developed herein uses the general structure of an L1 version developed earlier in the PLAN group by Ma et al (2004). A more advanced software called GSNRx^{TM} and developed subsequently (Petovello & Lachapelle 2006, Petovello et al 2007) was not available for use in this work. The structural differences between the GPS L1 and L5 signals were highlighted in Chapter 2. Implementation of the L5 acquisition, tracking and data demodulation algorithms developed herein in a software receiver represents a significant part of this thesis, and is described in Mongrédien et al (2007a). Specifically, a new acquisition module was developed to enable the sequential acquisition of the PRN and NH code delays, some data/pilot combining and also the introduction of an intermediate tracking step. The tracking module was extensively modified to allow some data/pilot combining and to include the Kalman filter-based tracking option. A new data demodulation module was also required to accommodate the format of the L5 navigation message; in particular, a new subframe synchronization algorithm and a Viterbi Decoder had to be developed. As a final note, the software, written in C/C++, was not optimized to operate in real-time as this was not necessary to meet the objectives of this thesis.

3.3.1 Global Receiver Architecture

The general architecture of a GPS receiver is shown in Figure 3-8.
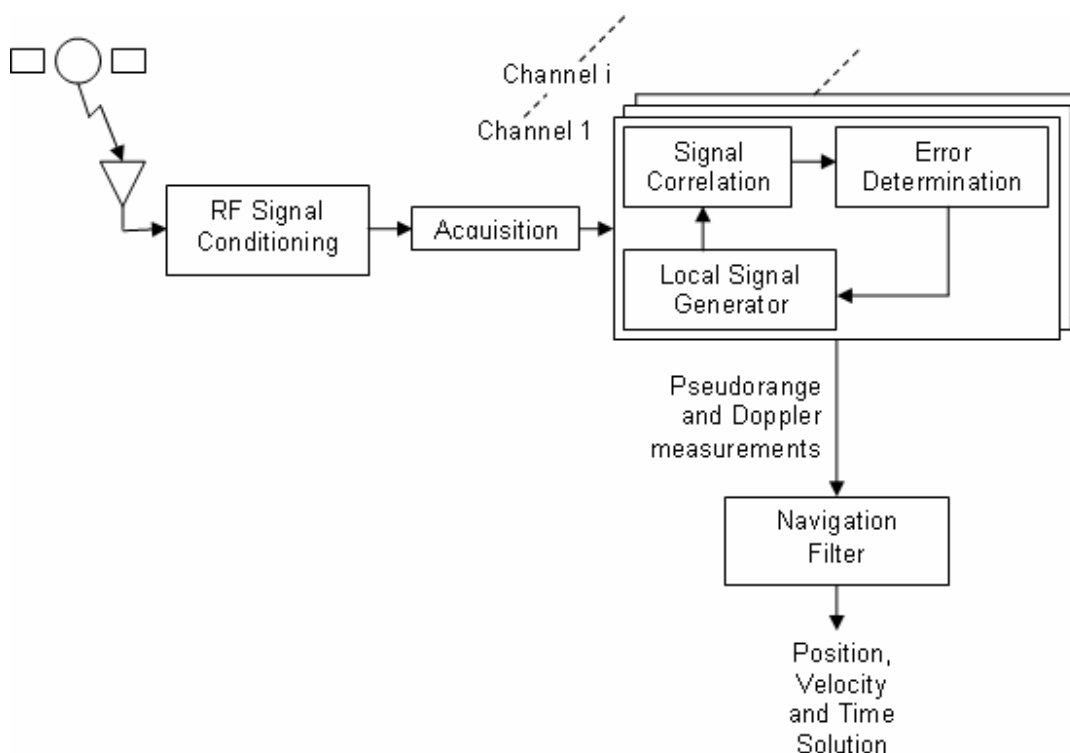
Figure 3-8 – High level block Diagram of a GPS receiver

The three main functions of a GPS receiver are: 1) RF signal conditioning, 2) signal processing and 3) navigation processing. RF signal conditioning comprises frontend filtering, signal down-conversion, sampling and quantization. As mentioned in the previous section, the RF signal part is performed by the frontend of the NovAtel Euro-L5 card. The signal and navigation processing parts are performed in software; their implementation is described in the next subsections.

3.3.2 Signal Processing

The signal processing part includes acquisition, tracking and data demodulation and relies on one key operation: the signal correlation.

Correlation

In its strict definition, correlation is the process of multiplying the incoming signal with the locally generated replica of the received spreading sequence and accumulating the result. In addition to the effects of external disturbances (such as noise or multipath) and frontend filtering (that limits the incoming signal spectrum), the correlation process is greatly affected by the presence of a carrier. For this reason, the correlation process presented herein also includes the frequency removal process. Frequency removal, or carrier wipe-off, is performed by multiplying incoming signal with the locally generated replica of the received carrier. It is important to note that, since the L5 signal uses a QPSK modulation, the correlation process has to be performed on both data and pilot channels.

The L5 correlation process, as it is performed on the data channel, is illustrated in Figure 3-9, although not accounting for the sampling and quantization effects. The incoming signal (given in Equation 2.9) is filtered and down-converted to the IF frequency by the front-end filter. Realizable front-end filters have some amplitude roll-off, however for theoretical purposes only "brick-wall" filters with linear phase response will be considered. These filters reject all out-of-band frequencies, pass all in-band frequencies with no magnitude adjustment, and have a linear phase response within the passband, introducing no distortion.
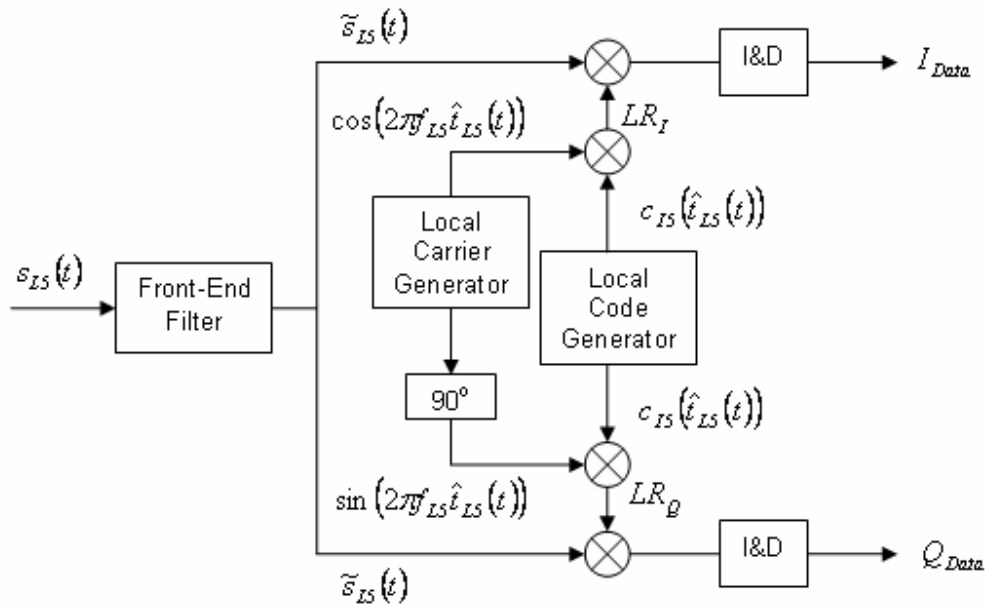
Figure 3-9 - Schematic Representation of I5 Correlation Process

Following this, the receiver generates local in-phase and quadra-phase replicas of the incoming signal that can be modelled as

$$LR_I = c_{L5}\left(\hat{t}_{L5}(t)\right)NH_{10}\left(\hat{t}_{L5}(t)\right)\cos\left(2\pi f_{IF}\hat{t}_{L5}(t)\right) \tag{3-6}$$

$$LR_Q = c_{I5}\left(\hat{t}_{L5}(t)\right)NH_{10}\left(\hat{t}_{L5}(t)\right)\sin\left(2\pi f_{IF}\hat{t}_{L5}(t)\right) \tag{3-7}$$

where $\hat{t}_{L5}(t) = (1+\hat{\eta})t - \hat{\tau}_{L5}$ is the receiver's estimation of the time delay and Doppler shift experienced by the signal during its propagation from the satellite to the receiver.

The (filtered) incoming signal is then multiplied by these replicas, and the resulting products passed through an *Integrate and Dump* (I&D) filter that performs the correlation. Although effectively performed as a summation, this operation can be modeled as (Van Dierendonck 1997)

$$I = \frac{1}{T}\int_0^{T_I} \tilde{s}_{L5}(t).LR_I(t)dt \tag{3-8}$$

$$Q = \frac{1}{T}\int_0^{T_I} \tilde{s}_{L5}(t).LR_Q(t)dt \tag{3-9}$$

where T_I is the coherent integration time and $\tilde{\bullet}$ represents the filtering operation by the front-end filter.

It is assumed that the difference between the received signal phase $\left(2\pi f_{IF} t_{L5}(t)\right)$ and the locally generated carrier phase $\left(2\pi f_{IF} \hat{t}_{L5}(t)\right)$ can be written as $2\pi \delta f t + \delta\phi$, where the frequency error δf and the phase error $\delta\phi$ remains constant over the integration interval. Similarly, it is assumed that the difference between the received and locally generated code phases can be written as $\delta\tau$, where the code delay error remains constant over the integration interval. Finally, assuming that the receiver front-end filter (with impulse response $h(t)$) has a one-sided bandwidth of B Hz, and that the correlation process does not straddle any data bit transition, the in-phase I and quadra-phase Q correlation values on the data channel can be approximated as (Holmes 2000)

$$I_{Data} = \frac{\sqrt{P}}{2} D_d \tilde{R}(\delta\tau)\frac{\sin(\pi\delta f T_I)}{\pi\delta f T_I}\cos(\delta\phi) + n_{I,Data} \tag{3-10}$$

$$Q_{Data} = \frac{\sqrt{P}}{2} D_d \tilde{R}(\delta\tau)\frac{\sin(\pi\delta f T_I)}{\pi\delta f T_I}\sin(\delta\phi) + n_{Q,Data} \tag{3-11}$$

and, the in-phase I and quadra-phase Q correlation values on the pilot channel can be approximated as (ibid)

$$I_{Pilot} = \frac{\sqrt{P}}{2}\tilde{R}(\delta\tau)\frac{\sin(\pi\delta f T_I)}{\pi\delta f T_I}\cos(\delta\phi) + n_{I,Pilot} \tag{3-12}$$

$$Q_{Pilot} = \frac{\sqrt{P}}{2}\tilde{R}(\delta\tau)\frac{\sin(\pi\delta f T_I)}{\pi\delta f T_I}\sin(\delta\phi) + n_{Q,Pilot} \tag{3-13}$$

where D_d is the sign of the navigation symbol bit, $\tilde{R}(x) = \int_{-B}^{B} G_{L5}(f)H(f)e^{-i.2\pi.f.x}df$ is the correlation of the filtered incoming spreading code with the locally generated code, H the Fourier transform of the frontend filter impulse response and $n_{I,Data}$, $n_{Q,Data}$, $n_{I,Pilot}$, $n_{Q,Pilot}$ are independent Gaussian noises with equal power.

Modelling the I&D filter as a simple integrator with equivalent one-sided rectangular bandwidth $1/2T_I$, Blanchard (1975) demonstrated that the noise components have the following power and auto-correlation function

$$P_n = \frac{N_0\tilde{R}(0)}{4T_I} \tag{3-14}$$

$$R_n(x) = \frac{N_0\tilde{R}(x)}{4T_I} \tag{3-15}$$

where $N_0/2$ is the incoming noise PSD.

Assuming perfect carrier wipe-off, the post-correlation SNR, on the in-phase component, is given by

$$SNR_{post} = \frac{2PT_I\tilde{R}^2(\delta\tau)}{N_0\tilde{R}(0)}. \tag{3-16}$$

Considering that the pre-correlation SNR, defined with the signal used before the correlation (and after front-end filtering) is given by

$$SNR_{pre} = \frac{P\widetilde{R}(0)}{N_0 B}$$

(3-17)

where $\widetilde{R}(0)$ can be seen as the power loss due to front-end filtering, the correlation gain G, defined as the ratio between the post- and pre-correlation SNRs, is given by

$$G = \frac{SNR_{post}}{SNR_{pre}} = \frac{2BT_I \widetilde{R}^2(\delta\tau)}{\widetilde{R}^2(0)}$$

(3-18)

which, assuming perfect code delay estimation, can be simplified as

$$G = 2BT_I.$$

(3-19)

Several conclusions can be drawn from the results shown above. First of all, it is easy to see from Equation 3.10 that, assuming all the parameters are accurately estimated, the navigation symbol bit sign fully appears on the data channel in-phase correlator output I_{Data}. The ability to accurately extract the navigation symbol bit is therefore conditioned by the post-correlation SNR given in Equation 3.16. It is clear that, as long as they do not straddle symbol bit boundaries, longer coherent integration times will increase the post-correlation SNR and ease the symbol bit sign determination. While a symbol bit sign transition does not occur every 10 ms, there is a potential for a transition. Consequently, coherent integrations on the data channel are limited to 10 ms. This problem, however, is alleviated on the pilot channel where no unknown data bit transitions occur.

The second limitation to increasing the correlation gain is due to the frequency mismatch between the local carrier replica and the incoming signal. As illustrated in Equations 3.10

and 3.11, frequency error attenuates the correlator outputs' amplitude according to a sinc function. The equivalent power attenuation therefore follows a sinc-squared function often termed the frequency power roll-off function. The power roll-off function is illustrated in Figure 3-10. This figure shows that the location of the first null of this function is determined by the coherent integration time T_I according to $f_{null} = 1/T_I$. This relation essentially describes the fact that a 1 Hz error over 1 s causes a 2π phase change between the incoming signal and the local carrier replica, negating all energy received. A frequency error of approximately 44% of the coherent integration time will attenuate the post-correlation SNR by approximately 3 dB.
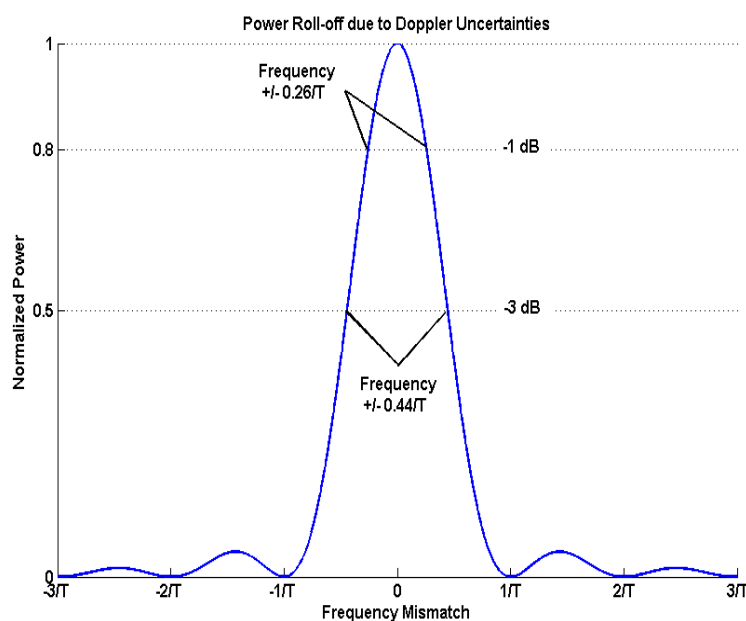
Figure 3-10 – Frequency Power Roll-off Function

The choice of the front-end filter will also play a role in the amount of signal power processed in the receiver since a narrow filter will cut out the secondary lobes of the

received signal spectrum. In the case of L5, the signal's main lobe occupies most of the allocated L5 frequency band. As shown in Van Dierendonck (1997), for a filter that would pass the signal's main lobe only (i.e. 2B = 20.46 MHz), the signal power loss would be 0.45 dB.

As shown in Figure 3-11, the filter also has an impact on the shape of the auto-correlation function. In particular, it can be seen that a narrow frontend filter (FE) bandwidth will tend to round off its main peak. This, in turn, will have an impact on the design of the receiver code tracking loop. This issue will be further addressed in Chapters 5 and 6.
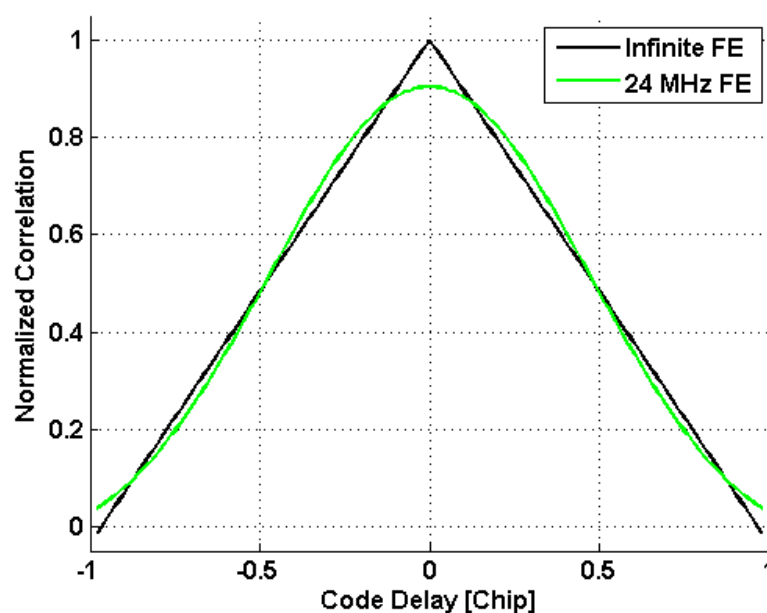
Figure 3-11 – Impact of the Frontend Filter Bandwidth on the Shape of the L5 PRN Auto-correlation Function

Acquisition

The software receiver first passes the IF samples into its acquisition module. The fundamental objectives of a receiver during signal acquisition are: 1) to determine which

satellites are visible, and 2) for each visible satellite, to calculate a coarse estimate of the received signal's code delay and Doppler frequency. Various implementations of the L5 signals' acquisition will be described and tested in Chapter 4.

Tracking

Upon successful signal acquisition, the IF samples are fed to the tracking module. This module consists of several channels (typically one for each satellite) tracking in parallel. The main objective of a receiver during signal tracking is to generate local replicas (consisting of a local spreading code and a local carrier) that match the incoming signals as closely as possible in order to perform, for each channel, effective code and carrier wipe-off and reliable navigation data bit decoding. The basic architecture of a single-channel tracking loop is also shown in Figure 3-8.

The samples are first passed through the correlation function. After accumulation, the correlator outputs are passed to an error estimation function that tries to accurately determine the errors in the code and carrier phase alignment. These estimates are then used, in a feedback loop, to update the code and carrier NCO and drive the local signal generation for the next epoch. Various implementations of the tracking error estimation function are possible. Two of them will be thoroughly described and compared in Chapters 5 and 6. *Constant Bandwidth* (CB) tracking is composed of a set of two or three tracking loops: a *Delay Lock Loop* (DLL) that tracks the spreading code delay, a *Phase Lock Loop* (PLL) that tracks the carrier phase and/or a *Frequency Lock Loop* (FLL) that tracks the Doppler frequency. *Kalman Filter* (KF) tracking on the other hand is composed

of a unique filter that jointly estimates the code delay, carrier phase and Doppler frequency of the received signals.

When a satellite is being tracked, it is important to know how well it is being tracked to ensure that the pseudorange, Doppler and carrier phase measurements passed to the navigation filter are reliable and accurate. This function is performed by the so-called lock detectors. The detectors used to confirm code, frequency and carrier lock are described in Appendix A.

Data Demodulation

The L5 navigation message decoding is done in three steps: 1) symbol bit sign recovery, 2) Viterbi Decoding, and 3) subframe synchronization.

Symbol bit recovery is performed herein using hard data bit decision (i.e. the symbol bit sign is set to one when the in-phase data prompt correlator output is positive). As an example, the in-phase data prompt correlator output probability distribution function of a high signal power satellite (approximated C/N_0 close to 50 dB-Hz) is shown in Figure 3-12. While in this case the distributions for positive and negative symbol bits are clearly separated, these distributions will tend to overlap when the incoming signal power decreases. Such overlaps can lead to unreliable symbol bit recovery and, ultimately, jeopardize the reliability of the predicted satellite position.

Viterbi Decoding of the L5 symbol bit stream is performed continuously (i.e. across subframe boundaries) using a five constraint length decoder. The implementation of Viterbi decoders is well documented (Forney 1973). However, two particular aspects of the decoder implemented herein require further explanation. First, the L5 data and

symbol bit boundaries are perfectly synchronized with those of the NH_{10} and NH_{20} sequences respectively (IS-GPS-705); this, in turn, can be used to initialize the decoder on the correct symbol bit. Second, the use of a Viterbi decoder introduces a delay that is a function of this decoder's constraint length. The 68 symbol bits delay introduced by the decoder used herein must be accounted for when determining the signal reception time.
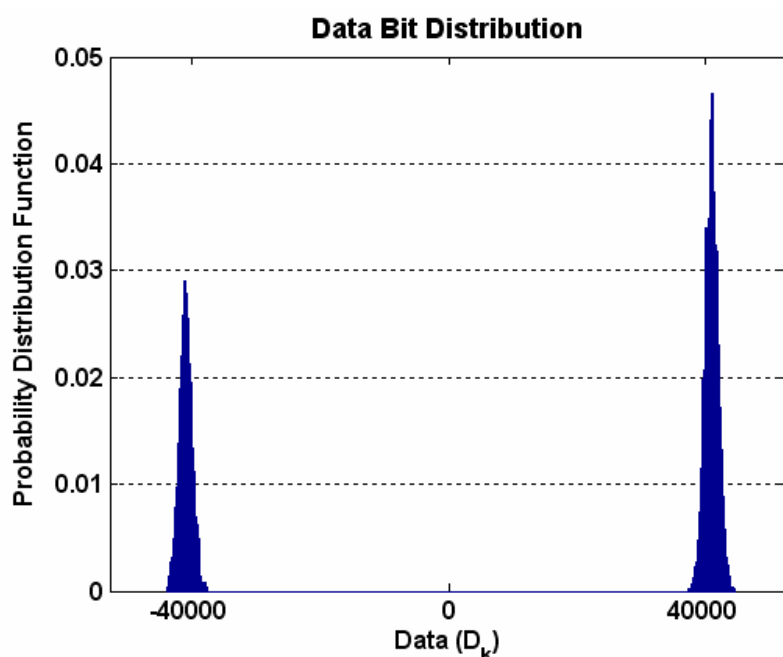
Figure 3-12 - Symbol Bit Probability Distribution Function

Subframe Synchronization relies on the successive detection of the following features: 1) preamble, 2) PRN number, 3) Z-count, and 4) cyclic redundancy check. Once the preamble is detected in the data stream, the synchronization algorithm checks that PRN number corresponds to the PRN of the satellite being tracked, that the Z-count is increasing by one from one subframe to the next, and that the parity of the subframe is correct. If any of these checks fail, the algorithm is reset to preamble detection. Once synchronization is confirmed, the navigation parameters can be read.

3.3.3 Navigation Processing

Position and velocity estimates are computed by the navigation processor using the raw pseudoranges, Doppler measurements and navigation bit stream provided by the signal processor. Using the raw data bit stream, the navigation processor can determine the satellite position, velocity and clock errors at the signal transmission time. Combining that information with the estimated satellite-receiver ranges and range rates provided by the receiver tracking loops, the navigation processor can derive final position and velocity estimates using least-squares or Kalman filtering (Axelrad & Brown 1997).

It is important to note that the natural measurements of a receiver tracking loops are not the pseudorange or Doppler measurements used in the navigation filter but rather the local code and carrier replicas used in the correlation function. Appendix B describes how the former can be obtained from the latter. Besides, the measurements made from the tracking loops, obtained with respect to receiver time, are affected by the local oscillator bias and drift. However, since the receiver clock errors are common to all the tracking channels, it is usual to consider the receiver clock bias and drift as unknowns in the navigation filter in addition to the three-dimensional user position and velocity.

Although Kalman filtering has been shown to enable accuracy gain under kinematic conditions and to provide smoother navigation solutions, a *Least-Squares Adjustment* (LSA) is used herein to obtain raw epoch-by-epoch navigation solutions which facilitate performance analysis. It uses pseudorange measurement to estimate the user position and receiver clock bias; similarly, it uses Doppler measurements to estimate the user velocity and receiver clock drift.

Least-Squares Adjustment (LSA)

The LSA process is a commonly used and well-known estimation technique. For the sake of clarity, the following discussion, based on Gelb (1974), reviews some of the important concepts.

GPS position (and velocity) computation is a parametric estimation problem where the measurement (observation) vector z relates to the unknown parameter (state) vector x as follows

$$z_k = H_k x_k + v_k \tag{3-20}$$

where the subscript k represents a quantity at the k$^{\text{th}}$ epoch, H is the design matrix which contains the "geometry" of the observation vector relative to the state vector and v is the measurement noise vector.

The least-squares solution $\hat{x}_k$ is found by minimizing the weighted sum of the squares of deviations $(z_k - H_k \hat{x}_k)$ given by (Gelb 1974)

$$J_k = (z_k - H_k \hat{x}_k)^T W_k^{-1} (z_k - H_k \hat{x}_k) \tag{3-21}$$

where J is the cost function to minimize, and W is the weighting function.

The solution, obtained by setting the derivation of Equation 3.21 (with respect to $\hat{x}_k$) to zero, and solving for $\hat{x}_k$ is given as (ibid)

$$\hat{x}_k = \left(H_k^T W_k^{-1} H_k\right)^{-1} H_k^T W_k^{-1} z_k \tag{3-22}$$

with estimated covariance

$$C_{\hat{x}k} = \left(H_k^T W_k^{-1} H_k\right)^{-1} \left(H_k^T W_k^{-1} C_{zk} W_k^{-1} H_k\right) \left(H_k^T W_k^{-1} H_k\right)^{-1} \tag{3-23}$$

where the superscript "-1" and "T" represent the matrix inverse and transpose operator respectively, and C is the covariance of the subscripted quantity.

To obtain the minimum variance for the estimated parameter, let $W_k = C_{Zk}$ so that Equations 3.22 and 3.23 reduce to

$$\hat{x}_k = \left(H_k^T C_{zk}^{-1} H_k \right)^{-1} H_k^T C_{zk}^{-1} z_k \qquad \textbf{(3-24)}$$

$$C_{\hat{x}k} = \left(H_k^T C_{zk}^{-1} H_k \right)^{-1}. \qquad \textbf{(3-25)}$$

Once the estimated state vector is obtained, the residual vector r can be computed as the difference between the actual observation and the predicted state

$$r_k = z_k - H_k \hat{x}_k. \qquad \textbf{(3-26)}$$

The residual vector indicates the extent to which the measurement model fits the actual data, and degree with which the measurements agree with each other.

Note that the navigation filter implemented herein uses a unique value for the variance of pseudorange and pseudorange rate measurements across all the visible satellites. Consequently the measurement covariance matrix is diagonal.

Now that the L5 generation and processing simulation tools have been reviewed, the generation of the truth data necessary for L5 performance analysis can be discussed.

3.4 Truth Determination

Generation of the truth data is accomplished by the hardware simulator that outputs receiver and satellite information files. In particular, the receiver file includes the simulated receiver position and velocity. Similarly, the satellite file contains the

simulated satellite position and velocity. The satellite file also includes and the simulated receiver-satellite range, pseudorange and Doppler.

To determine the tracking accuracy, the following approach is taken. Using the known receiver position and the computed satellite position, true pseudoranges are calculated for each satellite. True Doppler measurements are obtained in a similar fashion using the receiver and satellite velocity information. These true pseudoranges and Doppler measurements are then compared to the ones obtained from the tracking loops and the differences used to form an estimated measurement error. In the absence of ranging errors, the measurement error variance is a direct measure of the tracking variance. It is important to note, however, that this statement only holds true insofar as the satellite position and velocity are correctly estimated. To verify this, the values computed by the software receiver are time-matched and compared to the simulated ones. The agreement is found to be at the millimetre and sub-millimetre per second for position and velocity respectively.

Another limitation inherent to this test set-up is the accuracy of the hardware simulator itself. This accuracy is mostly limited by the quality of the clock used. The quoted accuracies are 1 cm and 1 mm/s RMS for the pseudorange and pseudorange rate errors (i.e. Doppler) respectively. It is important to bear in mind that these accuracies account for errors in simulated satellite induced and atmospheric biases; in the scenarios considered herein, the accuracy can be expected to be higher. Complete anticipated accuracies can be found in Spirent (2006).

CHAPTER FOUR: GPS L5 ACQUISITION

This chapter presents a discussion on how to efficiently implement the L5 signal acquisition given its structure. GPS signal acquisition is first introduced as a detection/estimation problem and, following this, the specifics of the L5 signal acquisition are reviewed in light of its structure. Particular emphasis is placed on understanding the impact of the two following L5 signal features: 1) the introduction of secondary NH codes that further modulate the primary PRN sequences, and 2) the presence of a data and pilot channel that equally share the broadcast signal power. A cascaded algorithm is then proposed for the sequential acquisition of the PRN and NH codes. In addition, several data/pilot combining schemes are proposed and tested with the objective of improving the detection performance of the L5 acquisition. The various acquisition strategies are compared against each other in terms of reliability and computational requirements.

4.1 The L5 Acquisition Problem

The fundamental objective of a GPS receiver during signal acquisition involves the identification of the individual satellite signals from the composite received signal as well as the extraction, for each of these individual satellites, of the coarse synchronization information that will enable subsequent GPS receiver operations including tracking, measurement formation and navigation solution derivation.

4.1.1 Detection/Estimation Problem in GPS Acquisition

From the correlation model of Section 3.3.2 it can be seen that, in addition to the PRN number, the unknown parameters in modeling the timing difference between a given satellite (transmitter) and the receiver are: 1) the code phase offset $\delta\tau$, 2) the frequency (or Doppler) offset δf, and 3) the phase offset $\delta\phi$.

The GPS acquisition problem can therefore be formulated as a parameter estimation problem where a signal is transmitted from a source with a set of unknown parameters denoted θ, where $\theta = [\delta\tau, \delta f, \delta\phi]$. The receiver can then use N successive observations of the received signal and a suitably chosen cost function to try to optimally estimate the set of transmitted parameters, with the resulting set of estimated parameters denoted $\hat{\theta}$. It is however important to bear in mind that the GPS acquisition problem differs from a pure estimation problem in the following ways. First, GPS signal acquisition is a coarse synchronization that is merely used to initiate the fine synchronization performed during signal tracking. As a result the objective during GPS signal acquisition is to obtain a coarse estimate of the unknown set of parameters θ. This implies that some parameters, such as the phase offset, can be regarded as nuisance parameters that do not need to be estimated. It also means that the estimation error does not need to be minimized in an absolute sense but should rather be constrained within pre-defined bounds. Second, since the coarse estimation of the received parameters can only be performed when the satellite of interest is present, the GPS signal acquisition is commonly approached as a detection/estimation problem.

From the above, the GPS signal acquisition can be seen, for each individual satellite, as a two-dimensional search in time and frequency. The time dimension corresponds to the unknown code phase offset (or, equivalently, to the unknown pseudorange between the satellite and the receiver) and the frequency dimension relates to the unknown Doppler offset (that is, to the relative satellite-user motion along the signal propagation path). As illustrated in Figure 4-1 this search space is divided into smaller cells where each cell corresponds to a particular "code phase delay - Doppler frequency offset" pair. In each cell, the incoming signal is correlated with the local code and carrier replicas generated with the code phase delay and Doppler frequency of that cell. This correlation value can be computed in many different ways (as will be discussed in Section 4.2.2) but is generically referred to as the test statistic.

It is important to note that the size of the full search space and that of the individual cell can vary. In particular, the ranges of code phase and frequency offsets that need to be searched are usually determined based on 1) the signal inherent characteristics (e.g. carrier frequency or PRN code length), 2) the type of acquisition performed (e.g. cold, warm or hot start), and 3) the expected level of receiver dynamics and oscillator instabilities. The cell size, on the other hand, is usually selected to ensure that the correlation losses (due to code and frequency mismatch) do not exceed a pre-defined permissible level. The choice of the cell size will condition, in part, the rapidity and reliability of the acquisition process.
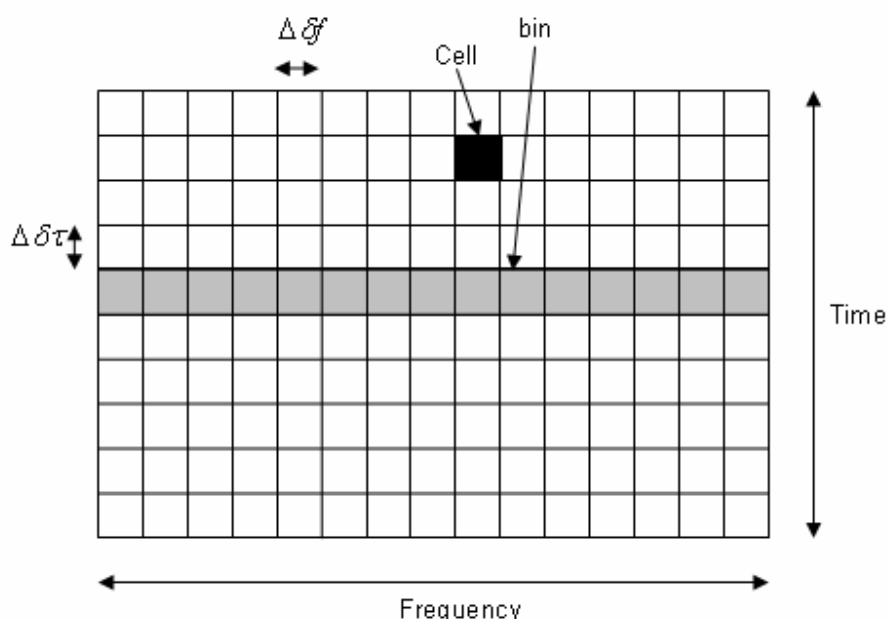
Figure 4-1 – Two-Dimensional GPS Acquisition Search Space

The full uncertainty region is first searched to locate the maximum correlation peak. In this cell, the signal detection process is then based on a binary hypothesis test where the two possible hypotheses are as follows: the signal is present (H_1) or absent (H_0). Accordingly, the detector can decide that the signal is either present (D_1) or absent (D_0). There are therefore four possible outcomes to binary hypothesis testing, and they are summarized in Table 4.1. Since it is not possible to jointly minimize the probability of false alarm (type I error) and the probability of missed detection (type II error), typical approaches attempt to minimize the probability of missed detection (P_M), which is equivalent to maximizing the probability of detection (P_D), for a fixed probability of false alarm (P_{FA}). This can be done following the classical Neyman-Pearson approach (Kay 1993).

Assuming that the *Probability Density Functions* (PDFs) of the test statistic under the

hypothesis that the signal is present $p(T;H_1)$ or absent $p(T;H_0)$ are known, the optimal

Neyman-Pearson detector is the one that decides that H_1 is true if

$$L(T) = \frac{p(T;H_1)}{p(T;H_0)} > \gamma \qquad \textbf{(4-1)}$$

where $L(T)$ is known as the likelihood ratio, and γ the threshold determined from

$$P_{FA} = \int_{R_1} p(x;H_0)dx = \alpha \qquad \textbf{(4-2)}$$

where $R_1 = \{T : L(T) > \gamma\}$ is the region of the test that maps into D_1.

Table 4.1 – Possible Outcomes for Binary Hypothesis Testing

Actual Situation	Decision Based on Statistical Test	
	Accept H$_0$	**Accept H$_1$**
H_0 is true	Correct Decision Probability: $1-\alpha$, P_R	**Type I Error; False Alarm** Probability: α, P_{FA}
H_1 is true	**Type II Error; Missed Detection** Probability: β, P_M	Correct Detection Probability: $1-\beta$, P_D

A common way of summarizing the performance of a *Neyman-Pearson* (NP) detector is

to plot P_D against P_{FA}. The resulting plot is commonly referred to as the *Receiver*

Operating Characteristics (ROC) curve. Alternatively, it is possible to plot P_D against

C/N_0 for a fixed P_{FA}; these curves, to be henceforth referred to as modified ROC, will be

used in Section 4.2.3.

It is important to recall that hypothesis H_1 and H_0 refer to the individual cell where the maximum test statistic is found, and not to the full search space. As discussed in O'Driscoll (2007) and Borio et al (2006), the overall performance of the GPS signal acquisition is not only conditioned by the test statistic employed but also by the acquisition search strategy.

Now that the generic GPS signal acquisition has been discussed, it is interesting to understand the particulars of the L5 signal acquisition problem.

4.1.2 L5 Acquisition Implementation Issues

When applying this detection/estimation approach to the L5 signal acquisition, it is important to take into account the characteristics of the L5 signal structure. First, the spreading sequences used to modulate both data and pilot channels on the L5 signal consist of two layers: the PRN and NH codes. It is then possible, when performing the code phase alignment (or, equivalently, the search in time), to define the code as the PRN code only or as the NH-modulated PRN code. Since the NH code alignment is required to proceed to a tracking state that includes the subframe synchronization and navigation message decoding (and therefore can lead to a navigation solution), the latter definition is taken herein. Several NH code acquisition strategies have been investigated in the past (Tran & Hegarty 2002, Macabiau et al 2003, Hegarty et al 2004b, Yang et al 2004, Hegarty 2006). They can be classified in two broad categories, namely the combined and cascaded schemes. The combined schemes try to acquire the PRN and NH code delays in a single step. This can be done on the pilot channel since, in the absence of unknown symbol bit transitions, the Q5 spreading sequence is fully periodic. This approach,

however, suffers from very stringent frequency requirements that can increase the computational load tremendously. In fact, the use of coherent integrations in excess of 20 ms not only amplifies the number of frequency and code bins that needs to be searched for but also augments the complexity of the correlation that needs to be performed in each cell of the search space. The cascaded schemes, on the other hand, implement the PRN and NH code delays acquisition in two steps. The first step (referred to as coarse acquisition) aims at roughly estimating the Doppler frequency and PRN code delay of the visible satellites while the second step (referred to as fine acquisition) provides the NH code delay and a refined Doppler frequency estimate. In light of the above it becomes obvious that the former approach is primarily used when the receiver is in re-acquisition mode or possesses some a priori time and/or frequency information (e.g. from an assistance network) that can help reduce the size of the search space. The cascaded approach is therefore followed in the framework of this dissertation.

Second, the L5 signal is broadcast using a QPSK modulation where the data and pilot channels are perfectly synchronized and modulated with quasi-orthogonal spreading sequences (as shown in Table 2.2). It is therefore possible to acquire the L5 signal using single or combined channel strategies. The latter strategy maximizes the available signal power (and therefore minimizes the risk of false acquisition) but generally increases the computational load. Various data/pilot combining strategies will be discussed in light of the coarse and fine acquisition steps in the next sections.

Now that the challenges of the L5 signal acquisition problem have been identified, the two following sections discuss the implementation of the coarse and fine steps of the cascaded L5 acquisition.

4.2 L5 Coarse Acquisition

The objective of an L5 receiver during coarse signal acquisition is to provide a coarse estimate of the received PRN code phase and frequency offset. The two-dimensional search implemented to this end is discussed hereinafter. Following this, various test statistics are presented and their detection performance compared.

4.2.1 Search Space Definition

During the coarse acquisition step, the PRN code period and the NH bit duration constrain the coherent integration time to exactly 1 ms. It is important to bear in mind, however, that at this stage the PRN code alignment has not yet been performed. This implies that, over a 1 ms coherent integration time, an NH bit sign transition can lead to destructive summations, negating all energy received. To circumvent this problem, a zero-padding strategy (Yang et al 2004) has to be implemented. Following this approach, 2 ms of incoming signal are correlated with 1 ms of locally generated samples appended by 1 ms of zeros; in this way, it is possible to ensure that a full 1-ms correlation peak will be found in the first millisecond of the resulting correlation.

The correlation process introduced in Section 3.3.2 was described in the time domain; however, it is possible, in software receivers, to implement it in the frequency domain (Yang 2000) using *Fast Fourier Transforms* (FFTs). This is done here to speed up the correlation process, as, in the frequency domain, all possible code offsets can be searched in one operation. To further improve the efficiency of this FFT-based algorithm two additional steps are taken: 1) the FFTs of all the local PRN codes are computed at the IF

and stored offline, and 2) the Doppler removal is implemented by applying a circular shift on the FFT of the incoming signal.

This correlation strategy readily settles the code and frequency resolution of the search space. By virtue of the shift theorem, the frequency resolution, f_D, of the Doppler removal is given by

$$f_D = \frac{f_S}{N} \tag{4-3}$$

where f_S is the sampling rate and N is the number of samples over which the FFT is performed.

Consequently, considering a 28 MHz complex sampling rate and accounting for the zero-padding, the Doppler removal offers a 500 Hz frequency resolution. Besides, taken over a full 10230-chip PRN code, this sampling rate provides a 0.35 chips code resolution. This leads to a maximum frequency and code error of 250 Hz and 0.18 chips, respectively. According to the correlation model developed in Section 3.3.2, this bounds the frequency and code power loss to 0.9 dB and 1.8 dB, respectively.

It is important to underline that, by performing the Doppler removal in the frequency domain, the potential effects of code Doppler are assumed negligible. These effects are rarely considered in GPS C/A acquisition; but, because of the fast L5 chipping rate, it is of major importance to assess their impact on the L5 correlation. In the case at hand, the coherent integration time is limited to 1 ms and the maximum Doppler error due to satellite motion is less than 4 kHz. Under such conditions, it can be shown that the maximum possible error is 0.03 chips; resulting in negligible resolution and/or power loss in terms of PRN code phase acquisition. In fact, it has been shown by Bastide (2004), and

confirmed by O'Driscoll (2007), that when using a 1 ms coherent integration time, the code Doppler effects can be neglected up to 200 ms total pre-detection time.

Now that the L5 coarse acquisition search space has been thoroughly described, it is interesting to assess the detection performance of various common test statistics. These test statistics are introduced as single bit strategies (where the total pre-detection integration time is set to exactly one code period). They can, however, be readily extended to several bits as illustrated in Figure 4-2.
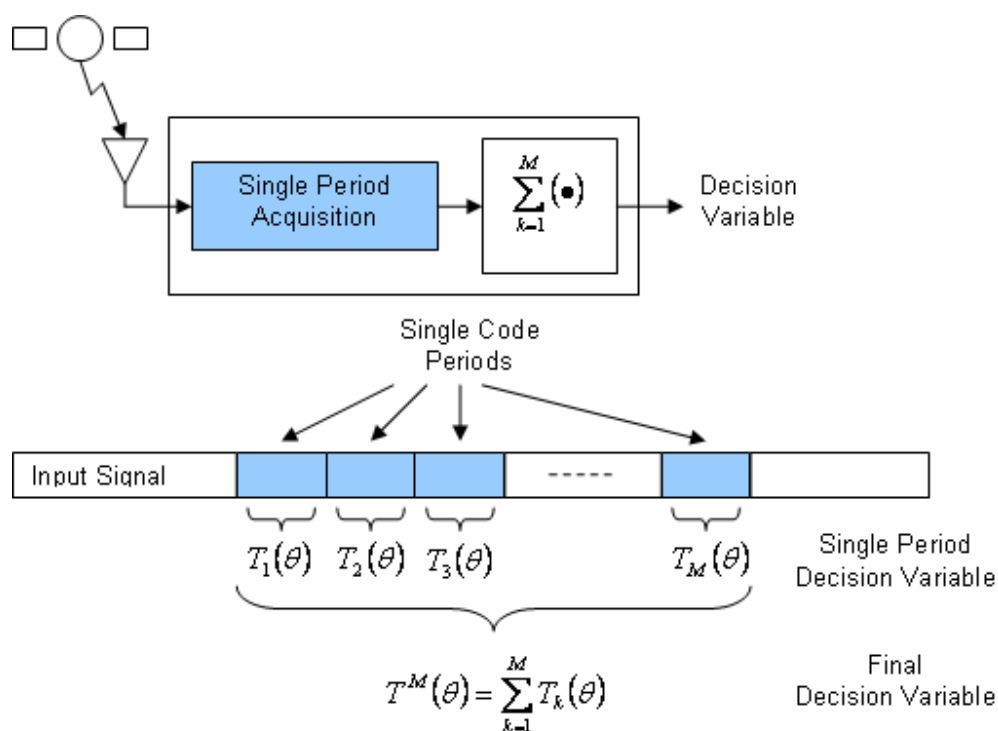
Figure 4-2 – Generic Acquisition Scheme with Non-Coherent Combining of M Variables Obtained on a Single Code Period (Borio 2007)

The acquisition test statistic is defined, in each cell of the two-dimensional search space, as the correlation between the incoming signal and the local code and carrier replicas. Four such correlation strategies are presented in the next subsection.

4.2.2 L5 Coarse Acquisition Strategies

Four correlation strategies are discussed in this section for the coarse acquisition of the L5 signal. They are the 1) single, 2) non-coherently combined, 3) coherently combined and 4) differentially combined channel strategies.

Single Channel Acquisition

Using the orthogonality and synchronicity properties of the data and pilot spreading sequences, it is possible to ignore one of the two channels and to acquire the L5 signal using a single channel. This process is equivalent to the conventional acquisition of single component signals such as the C/A signal. The corresponding test statistic is given by

$$T_{SC}(\delta f, \delta \tau) = I_X^2 + Q_X^2 \tag{4-4}$$

where the subscript X can refer to a correlation on either the data ($X = data$) or the pilot ($X = pilot$) channel, and the dependence of T_{SC} upon the phase offset $\delta \phi$ is removed by the squaring and summing operations.

It has been mentioned in Section 3.3.2 that the in-phase and quadra-phase components are two independent white Gaussian *Random Variables* (RVs) with variance $\sigma_N^2 = \dfrac{N_0 \tilde{R}(0)}{4T_I}$. Accordingly, it can be inferred that the test statistic T_{SC} is chi-square (χ^2) distributed with two degrees of freedom. When the signal is present, T_{SC} is a non-central χ^2 RV with non-centrality parameter λ, and when the signal is absent, T_{SC} is a central χ^2 RV. Using the correlation model developed in Section 3.3.2 and neglecting the code and frequency errors, the non-centrality parameter λ can be approximated by

$$\lambda \approx \frac{P}{4}\tilde{R}^2(0)$$

(4-5)

where $\tilde{R}(0)$ accounts for the effects of front-end filtering.

Using the properties of non-central and central χ^2 RVs (Proakis 2000), and assuming a threshold γ, the probabilities of false alarm and detection of the single channel test statistic are, respectively

$$P_{FA}^{SC} = \exp\left(-\gamma\frac{2T_I}{N_0\tilde{R}(0)}\right)$$

(4-6)

$$P_D^{SC}(\gamma) = Q_1\left(\sqrt{\frac{P\tilde{R}(0)T_I}{N_0}}, 2\sqrt{\gamma\frac{T_I}{N_0\tilde{R}(0)}}\right)$$

(4-7)

where $Q_K(a,b)$ is the generalized Marcum Q-function (Marcum 1960), of order K.

In addition to its simplicity, this approach offers the advantage of a low computational burden (since the correlation is only implemented on one channel). However it only makes use of half of the incoming signal power, which results in a 3 dB performance loss, relative to an ideal data/pilot combined correlation strategy.

Non-Coherent Channel Combining

The simplest strategy in attempting to recombine the power from the data and pilot channels is the non-coherent combining strategy. This approach is discussed, for instance, in Bastide et al (2002). The corresponding acquisition test criterion is given by

$$T_{NC}(\delta f, \delta\tau) = I_{data}^2 + Q_{data}^2 + I_{pilot}^2 + Q_{pilot}^2$$

(4-8)

The test statistic T_{NC} is chi-square (χ^2) distributed with four degrees of freedom. T_{NC} is a central χ^2 RV when the signal is absent, and a non-central χ^2 RV with non-centrality parameter $2\lambda \approx \frac{P}{2}\tilde{R}^2(0)$ when it is present.

Assuming a threshold γ, the probabilities of false alarm and detection of the non-coherently combined test statistic are, respectively

$$P_{FA}^{NC} = \exp\left(-\gamma\frac{2T_I}{N_0\tilde{R}(0)}\right)\left(1 + \gamma\frac{2T_I}{N_0\tilde{R}(0)}\right) \qquad \text{(4-9)}$$

$$P_D^{NC}(\gamma) = Q_2\left(\sqrt{\frac{2P\tilde{R}(0)T_I}{N_0}}, 2\sqrt{\gamma\frac{T_I}{N_0\tilde{R}(0)}}\right). \qquad \text{(4-10)}$$

The benefits of recombining the power of the data and pilot channels were demonstrated in Bastide et al (2002); however, knowing that the coherent integration time is limited to 1 ms, this approach may suffer from high squaring losses for low incoming signal power. In order to maximize the available power, different combining strategies can be envisioned. To this end, Yang et al (2004) and Borio (2007) respectively introduce a coherent and differential data/pilot combining strategy for the GPS L5 and Galileo E5a signals. The statistical properties of the coherent and differential combining algorithms are derived in Borio (2007) and are repeated here for convenience.

Coherent Channel Combining

The coherent channel combining algorithm, introduced in Yang et al (2004) relies on the perfect orthogonality of the data and pilot channels. By definition the pilot channel is

transmitted a quarter of a cycle behind the data channel. In the presence of secondary code and navigation data bits, and after Doppler removal, this results in the data and pilot correlation outputs being either aligned or in phase opposition. It is then possible to recombine them prior to squaring, according to these two hypotheses, and select the one with the highest amplitude. Accordingly, the coherent combining test statistic is given by

$$T_{CC}(\delta f, \delta \tau) = \max[T^+(\delta f, \delta \tau); T^-(\delta f, \delta \tau)] \tag{4-11}$$

where the coherently recombined data/pilot correlation under the assumptions that the data and pilot correlations are aligned, $T^+(\delta f, \delta \tau)$, or in phase opposition, $T^-(\delta f, \delta \tau)$, can be expressed as

$$T^\pm(\delta f, \delta \tau) = (I_{pilot} \pm I_{data})^2 + (Q_{pilot} \pm Q_{data})^2 \ . \tag{4-12}$$

Since the independent in-phase and quadra-phase noise components on the data and pilot channels are summed before they are squared this strategy reduces the squaring losses. By proving the independence of $T^+(\delta f, \delta \tau)$ and $T^-(\delta f, \delta \tau)$, Borio (2007) shows that the following relationship holds

$$P(T_{CC}(\delta f, \delta \tau) > \gamma) = 1 - P(T^+(\delta f, \delta \tau) < \gamma) P(T^-(\delta f, \delta \tau) < \gamma) \tag{4-13}$$

where the RVs $T^+(\delta f, \delta \tau)$ and $T^-(\delta f, \delta \tau)$ are χ^2 distributed with two degrees of freedom and variance $2\sigma_N^2 = \dfrac{N_0 \tilde{R}(0)}{2T_I}$. When the signal is absent, both RVs are central; and when the signal is present, one of the two RVs $T^+(\delta f, \delta \tau)$ and $T^-(\delta f, \delta \tau)$ is central and the other non-central with non-centrality parameter $4\lambda \approx P\tilde{R}^2(0)$.

From the above, Borio (2007) demonstrates that the probabilities of false alarm and detection of the coherently combined test statistic are, respectively

$$P_{FA}^{CC} = 1 - \left(1 - \exp\left(-\gamma \frac{T_I}{N_0 \tilde{R}(0)}\right)\right)^2 \qquad (4\text{-}14)$$

$$P_D^{CC} = 1 - \left(1 - \exp\left(-\gamma \frac{T_I}{N_0 \tilde{R}(0)}\right)\right)\left(1 - Q_1\left(\sqrt{\frac{2P\tilde{R}(0)T_I}{N_0}}, \sqrt{\gamma \frac{2T_I}{N_0 \tilde{R}(0)}}\right)\right). \qquad (4\text{-}15)$$

Differential Channel Combining

The differential channel combining algorithm is introduced in Borio (2007) as an adaptation of the traditional differentially coherent combining scheme used for C/A signal acquisition (e.g. O'Driscoll 2007, Shanmugam 2008). Instead of taking the dot-product multiplication of two consecutive correlator outputs as is done for differential C/A acquisition, the differential combining scheme proposed for QPSK signals (such as the L5 signal) is based on the dot-product multiplication of the data and pilot correlator outputs.

The traditional algorithm relies on the assumption that the phase offset affecting two consecutive correlations is constant to cancel the dependence of the differentially combined test statistic upon $\delta\phi$, and on the independence of the consecutive noise term to induce lower noise amplification than the non-coherent combining algorithm. When considering the L5 signal, the data and pilot channels are broadcast with a 90 degree phase offset and are affected by the same delay and Doppler frequency. Consequently, after correlation, the data and pilot correlator outputs are either in phase or in opposition.

This implies that the differentially coherent test statistic T_{DC} will not depend on $\delta\phi$; however, it also means that its sign will be conditioned by the relative sign of the secondary codes and navigation symbol bit. To remove this dependence, an absolute value operator is introduced. Finally, the differentially coherent test statistic is given by

$$T_{DC}(\delta f, \delta\tau) = abs[I_{data} I_{pilot} + Q_{data} Q_{pilot}]. \tag{4-16}$$

Remembering that the data and pilot correlator outputs are independent Gaussian random variables with variance σ_N^2, the differentially coherent test statistic can be rewritten as the difference of two independent χ^2 random variables with two degrees of freedom and

variance $2\sigma_N^2 = \dfrac{N_0 \tilde{R}(0)}{2T_I}$.

From the above, Borio (2007) demonstrates that the probabilities of false alarm and detection of the coherently combined test statistic are, respectively

$$P_{FA}^{DC}(\gamma) = \exp\left(-\gamma \frac{4T_I}{N_0 \tilde{R}(0)}\right) \tag{4-17}$$

$$P_D^{DC}(\gamma) = \begin{cases} \dfrac{1}{2}\exp\left(-\dfrac{(8\gamma + \tilde{R}^2(0)P)T_I}{2N_0\tilde{R}(0)}\right) + Q_1\left(\sqrt{\dfrac{2P\tilde{R}(0)T}{N_0}}, \sqrt{\gamma\dfrac{8T_I}{N_0\tilde{R}(0)}}\right) \\ -\dfrac{1}{2}\exp\left(-\dfrac{(8\gamma - \tilde{R}^2(0)P)T_I}{2N_0\tilde{R}(0)}\right)Q_1\left(\sqrt{\dfrac{P\tilde{R}(0)T}{N_0}}, 4\sqrt{\gamma\dfrac{T_I}{N_0\tilde{R}(0)}}\right) \end{cases}. \tag{4-18}$$

Now that the theoretical performance of the four correlation strategies have been reviewed, it is interesting to study their detection performance.

4.2.3 Detection Performance

The detection performance of the four aforementioned correlation strategies are compared theoretically and empirically using modified ROC curves and *Post-correlation SNR* (PSNR) coefficients respectively.

Modified ROC curves

In Figure 4-3, the probability of detection of the four acquisition strategies are plotted against the incoming C/N$_0$ for a fixed probability of false alarm $P_{FA} = 10^{-4}$. As suggested in Bastide (2004), the probability of false alarm is set to 10^{-4} rather than 10^{-3} (as is typically used for C/A signal acquisition) to account for the fact that the L5 uncertainty region is approximately ten times bigger than that of GPS C/A. Note that the results displayed in Figure 4-3 account for the effects of frontend filtering but not for those of code delay and Doppler uncertainty. As expected, and already reported in Bastide et al (2002) and in Yang et al (2004), single and coherently combined channel acquisition offer the worst and best detection performance, respectively. The low performance of the single channel acquisition is a direct consequence of the fact it only uses half of the available power. Conversely, the good performance of the coherently combined acquisition results from the optimal use that this strategy makes of all the available power. However, it is important to point out that for low C/N$_0$, where the relative data/pilot sign recovery becomes unreliable, the performance of all data/pilot combining methods tends to merge.

As suggested in Bastide et al (2002) the L5 acquisition threshold is taken as the incoming signal C/N$_0$ required to reach the probability of detection $P_D = 0.9$. With the parameters used herein, the acquisition threshold can be approximated at 42 dB-Hz.
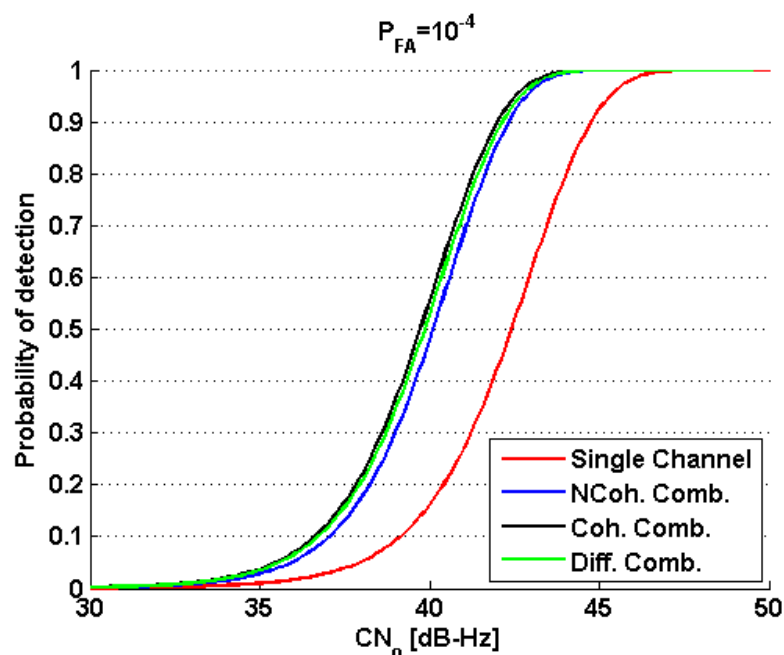
Figure 4-3 – Probability of Detection versus Total C/N$_0$ for Various L5 Acquisition Strategies Using 1 ms Coherent Integration

Since intra-system cross-correlation peaks are the main cause of false alarms during signal acquisition, a more reliable test statistic is desired. To this end, the common approach is to assume the presence of a cross-correlation peak due to a strong interfering satellite in the incorrect search space bins. Hegarty et al (2003) introduced two cross-correlation levels: one at 19 dB-Hz when the cross-correlation occurs on both channels simultaneously and another at 16 dB-Hz when it affects a unique channel. Although seldom encountered in real life, the worst case is considered here. Another common step in making the signal detection more reliable is to increase the total pre-detection

integration time using M summations of the test statistic T. Both effects are illustrated for the non-coherently combined strategy in Figure 4-4.

The resulting test statistic T_{NC}^{M} is a non-central χ^2 RV under H_1 and H_0, and the non-centrality parameters can be approximated, respectively, as

$$\lambda_1 \approx \frac{MP\widetilde{R}^2(0)}{2} \tag{4-19}$$

$$\lambda_0 \approx \frac{MP_I\widetilde{R}^2(0)}{2} \tag{4-20}$$

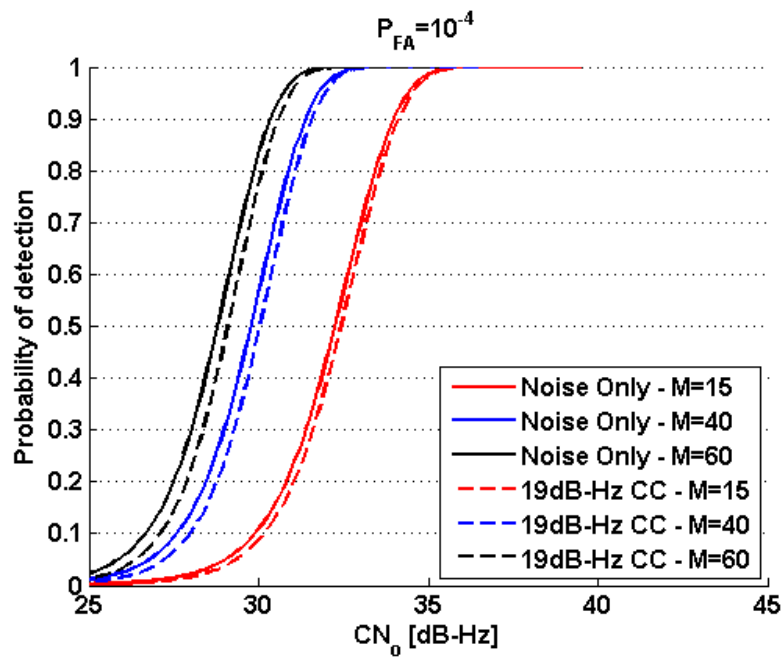where P_I is the cross-correlation level.

Figure 4-4 – Probability of Detection versus Total C/N$_0$ in the Presence of Noise and Cross-Correlation (CC) Using 1 ms Coherent Integration and Various Non-Coherent Summation Numbers

As expected, and already reported in Hegarty et al (2003), the use of non-coherent summations can help improve the detection performance of the non-coherently combined strategy. This improvement, however, tends to vanish when the C/N_0 decreases since the squaring losses increase. It is anticipated that similar trends would be observed for the other L5 coarse acquisition strategies.

Similarly, Figure 4-4 shows that, in the presence of cross-correlation peaks the incorrect search space cells, the detection performance of the non-coherently combined acquisition strategy degrades, but only marginally. However, it is important to recall that, as illustrated in Table 2.2, the L5 PRN codes were designed to reduce the occurrence of intra-system cross-correlation peaks or, when cross-correlations do occur, to limit their time duration (Spilker & Van Dierendonck 2001).

Empirical Detection Performance – PSNR coefficients

To confirm the theoretical detection performance of the four acquisition strategies presented above, their PSNR is also computed using (Shanmugam 2008)

$$PSNR = 10\log_{10}\left[\frac{\left(T\left(\hat{\theta} = \theta\right) - E\left[T\left(\hat{\theta} \neq \theta\right)\right]\right)^2}{\text{var}\left[T\left(\hat{\theta} \neq \theta\right)\right]}\right] \tag{4-21}$$

where the values $T\left(\hat{\theta} = \theta\right)$, $E\left[T\left(\hat{\theta} \neq \theta\right)\right]$ and $\text{var}\left[T\left(\hat{\theta} \neq \theta\right)\right]$ are estimated over successive search spaces by averaging, respectively, the maximum, mean and variance of the test statistic.

O'Driscoll (2007) shows that, when applied to a mean-shifted Gaussian detection problem, the PSNR corresponds to the *Deflection Coefficient* (DC) and, therefore, can be

used to exactly characterize the detection performance of this problem (Kay 1993). This relationship, however, does not hold for non-Gaussian detection problems. In such cases, empirical ROC curves provide the most relevant insight in terms of detection performance. However, in cases where the true code delay and Doppler offset of the incoming signal cannot be straightforwardly determined (e.g. when using real or hardware simulated data), the estimation of the probabilities of detection and false alarm over a large number of samples can become very tedious. Under these circumstances, empirical PSNR values can be used as a good approximation (Shanmugam 2008).

Empirical PSNR coefficients are shown in Figure 4-5. For each PSNR coefficient (i.e. for each acquisition strategy and each C/N_0), the values for the maximum, mean and variance of the test statistic (used in Equation 4.21) are averaged over 1,000 two-dimensional search spaces.
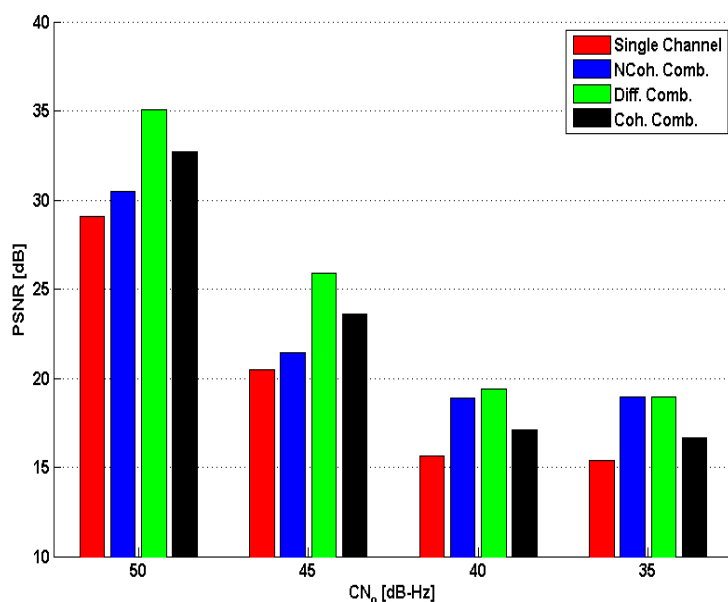

Figure 4-5 – Acquisition Sensitivity for Single versus Combined Channel Scenarios

As expected from the theoretical ROC curves displayed in Figure 4-3, the data/pilot combined strategies clearly outperform the single channel acquisition for the entire range of C/N_0. Amongst these combined implementations and at high C/N_0, the differential combining approach seems to provide the higher PSNR, followed by the coherent and non-coherent combining strategies. At lower C/N_0, the performance of coherent and non-coherent combining degrades and, as a result, the performance of the combined implementations tends to merge. While these trends do not follow those observed in terms of ROC, where the coherent combining strategy provides the highest detection performance, it is important to recall that, for non-Gaussian problems, the PSNR is not an exact approximation of the detection performance. In fact, the superiority of the differential combining strategy in terms of PSNR can be explained by the low variance of the differential detector. Also, the ROC curves shown in Figure 4-3 are derived under the assumption that only noise is present under H_0. In reality, some cross- and auto-correlation side peaks are present in all the cells of the search space and modify the distribution of the test statistic under H_0. In particular, it can be expected that the effects of cross- and auto-correlation side peaks on the coherent and differential combining will be magnified at low C/N_0.

4.2.4 False Frequency Acquisition

So far, the false alarm issue was discussed in the time domain only (that is, based on the correlation properties of the PRN codes), overlooking its potential occurrence in the frequency domain. However, assuming no noise and no code delay uncertainty, and using the power roll-off function defined in Section 3.3.2, it can be anticipated that, along the

frequency axis, the ratio between two neighbouring peaks will vary between 0 dB and 4 dB. In fact, Figure 4-6 illustrates that when the true Doppler frequency is located in the middle of two frequency bins, the receiver can easily acquire the wrong coarse frequency estimate, leading to an initial frequency error that slightly exceeds 250 Hz. The consequences of such error will be further discussed in Section 4.3.3.
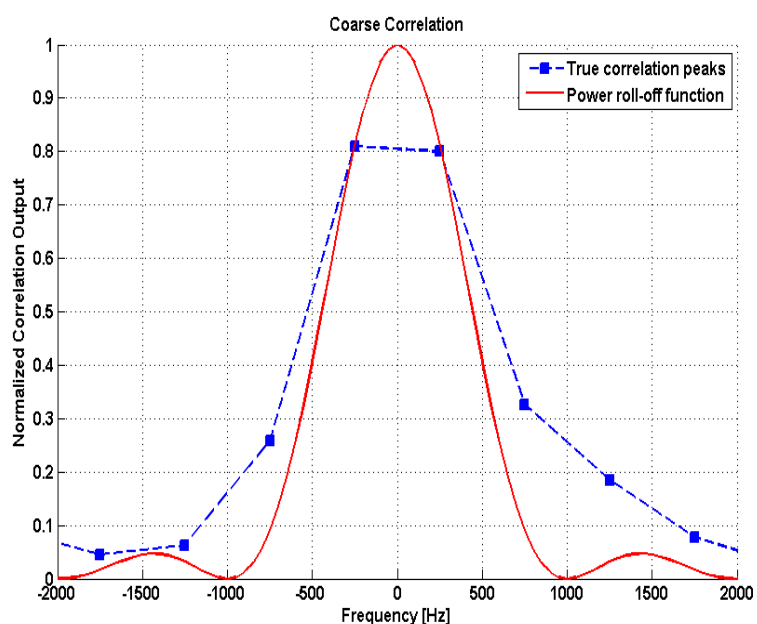
Figure 4-6 – Correlators' Output along the Frequency Axis, at the Correct PRN Code Delay

Now that the coarse L5 signal acquisition step has been thoroughly discussed, the following section discusses the implementation of the fine L5 signal acquisition step.

4.3 L5 Fine Acquisition

Assuming a successful (and unbiased) coarse acquisition, the PRN code phase offset is known within ±0.18 chip and the PRN Doppler frequency within ±250 Hz. The next

required step is then to acquire the NH code phase offset. In order to do so, the complex 1-ms coherent integration peaks need to be correlated with the locally generated NH codes. The search implemented to this end is discussed hereinafter and, in particular, the data/pilot combining and frequency sensitivity issues are addressed.

4.3.1 Data/Pilot Combining

It is possible to recombine the data and pilot channels so as to increase the overall SNR. This approach, however, suffers from the presence of unknown data bit transitions on the data channel, and from the discrepancies between the data and pilot NH codes' periods. The pilot channel-only strategy, on the other hand, benefits from its ease of implementation (as enabled by the full periodicity of the Q5 spreading sequence). Besides, this pilot-only strategy allows direct and simultaneous acquisition of the NH_{20}, NH_{10} and data bit boundaries (when a combined approach would only give the NH_{10} and data bit boundaries), and takes advantage of the superior NH_{20} code correlation properties (Shanmugam 2008). In light of the above, the pilot-only approach is adopted here.

4.3.2 Frequency Error Sensitivity

Correlating the complex 1-ms coherent integration peaks with the locally generated NH_{20} code is somewhat similar to performing a coherent integration over the full NH_{20} code period and thus necessitates a reduction of the frequency uncertainty. More explicitly, Equations 3.12 and 3.13 show that frequency errors will affect the complex correlation peaks in the two following ways: first they will result in a power degradation through the sinc term and second, they will induce a phase rotation via the sine and cosine terms. As

shown in Macabiau et al (2003), and illustrated in Figure 4-7, this significantly degrades the NH_{20} code correlation for a frequency error as small as 30 Hz.
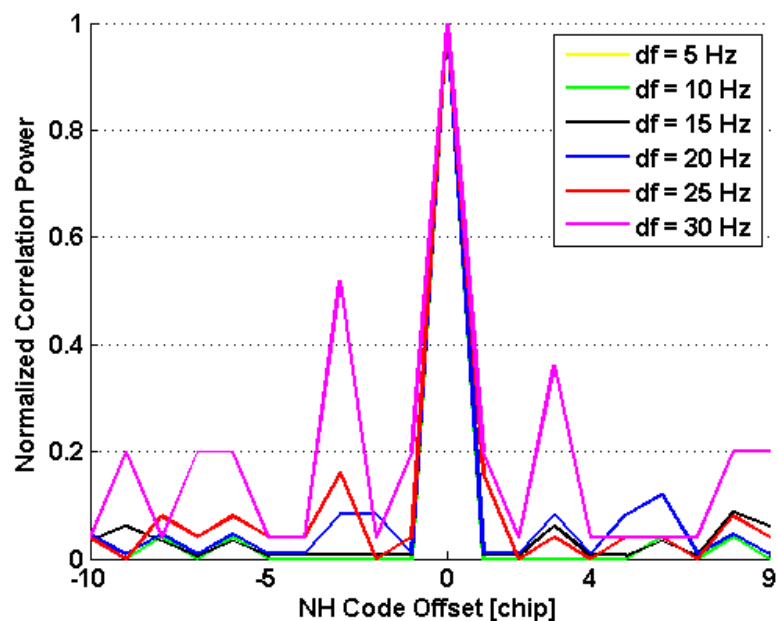
Figure 4-7 – NH_{20} Correlation Properties in The Presence of Frequency Errors

To reduce the frequency uncertainty, two methods have been previously discussed. The first one, introduced by Macabiau et al (2003), implements a PRN-only tracking step prior to NH code phase acquisition. This step is introduced to ensure minimal frequency error and to preserve the NH correlation properties. The second method, suggested by Yang et al (2004), implements the NH code alignment directly after the coarse acquisition. The Doppler removal is performed at the correlation stage by generating the local NH code at various frequencies within a ± 250 Hz range, using 25 Hz steps. The latter implementation, however, provides poorer detection performance as it does not address the power degradation effect. In addition, the direct NH acquisition strategy proposed by Yang et al (2004) might suffer from PRN correlation peak migration. This

issue, discussed by Bastide (2004), may arise when several non-coherent summations are needed to extract the NH correlation peak since the received code phase delay may shift over long pre-detection integration times. Given the above, the first strategy is selected, and the PRN-only tracking step implemented to this end is described in the following subsection.

4.3.3 One-dimensional Fine Acquisition

The PRN-only tracking step implemented prior to the NH_{20} code phase acquisition is a 1-ms FLL-based strategy. To validate the use of this intermediate tracking step, it is of major importance to ensure that 1) the respective FLL and DLL pull-in ranges encompass the frequency and code delay uncertainties at the coarse acquisition output, and 2) the PRN-only tracking threshold is above the acquisition threshold.

Pull-in Range and Sensitivity Analysis

The FLL pull-in range is conditioned by both the discriminator and coherent integration time used, and while the coherent integration time is constrained to exactly 1 ms, several FLL discriminators are available. At this stage, the FLL discriminator needs to fulfill the two following requirements. First, it needs to be insensitive to NH bit transitions and second, it must possess the widest linear tracking region possible to shorten the convergence time of the PRN-only tracking step. To this end, the *Decision Directed* (DD) discriminator described in Ward et al (2006) is chosen. It can be expressed, on either channel, and in units of radians per second, as (ibid)

$$D_{DD} = \frac{sign(dot).cross}{T_I} \tag{4-22}$$

with

$$dot = I_{P,k-1}Q_{P,k} - I_{P,k}Q_{P,k-1} \qquad \textbf{(4-23)}$$

$$cross = I_{P,k-1}I_{P,k} + Q_{P,k-1}Q_{P,k} \,. \qquad \textbf{(4-24)}$$

Assuming no external disturbances, Appendix A shows that the dot and cross terms can be approximated as

$$dot = \frac{P}{4}\tilde{R}^2(\delta\tau)D_{NH}^2 \sin(2\pi\delta f T_I) \qquad \textbf{(4-25)}$$

$$cross = \frac{P}{4}\tilde{R}^2(\delta\tau)D_{NH}^2 \cos(2\pi\delta f T_I) \qquad \textbf{(4-26)}$$

where D_{NH}^2 is the product of the successive NH bit signs.

The output of this discriminator is shown in Figure 4-8. It can be seen that the DD discriminator has a pull-in range of ± 250 Hz, which matches the Doppler uncertainty after coarse acquisition. However, the DD discriminator exhibits sharp edges that might cause some problems when the frequency error approaches the limits of the pull-in region.

The DLL pull-in range is determined by the *Early-Late Spacing* (ELS) used. As specified earlier the code phase offset is known within a ± 0.18 chip range, constraining the ELS to values greater than 0.4 chips. While this can appear unusually wide compared to common ELS used for narrow correlators, it is important to recall that the narrow spacing technology, described by Van Dierendonck et al (1992) for the C/A signal, cannot be applied to the L5 signal (Betz & Kolodzieski 2000). The ELS is therefore set to one chip, which encompasses the code phase uncertainty after coarse acquisition.
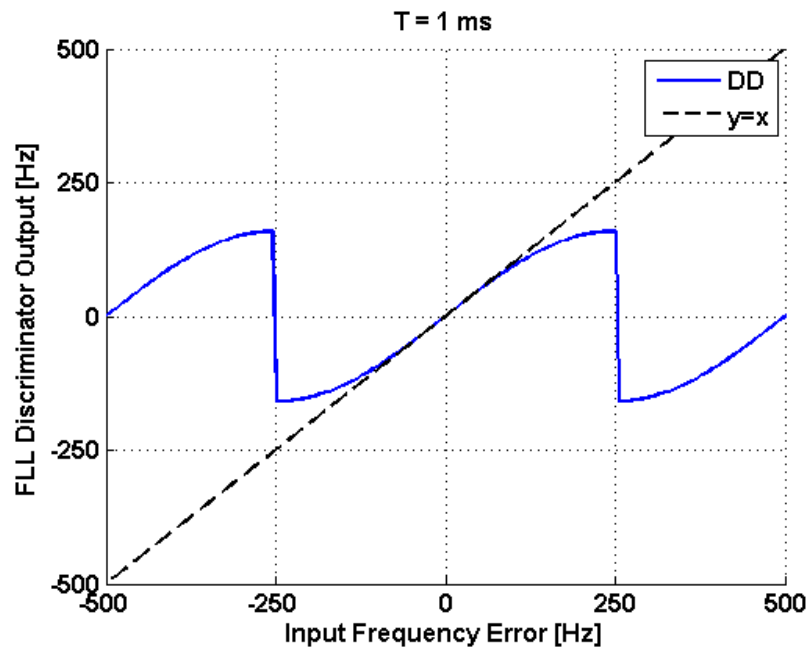
Figure 4-8 – FLL Discriminators Output Using 1 ms Coherent Integration

It is a well-known fact (e.g. Raquet 2003, Ray 2004) that the overall sensitivity of a tracking channel is determined by the sensitivity of its carrier loop. The FLL tracking sensitivity, in turn, can be determined using the following rule-of-thumb (Ward et al 2006)

$$3\sigma_{FLL,noise} + \theta_e \leq \frac{1}{4T_I} \tag{4-27}$$

where θ_e is the dynamic stress error and $\sigma_{FLL,noise}$ the frequency error standard deviation due to noise.

Considering a static receiver, and using the theoretical frequency tracking error variance given in Ward et al (2006), the loss of lock threshold of an FLL using 1-ms coherent

integrations and a 10-Hz loop bandwidth is approximately 25 dB-Hz, which is well below the sensitivity of the acquisition strategies discussed in Section 4.2.2.

Now that the use of an intermediate tracking step has been validated, issues regarding its optimization can be addressed. In particular the benefits of combining the data and pilot channels will be discussed and ways to confirm the tracking lock will be investigated.

Data/Pilot Combined Tracking

It is important to bear in mind that the 25 dB-Hz sensitivity threshold established earlier refers to the available tracking power which, in the L5 case, might differ from the incoming signal power due to the effective power split between the data and pilot channels. This implies that, using data/pilot combining strategies, it is possible to maximize the amount of available tracking power and, therefore, to improve the PRN-only tracking sensitivity. Several data/pilot combining algorithms have been investigated in the past (e.g. Julien 2005, Muthuraman 2007), however, it is important to bear in mind that these strategies were introduced in the context of full tracking, where the pilot channel outperforms the data channel. In the frame of PRN-only tracking, however, both channels are still affected by unknown NH bit signs transitions and, therefore, exhibit the same tracking performance. Accordingly, the simplest way to recombine the data and pilot channel powers, for both code and carrier tracking loops, is to use composite discriminators (e.g. Hegarty 1999). These composite discriminators can merely be defined as the weighted sum of the data and pilot discriminator outputs. This strategy is implemented herein on both code and carrier tracking loops.

Lock Detector and False Frequency Lock

It is important, prior to attempting any NH code alignment, to ensure that the signal is effectively being tracked. To this end, the FLL lock detector derived in Appendix A is implemented. Ideally, an FLL detector locked around 0.95 would guarantee a frequency error around 25 Hz. However, as illustrated in Figure 4-9, this detector is very noisy (even after smoothing) and therefore cannot be used as a reliable frequency error estimator. In addition, this lock detector is unable to detect false frequency locks (500 Hz offset). As mentioned in Section 4.2.4, the coarse acquisition frequency error can slightly exceed 250 Hz. Examining Figure 4-8, it is straightforward to understand that with such an input frequency error, the FLL discriminator could easily undergo a frequency slip that would result in a 500 Hz tracking error. It can be inferred, by analyzing Equations 3.10 to 3.14, that such frequency errors will affect the correlator outputs in the two following way: first, and according to the power roll-off function shown in Figure 3-10, they will attenuate the in-phase data and pilot correlator outputs by approximately 4 dB and second, due to the sine and cosine terms, they will reverse their sign every two milliseconds.

As illustrated in Figure 4-10 the occurrence of such sign change degrades the NH_{20} correlation properties by 2 dB which, as demonstrated in Figure 4-11, is not sufficient for a strong signal to prevent the acquisition of the received NH_{20} code phase offset and the transition into full tracking. Conversely, Figure 4-11 shows that the occurrence of such sign change negates all energy received on the data channel and thus prevents any further navigation message decoding operations.
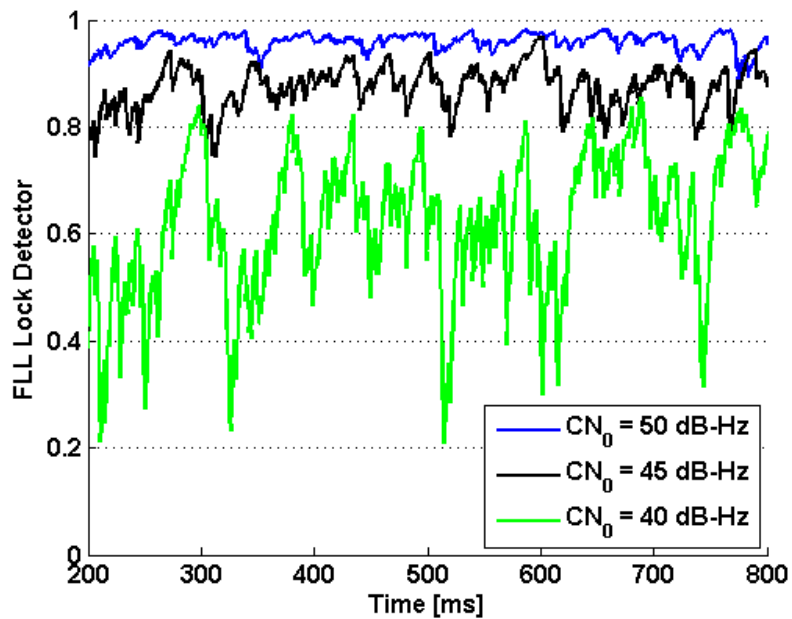
Figure 4-9 –Smoothed FLL Detector versus Time for Various C/N₀
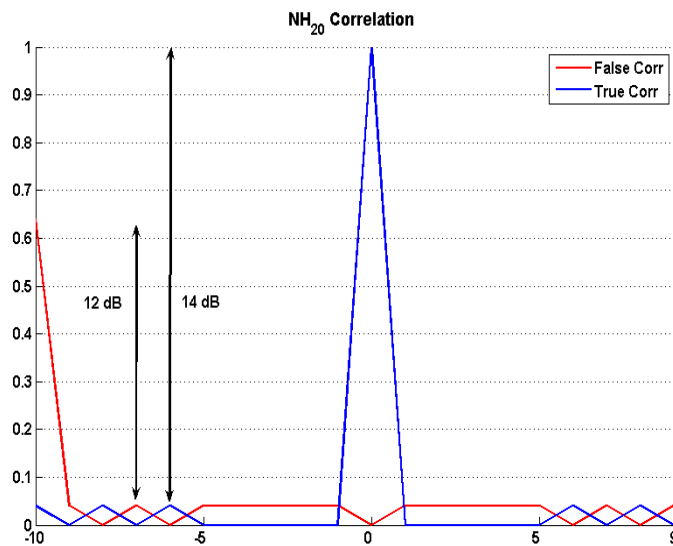
Figure 4-10 – NH20 Normalized Correlation Function Power in the Presence of Periodic 90° Phase Shifts
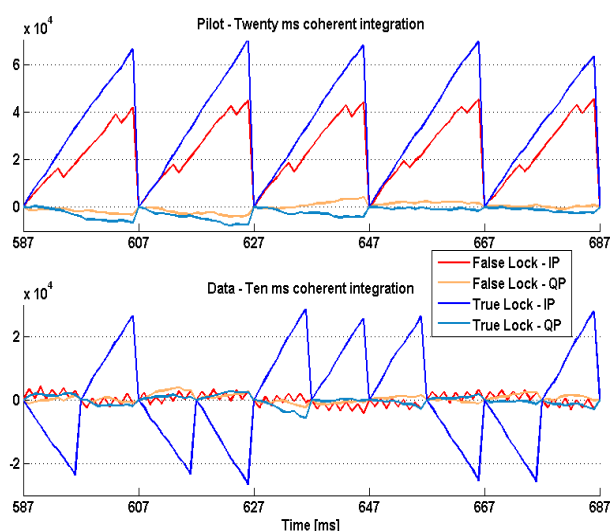
Figure 4-11 – Pilot and Data Correlator Outputs in the Presence of Periodic 90° Phase Shifts

The occurrence of these false frequency locks (500 Hz offset), however, is uncommon. In addition, they can easily be detected once the channel is in full tracking mode by continuously failing subframe synchronization. In light of the above, the one-dimensional L5 fine acquisition strategy provides a computationally efficient way of acquiring the data and pilot NH code offsets and of reliably performing data bit synchronization.

4.4 Conclusions on GPS L5 Acquisition

Signal acquisition is always a challenging part in the implementation of a standalone GPS receiver since it requires the simultaneous estimation of numerous parameters. This challenge is further exacerbated when long and precise ranging codes (such as the P(Y) or L5 codes) are used. In this context, the L5 signal was merely designed to enable direct cold start acquisition without the C/A code and to facilitate re-acquisition (Spilker & Van Dierendonck 2001).

It has been observed that the direct GPS L5 signal cold start acquisition is greatly affected by the introduction of NH codes on the data and pilot channels. First, the secondary codes constrain the duration of the coherent integration to 1 ms which, in turn, limits the correlation gain achieved during PRN code acquisition. Second, their correlation properties degrade rapidly in the presence of residual Doppler error.

Similarly, it was demonstrated that the separation of the GPS L5 signal power between two orthogonal channels induces some detection performance losses. While the single channel acquisition strategy results in an approximate 3 dB loss (compared to the conventional acquisition of single component signal that would be transmitted with the full L5 power), the combined acquisition approaches can greatly reduce this loss for common C/N_0 but at the cost of an increased computational load. In addition to the power losses induced by the introduction of an L5 dataless channel, the L5 acquisition suffers from increased frontend filtering losses that further reduce the effective C/N_0 of the incoming L5 signals.

However, it is important to bear in mind that GPS L5 acquisition benefits from the increased PRN code cross-correlation protection and improved narrow-band interference mitigation capability of the L5 spreading code.

CHAPTER FIVE: GPS L5 CONSTANT BANDWIDTH TRACKING

This chapter deals with how to efficiently implement constant bandwidth carrier and code tracking of the GPS L5 signal. Constant bandwidth tracking refers, in the framework of this dissertation, to code and carrier tracking loops derived from control theory. This theory has been developed in the analog domain and can only be adapted to the case of a discrete GPS signal within the framework of the continuous update approximation (Ward et al 2006). The discussion that follows is placed within this framework, which limits the range of workable pairs for the values "coherent integration time – loop filter bandwidth". Following the common usage, the code and carrier tracking loops are studied individually, assuming perfect tracking from the other loop. At first, two carrier tracking architectures, namely the *Phase Lock Loop* (PLL) and the *Frequency Lock Loop* (FLL), are described. The main error sources for carrier phase and frequency tracking are reviewed and the tracking performance allowed by the various carrier phase and frequency tracking implementations discussed, confirming the advantages of dataless channels for carrier tracking. Following this discussion, code tracking is investigated. A common code tracking architecture, namely the *Delay Lock Loop* (DLL), is first described and its main error sources are reviewed. Then, the code tracking sensitivity is discussed, and the benefits of pilot tracking highlighted. Finally, the performance of an algorithm that coherently combines the data and pilot channels at the correlator level is assessed in terms tracking accuracy and sensitivity, which is one of the main contributions of this work.

5.1 GPS L5 Carrier Phase Tracking

As discussed in Van Dierendonck (1997), Ward et al (2006) or Misra & Enge (2006), carrier tracking can be performed using either a PLL or an FLL. The main distinction between these loops is that while the FLL aims at producing a zero frequency error (that is, a constant phase error), the PLL aims at generating a zero phase error. As a consequence, FLLs tend to converge faster and to be more robust than PLLs (Ward et al 2006). However, the fact that FLLs do not guaranty a zero phase error also implies that they do not directly allow bit sign recovery and navigation message decoding. Consequently FLL tracking is primarily used as an intermediate step that can ease the transition into a more accurate PLL tracking (Van Dierendonck 1997). Both strategies are nevertheless presented here. To this effect, the following subsections review the general PLL and FLL theories applied to carrier tracking on both data and pilot channels.

5.1.1 General PLL Theory

A generic PLL architecture is given in Figure 5-1. The signal enters the PLL after downconversion, filtering, sampling and signal acquisition. Following code and carrier wipe-off, the in-phase and quadra-phase prompt correlations are passed to a discriminator that estimates the average phase error over the previous integration interval. This phase error estimate is then fed to a low-pass filter that is meant to reduce the noise without removing any useful signal information (such as phase shifts due to dynamic and/or clock jitter). This filtered estimate is finally used to update the local carrier NCO and drive the local carrier replica over the next integration period.
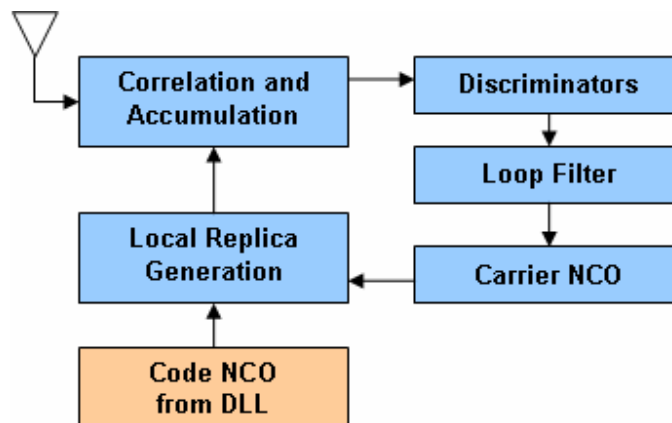
Figure 5-1 – Generic PLL Architecture

The three parameters that critically influence the overall performance of the PLL are the coherent integration time, the discriminator and the loop filter. In this regard the advantage of pilot tracking is two-fold since it enables the use of pure PLL discriminators and/or longer integration times. Nevertheless, in order to provide an insightful comparison between data and pilot tracking the integration time for both PLLs is set to 10 ms (which corresponds to the symbol bit duration on L5). In order to remain within the scope of the continuous update assumption and to design a loop that is insensitive to constant receiver acceleration, a third order loop with 10-Hz one-sided bandwidth (B_L) is implemented. A carrier tracking loop that is insensitive to data modulation is usually called a Costas loop and will be used for tracking on the data channel. The PLL and Costas discriminators selected for pilot and data tracking respectively are the *Coherent* (Coh) and *Dot-Product* (DP) discriminators. They are given as (Ward et al 2006)

$$D_{Coh} = Q_P \tag{5-1}$$

$$D_{DP} = I_P Q_P. \tag{5-2}$$

From the correlation model developed in Section 3.3.2, and assuming no external disturbances, they equal

$$D_{Coh} = \frac{\sqrt{P}}{2}\tilde{R}(\delta\tau)\sin(\delta\phi) \approx \frac{\sqrt{P}}{2}\tilde{R}(\delta\tau)\delta\phi \tag{5-3}$$

$$D_{DP} = \frac{P}{4}\tilde{R}^2(\delta\tau)\sin(2\delta\phi) \approx \frac{P}{2}\tilde{R}^2(\delta\tau)\delta\phi. \tag{5-4}$$

The DP discriminator is insensitive to 180° phase jumps due to symbol bit change since it is based on the product of the in-phase and quadra-phase prompt correlator outputs that will change sign simultaneously if a symbol bit change does occur. It should be noted that, as a result of this multiplication, the DP discriminator tracks twice the carrier phase error which reduces its stability and linearity domains, and introduces several lock points separated from the zero phase error by π radians (which can lead to half cycle slips). Another consequence of that multiplication is that it introduces additional noise terms that can reduce the PLL tracking accuracy and sensitivity.

In light of the above, and as illustrated in Figure 5-2, the main advantage of the Coh discriminator resides in its extended linear tracking region (twice that of the DP discriminator) that, as demonstrated in Julien (2005), can improve the PLL tracking sensitivity by up to 6 dB.
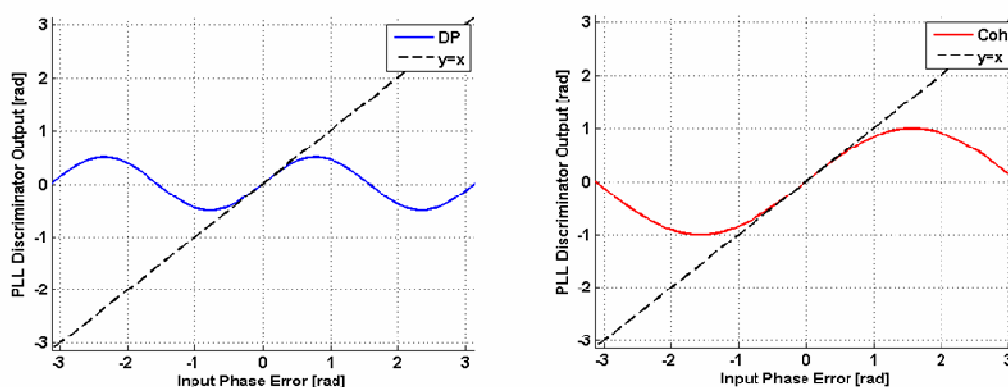
Figure 5-2 – Mean DP and Coh Discriminator Outputs

Another benefit of the Coh discriminator is that it no longer exhibits stable lock points separated from the zero phase error by π radians which implies that it is not subject to half cycle slips. In contrast, the Coh discriminator can only be affected by full cycle slips that do not compromise the parity of the decoded navigation message.

On a final note, the DP and Coh discriminators both require an external normalization to remove the impact of incoming signal power on their respective outputs.

5.1.2 Generic FLL Architecture

The generic FLL architecture is very similar to that of the PLL described above with the major difference that the FLL discriminator relies on in-phase and quadra-phase correlator outputs taken over two consecutive correlation intervals and recombined into dot and cross products, as previously shown in Equations 4.23 and 4.24. These composite correlator outputs are then passed to a discriminator that estimates the average frequency error over the previous integration interval. This frequency error estimate is then low-pass filtered before being used in a feedback loop to drive the local carrier generation over the next integration period. The overall performance of an FLL is essentially

conditioned by the same parameters as the PLL. In order to provide a fair comparison of the two carrier tracking loops, similar settings are chosen for the PLL and the FLL. In other words, the coherent integration time and the one-sided loop filter bandwidth (B_L) are set to 10 ms and 10 Hz respectively. However, since the FLL tracking loop involves, through the discriminator it uses, one more integrator than the PLL, a second-order loop is implemented. An FLL that is insensitive to data modulation will hereinafter be referred to as a Costas loop and will be used for the tracking on the data channel. By analogy with the PLL, the pure FLL and Costas discriminators implemented for pilot and data tracking respectively are the *cross* (Cross) and *Composite Dot-Produc*t (CDP) discriminators. They are given as (Ward et al 2006)

$$D_{Cross} = \frac{cross}{T_I} \tag{5-5}$$

$$D_{CDP} = \frac{cross \times dot}{T_I}. \tag{5-6}$$

From the correlation model developed in Section 3.3.2, and assuming no external disturbances, they equal

$$D_{Cross} = \frac{P}{4T_I}\tilde{R}^2(\delta\tau)\sin(2\pi\delta f T_I) \approx \frac{P}{4}\tilde{R}^2(\delta\tau)2\pi\delta f \tag{5-7}$$

$$D_{CDP} = \frac{P^2}{16T_I}\tilde{R}^4(\delta\tau)\sin(4\pi\delta f T_I) \approx \frac{P^2}{8}\tilde{R}^4(\delta\tau)2\pi\delta f \;. \tag{5-8}$$

Since the CDP discriminator is based on the product of two components (the dot and cross) that change sign simultaneously, it is insensitive to 180° phase jumps due to

symbol bit transition. As a result however, the CDP discriminator tracks twice the frequency error and is affected by additional noise terms.

In contrast, and as illustrated in Figure 5-3, the Cross discriminator possesses an extended linear tracking region (twice that of the CDP discriminator) that, as will be demonstrated hereinafter, can help improve the FLL tracking sensitivity by approximately 6 dB.
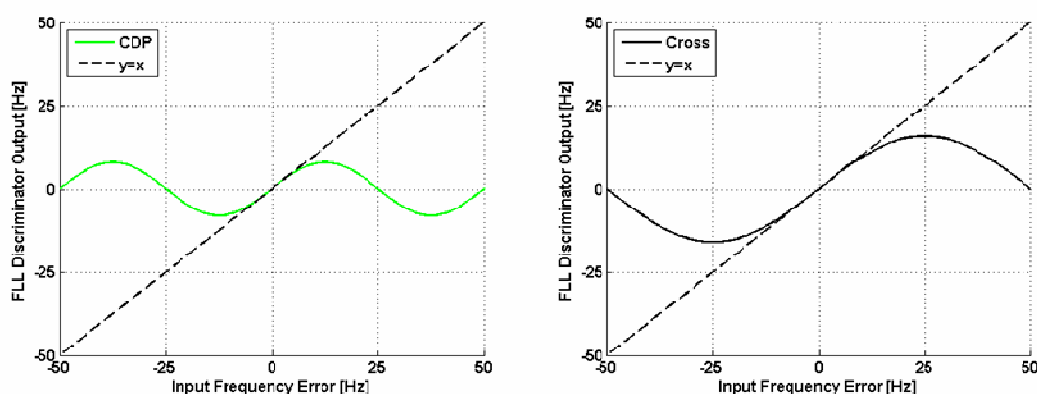
Figure 5-3 – Mean CDP and Cross Discriminator Outputs

On a final note, the CDP and Cross discriminators both require an external normalization to remove the impact of signal power on their respective outputs.

Now that the PLL and FLL architectures have been reviewed, the following subsection briefly introduces the error sources that can affect their performance.

5.1.3 Carrier Tracking Error Source and Sensitivity Analysis

The most important error sources affecting the carrier tracking loop performance are thermal noise, oscillator phase noise, and dynamics. Considering all these error sources, the total PLL jitter and its rule-of-thumb tracking threshold can be expressed as (Ward et al 2006)

$$3\sigma_{PLL} = 3\sqrt{\sigma_{PLL,T}^2 + \sigma_{PLL,A}^2} + \theta_e \le \frac{L_\phi}{4} \qquad\qquad \textbf{(5-9)}$$

where $\sigma_{PLL,T}$, $\sigma_{PLL,A}$ and θ_e are the PLL tracking error due to noise, oscillator phase noise, and dynamics respectively; L_ϕ is the two-sided pull-in range of the phase discriminator that equals π and 2π for the DP and Coh discriminators, respectively.

Considering that the oscillator phase errors remain constant over two consecutive integration intervals, the total FLL jitter and its rule-of-thumb tracking threshold can be expressed as (Ward et al 2006)

$$3\sigma_{FLL} = 3\sigma_{FLL,T} + f_e \le \frac{L_f}{4} \qquad\qquad \textbf{(5-10)}$$

where $\sigma_{FLL,T}$ and f_e are the FLL tracking error due to noise and dynamics respectively; L_f is the two-sided pull-in range of the FLL discriminator that equals $1/2T_I$ and $1/T_I$ for the CDP and Cross discriminators, respectively.

The model for all these error sources can be found, for instance, in Blanchard (1975), Irsigler & Eissfeller (2002), Julien (2005) and Ward et al (2006). Suffice to say here that their impact on carrier tracking accuracy and sensitivity will be conditioned, for both PLL and FLL, by 1) the choice of the discriminator, 2) the design of the loop filter (e.g. order and bandwidth) and 3) the coherent integration time used. It is not possible, however, to jointly minimize the impact of all these error sources. As a consequence, the design of a carrier tracking loop involves some trade-offs. Specifically it has been demonstrated (Ward et al 2006) that smaller loop bandwidths and longer coherent integration times will help reduce the carrier tracking error due to noise. On the other hand, the loop filter

bandwidth should be sufficiently wide to not remove any signal dynamic information (due to dynamics and/or clock jitter), and the coherent integration time should be short enough to ensure good loop response to sudden signal change.

For the sake of clarity, Table 5.1 summarizes the loop parameters used in the framework of this dissertation.

Table 5.1 – Carrier Tracking Loop Parameters

	PLL		FLL	
	Data	**Pilot**	**Data**	**Pilot**
Integration Time	10 ms	10 ms	10 ms	10 ms
Loop Order	3	3	2	2
Loop Bandwidth	10 Hz	10 Hz	10 Hz	10 Hz
Discriminator	DP	Coh	CDP	Cross

Now that the generic data and pilot carrier tracking has been presented, it is interesting to compare the sensitivity and accuracy of these various carrier tracking implementations.

5.2 L5 Carrier Tracking in the Presence of Noise

The first step in evaluating the tracking performance of the various carrier tracking implementations presented above is to look at their behaviour in the presence of white noise only. To this end, the signal power profile shown in Figure 5-4 is applied to the simulated signal, and a static receiver is assumed.
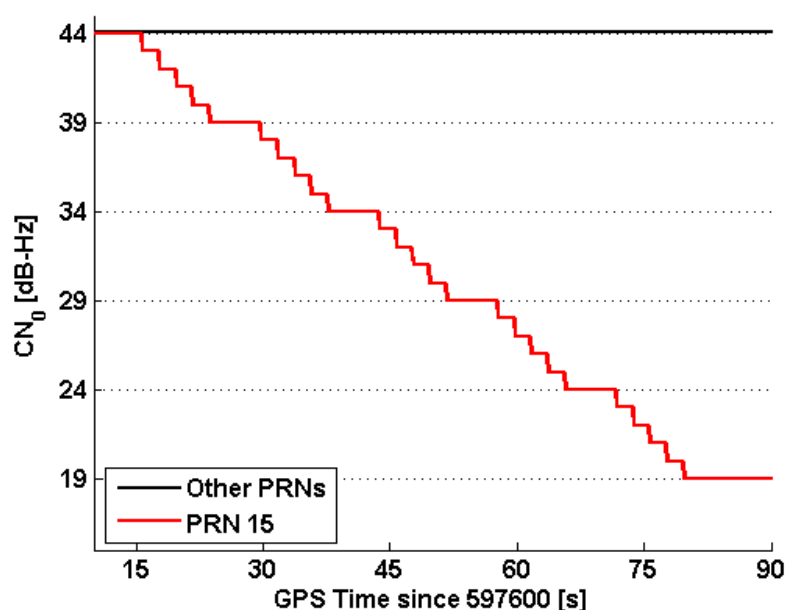
Figure 5-4 – Simulated Equivalent C/N$_0$ Profile for All Simulated Satellites

In this equivalent C/N$_0$ profile, the signal power for PRN 15 is dropped in five 5-dB steps from 44 to 19 dB-Hz. The power of the remaining satellites is held constant at 44 dB-Hz in order to maintain high quality receiver clock bias and clock drift estimates. Examining Figure 5-4, it is important to bear in mind that the C/N$_0$ values shown are those of the full L5 signal. This implies that the effective C/N$_0$ seen by the receiver on the data and pilot channels of PRN 15 will decrease from 41 to 16 dB-Hz.

When evaluating the impact of thermal noise on various tracking implementations, it is interesting to first look at the response of their discriminators to thermal noise stress.

5.2.1 Impact on Mean Carrier Discriminator Outputs

The approach taken herein is purely empirical. Every carrier tracking loop update, the value of the normalized and unfiltered discriminator outputs is recorded. It is then

straightforward to generate the distribution of these discriminator outputs. Since the FLL
and PLL discriminators do not estimate the local carrier replica misalignment at the same
level, their behaviour is studied independently.

PLL Discriminator

The distribution for the normalized Coh and DP discriminator outputs is shown in Figure
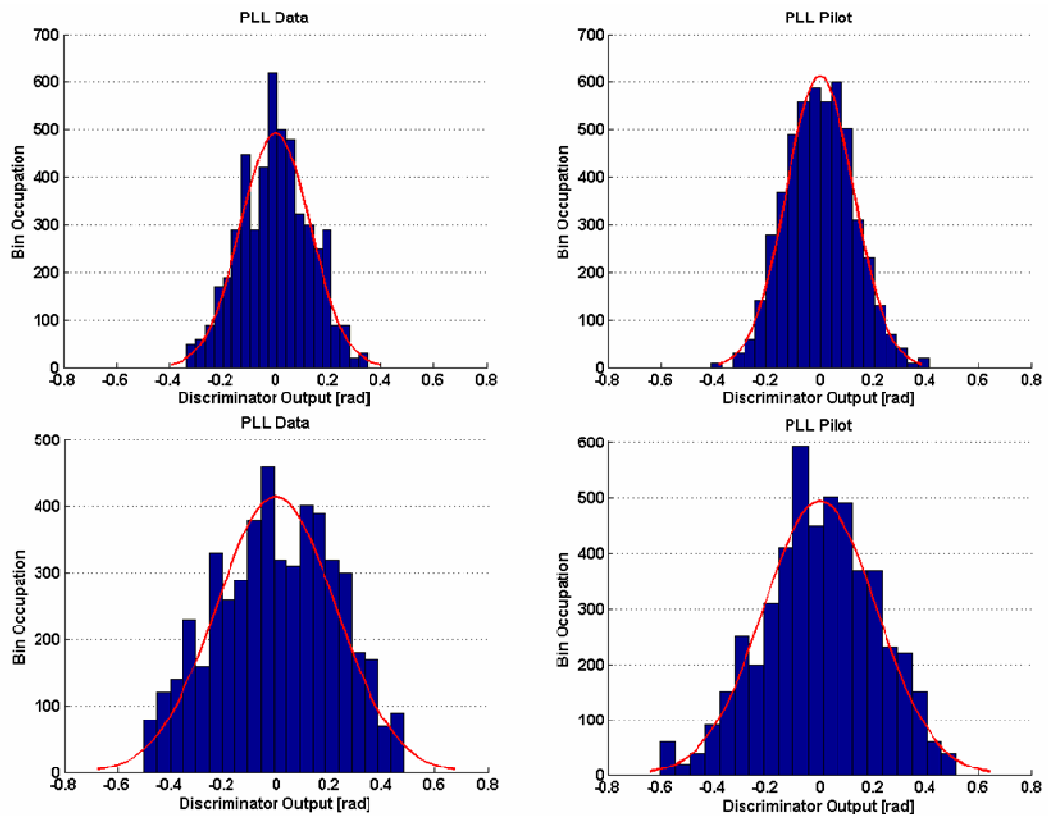5-5, along with a normal envelope, for two values of estimated C/N_0.

**Figure 5-5 - Histogram of the Dot-Product (Left) and Coherent (Right)
Discriminator Outputs for a C/N_0 of 36 (Top) and 31 (Bottom) for a Coherent
Integration Time of 10 ms**

For a 36 dB-Hz C/N_0, the Coh and DP discriminator outputs follow zero-mean Gaussian distributions. This indicates that both discriminators are operating in their linearity range and, therefore, that the tracking is stable. Examining the jitter of these distributions, it is interesting to note that the normalized DP discriminator has a greater jitter than the normalized Coh discriminator. This derives from the fact that the DP discriminator uses the product of the in-phase and quadra-phase correlator outputs while the Coh discriminator only uses the quadra-phase correlator output. As a result of the noise increase, the distributions for both discriminators tend to flatten when the C/N_0 decreases to 31 dB-Hz.

Finally, it is important to note that the DP and Coh discriminator output ranges are bounded and that, when the discriminator output values eventually reach these inherent boundaries, the distributions becoming non-Gaussian. The fact that the normalized Coh discriminator has a wider output range explains its superior resistance to noise compared to the normalized DP discriminator.

FLL Discriminators

Similarly, Figure 5-6 shows the distribution of the normalized Cross and CDP discriminator outputs for the same two values of C/N_0. Their distributions follow the same general trend as those of the normalized Coh and DP discriminators, which implies that the Cross discriminator offers a superior resistance to noise than the CDP discriminator. This is important as it supports the assumption that the presence of a dataless channel can also bring significant improvements to frequency tracking.
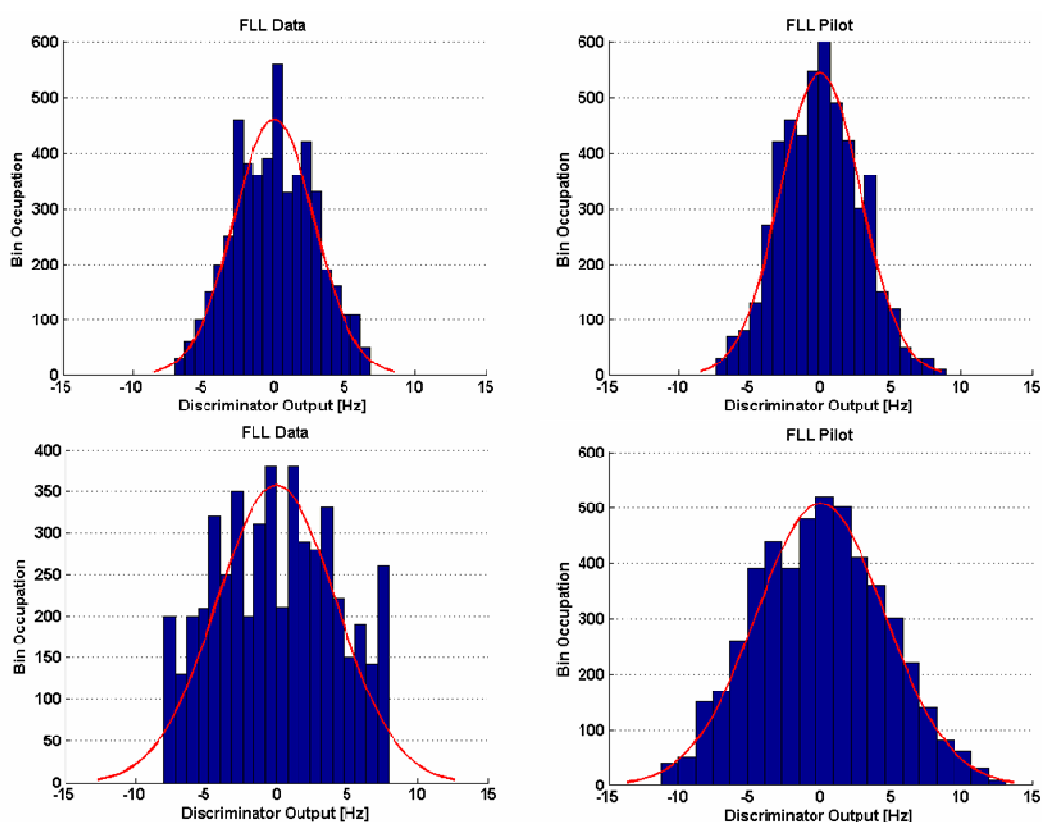
**Figure 5-6 - Histogram of the Composite Dot-Product (Left) and Cross (Right)
Discriminator Outputs for a C/N$_0$ of 36 (Top) and 31 (Bottom) for a Coherent
Integration Time of 10 ms**

Despite these similarities, the FLL discriminators remain more susceptible to thermal
noise stress than the PLL discriminators. This is a consequence of the fact that the FLL
discriminators are based on the multiplication of in-phase and quadra-phase correlator
outputs from two consecutive integration periods.

Now that the behaviour of each discriminator has been investigated, it is interesting to
assess the overall impact of white noise on carrier tracking loop performance.

5.2.2 Impact on Overall Carrier Tracking Accuracy

Accounting for frontend filtering effects, the theoretical PLL tracking error variance due to Gaussian noise when using the DP and Coh discriminators (assuming perfect normalization and perfect code tracking) can be expressed, in radians squared, as (Julien 2005)

$$\sigma^2_{PLL,T,DP} = \frac{B_L\left(1 - 0.5 B_L T_I\right)}{\frac{C}{N_0} . \int_{-B}^{B} G_{L5}(f).df}\left(1 + \frac{1}{2\frac{C}{N_0}T_I\int_{-B}^{B}G_{L5}(f).df}\right) \tag{5-11}$$

$$\sigma^2_{PLL,T,Coh} = \frac{B_L\left(1 - 0.5 B_L T_I\right)}{\frac{C}{N_0}\int_{-B}^{B}G_{L5}(f).df} . \tag{5-12}$$

Because the phase discriminators only use the in-phase and quadra-phase prompt correlator outputs, the filter loss due to frontend filtering has an impact only on the equivalent C/N_0, and since the Coh discriminator does not originate from the product of the correlator outputs, it does not suffer squaring losses. This was already observed in Figure 5-5 and implies that it should perform better at low C/N_0 than the DP discriminator.

Similarly, the theoretical FLL tracking error variance due to Gaussian noise when using the CDP discriminator (assuming perfect normalization and perfect code tracking) can be approximated, in radians squared per second squared, as (Ward et al 2006)

$$\sigma^2_{FLL,T,CDP} = \frac{4FB_L}{T_I^2 \frac{C}{N_0}\int_{-B}^{B}G_{L5}(f).df}\left(1 + \frac{1}{T_I \frac{C}{N_0}\int_{-B}^{B}G_{L5}(f).df}\right) \tag{5-13}$$

where F is 1 at high C/N$_0$, and 2 near threshold.

Since the Cross discriminator is not derived from the product of the composite dot and cross correlator components, it does not suffer from squaring losses and, therefore, can be approximated as

$$\sigma^2_{FLL,T,Cross} = \frac{4FB_L}{T_I^2 \frac{C}{N_0} \int\limits_{-B}^{B} G_{L5}(f).df} .$$

(5-14)

In order to compare the accuracy of the frequency and phase tracking loops, it is possible to design the PLL as a frequency lock loop and, consequently, to derive its frequency estimation error. This was done in Julien (2005) who demonstrated that the frequency error derived from a PLL could be expressed, in radians squared per second squared, as

$$\sigma^2_{PLL,T,f} = \frac{\kappa(B_L).4\pi^2.B_L^2}{3} \sigma^2_{PLL,T}$$

(5-15)

where κ is a constant that depends on the loop filter bandwidth and approximately equals 4 for a 10 Hz loop filter bandwidth.

The frequency estimation error in white noise derived from Equations 5.11 to 5.15 for an L5 carrier tracking loop using a 10 Hz loop filter and a 10 ms coherent integration time is shown in Figure 5-7 for both FLL and PLL implementations. The PLLs are expected to produce frequency estimates that are significantly more accurate than the ones originating from the FLLs. Similarly the Coh and Cross discriminators are expected to respectively outperform the Cross and CDP discriminators for C/N$_0$ values below 30 dB-Hz.
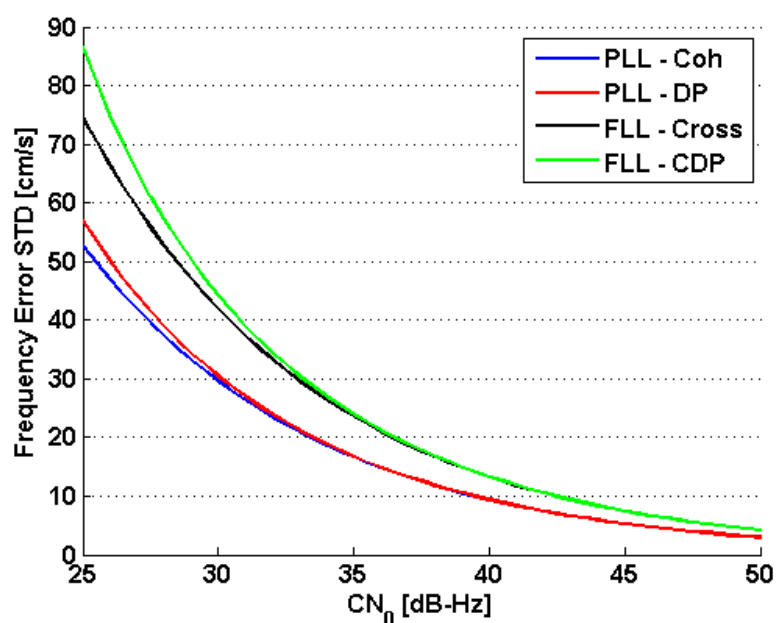
Figure 5-7 – Frequency Tracking Error in White Noise

In addition to enabling direct comparison of the FLL and PLL resistance to white noise, the results shown in Figure 5-7 illustrate 1) the typical frequency error of the Doppler measurements derived from the carrier tracking loops, 2) the accuracy of the carrier aiding used for code tracking, and 3) the amount of power attenuation that the correlator outputs will undergo during carrier wipe-off due to frequency inaccuracies.

To confirm these theoretical results, Figure 5-8 shows the estimated *Standard Deviation* (STD) of the Doppler measurement derived from the four phase and frequency tracking loops discussed above. It is important to note that the effects of satellite and receiver clock errors have been removed from the Doppler measurements prior to any STD estimation. This implies that stored satellite clock corrections were applied to the Doppler measurement derived from the data and pilot FLLs.
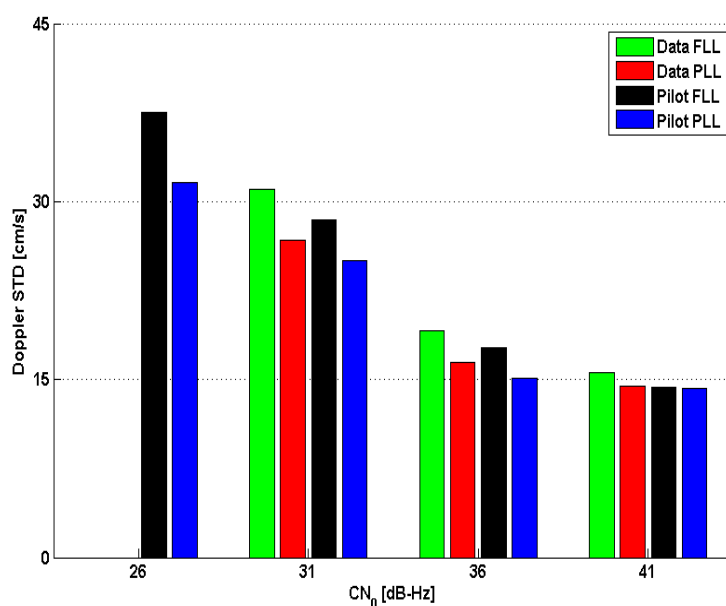
Figure 5-8 – Estimated Doppler STD versus C/N$_0$ for Various Carrier Tracking Implementations

In agreement with the theoretical results shown in Figure 5-7, the Doppler measurements derived from pilot tracking are less noisy than the ones derived from data tracking. Similarly, the Doppler measurements obtained from frequency tracking are noisier than the ones obtained from phase tracking. However, it is interesting to note that for high C/N$_0$, the difference between phase and frequency tracking is not as high as expected from the theory. It is however important to remember that the values shown in Figure 5-7 are obtained assuming perfect code tracking and perfect normalization. In the presence of code tracking and normalization imperfections, the performance gap between phase and frequency tracking can be expected to diminish.

Now that the impact of white noise on carrier tracking accuracy has been assessed, it is of major interest to investigate its effect on carrier sensitivity.

5.2.3 Impact on Overall Carrier Tracking Sensitivity

To illustrate the sensitivity of the various carrier tracking implementations, Figure 5-9 shows the estimated Doppler frequency obtained when the receiver is "forced" into each of these tracking modes (this implies, for instance, that no attempts are made by the receiver to re-acquire the satellite, even when its lock detectors go below the authorized thresholds).
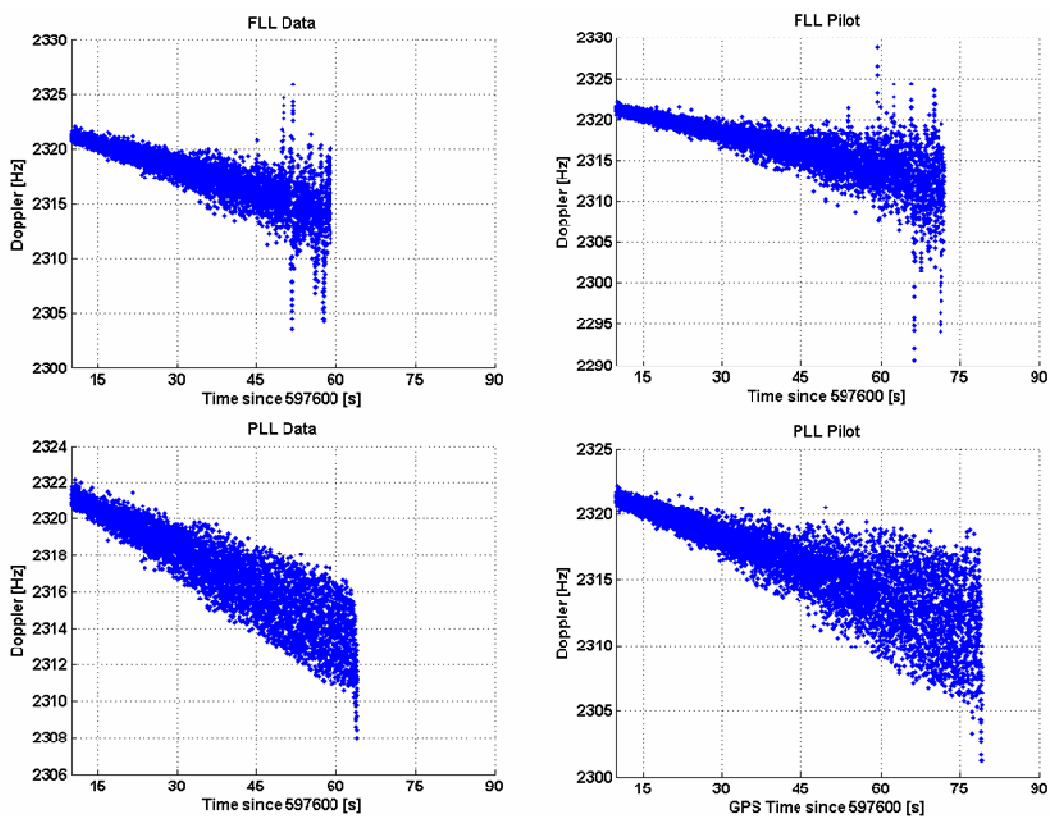

Figure 5-9 – Estimated Doppler for the Data (Left) and Pilot (Right) Only Frequency (Top) and Phase (Bottom) Tracking Loop

Comparing the signal power profile shown in Figure 5-4 with the estimated Doppler frequencies shown in Figure 5-9, it can be inferred that, for this data set, the data and pilot FLLs lose lock at approximately 25 and 20 dB-Hz, respectively. For the data and

pilot PLLs, these values drop to 22 and 17 dB-Hz, respectively. These values closely match the theory since Equation 5.10 approximates the data and pilot FLL tracking thresholds at approximately 24 and 19 dB-Hz, respectively; and Equation 5.9 approximates the data and pilot PLL tracking thresholds at approximately 23 and 18 dB-Hz, respectively. It is interesting to note that the tracking threshold values obtained empirically are 1 or 2 dB below the expected theoretical values. It should be noted, however, that while the theoretical values indicate the C/N_0 at which the tracking can no longer be considered reliable, the empirical values are taken when the tracking loops effectively lose lock.

When comparing data and dataless carrier tracking implementations, it can be seen that the sensitivity gain enabled by using pure rather than Costas discriminators is approximately 5 dB. Besides, this value does not account for the fact that longer integration time could be used on the pilot channel to further reduce the impact of noise on the correlator outputs and, therefore, bring the pilot tracking threshold even lower. This approach, however, must be used with care since the use of very long coherent integration might hamper, for stand-alone receivers, the tracking loop reaction to receiver dynamics and/or oscillator frequency noise.

Figure 5-9 also shows that for a static receiver the phase tracking threshold is approximately 3 dB lower than the frequency tracking threshold for both data and pilot implementations. It is important to bear in mind that this result was obtained by carefully differentiating the behaviour of data-only and pilot-only tracking implementations for both the FLL and PLL. Because FLLs are more commonly used as an intermediate tracking step, the distinction between data and pilot tracking, although common for PLLs,

is rarely made for FLLs. It is then possible, when comparing the sensitivity of the data PLL with that of the pilot FLL, to erroneously conclude that frequency tracking offers lower tracking thresholds than phase tracking. In light of the above, and considering that FLL tracking does not enable navigation message decoding, the use of pure frequency tracking is not recommended beyond its common use as an intermediate tracking step. Each data set being unique, the results given here are not meant to establish hard recommendations but rather to illustrate the general trends observed for carrier tracking in the presence of white noise.

Now that the impact of white noise on carrier tracking accuracy and sensitivity has been assessed, it is of major interest to evaluate the impact of oscillator frequency noise and dynamics on phase tracking accuracy.

5.3 L5 Carrier Tracking in the Presence of Oscillator Frequency Noise and Dynamics

As explained in Section 3.1.5, oscillator frequency noise is the result of the instability of the oscillator central frequency that produces some phase jitter at the local carrier replica level. For a third order loop, the tracking error variance due to oscillator phase noise can be expressed, in radians, as (Blanchard 1975)

$$\sigma_{PLL,A}^2 = 2\pi^2 f_{Osc}^2 \left(\frac{\pi^2 h_{-2}}{3\omega_L^3} + \frac{\pi h_{-1}}{3\sqrt{3}\omega_L^2} + \frac{\pi h_0}{6\omega_L} \right) \tag{5-16}$$

where f_{Osc} is the natural frequency of the oscillator and $\omega_L \cong 1.7 B_L$ for a third-order loop. Figure 5-10 shows the phase estimation error due to oscillator frequency noise.
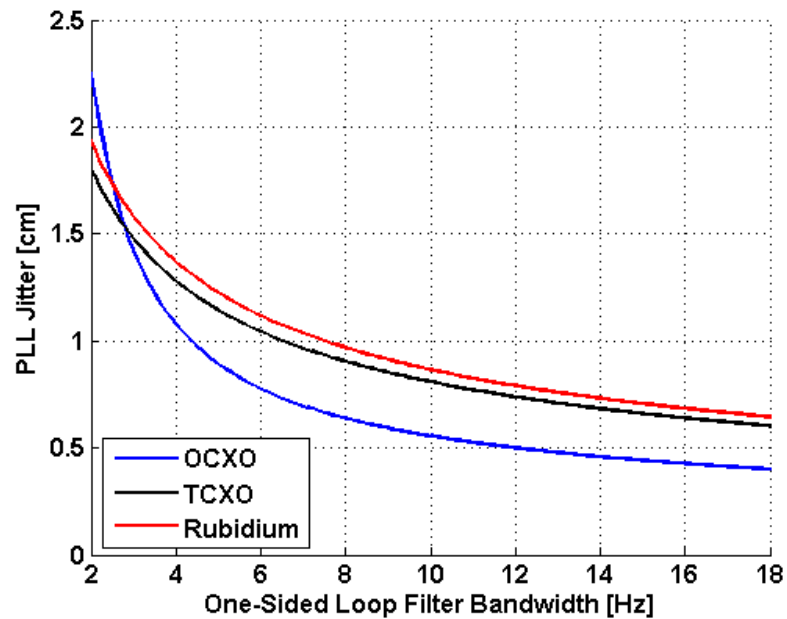
Figure 5-10 – Frequency Error Jitter Due to Oscillator in Third-Order PLL at L5

The oscillator frequency noise in a third-order PLL is at the sub-centimetre level for OCXO, TCXO and rubidium oscillators. Amongst these oscillators, and with the filter bandwidth used, the oscillator that provides the lowest phase jitter is the OCXO followed by the TCXO and the rubidium, with differences at the millimetre level.

To confirm these theoretical results Figure 5-11 shows the estimated Doppler measurement STD derived at various C/N_0 values from the data and pilot PLLs when data sets are collected using either of these oscillators as an external *Frequency and Time Standard* (FTS).
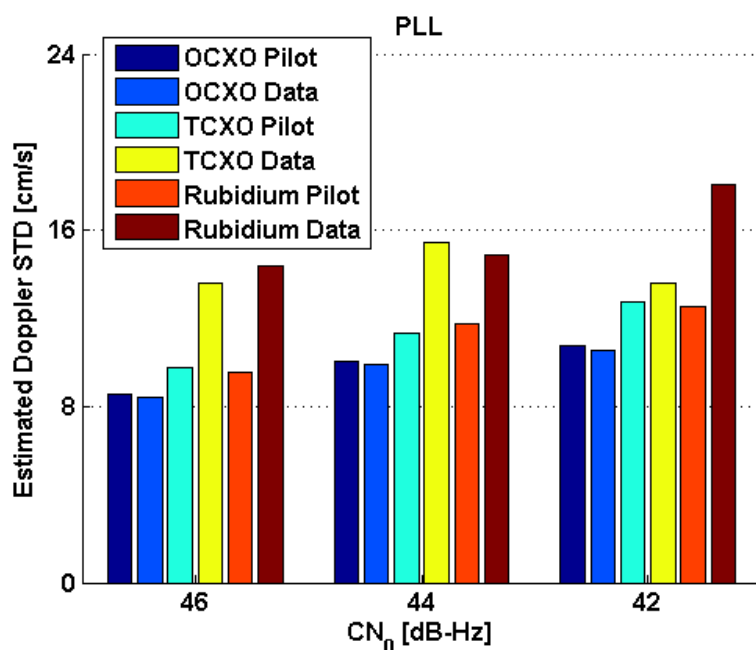
Figure 5-11 - Estimated Doppler STD versus C/N$_0$ using Various External Oscillator References and PLL Implementations

In agreement with the theory, the oscillator that offers the highest accuracy is the OCXO, followed by the TCXO and Rubidium. It is important to note that the variations observed across the various C/N$_0$ do not result from variations in the oscillator frequency noise but rather depend on the level of thermal noise experienced by the PLL.

Due to the short wavelength of the GPS L5 signal (~25 cm), the PLL will be very susceptible to user dynamics since it can rapidly lead to an error greater than the stable tracking domain boundaries, thereby provoking cycle slips. In order to track most dynamics without bias, higher order loops are preferred. Third order loops are commonly used for GNSS PLLs and should only be affected by jerk and higher order dynamics. For a third order loop, the tracking error variance due to dynamics can be expressed, in radians, as (Blanchard 1975)

$$\theta_e(t) = 2\pi \frac{\dfrac{dR^3}{dt^3}}{\omega_L^3} \tag{5-17}$$

where $\dfrac{dR^3}{dt^3}$ is the LOS jerk stress expressed in cycles per second.

To analyse the influence of receiver dynamics on carrier tracking, a kinematic data set is required. To this end, the receiver is set to travel eastward with a constant velocity of 5 m/s (after a static period and a short acceleration). While this motion profile does not include any jerk or higher order dynamics, it can provide a useful insight into the effective resistance of the phase tracking loop to second order dynamics.

Figure 5-12 shows the estimated three-dimensional velocity STD obtained when data and pilot PLLs are used to track the satellites seen by a static and a kinematic receiver.
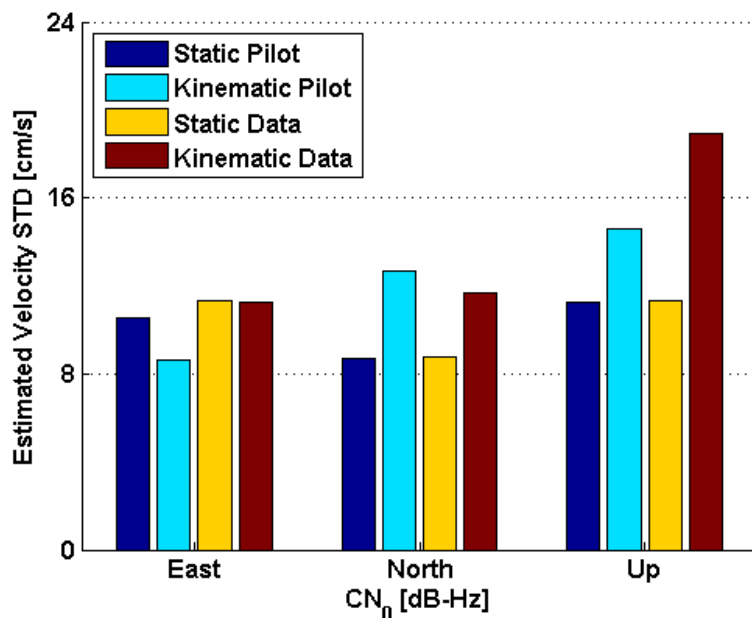

Figure 5-12 - Estimated Three-Dimensional Velocity STD for Static and Kinematic Receivers using Various PLL Implementations

Figure 5-12 shows that even though the third order carrier tracking loop can easily accommodate acceleration dynamics, the resulting velocity estimates get noisier when the receiver is moving.

Following this discussion on L5 carrier tracking it is important to study the performance of L5 code tracking since it is the code tracking loop that provides the user with the robust pseudorange measurements than are commonly used in the navigation filter to estimate the receiver position.

5.4 GPS L5 Code Tracking

As discussed in Van Dierendonck 1(997), Ward et al (2006) and Misra & Enge (2006), code tracking is commonly performed using a DLL.

5.4.1 Generic DLL Architecture

A typical DLL architecture is shown in Figure 5-13. The principle of a DLL is very similar to that of a PLL. The main distinction between these loops is that, in addition to the prompt correlators' output, the DLL also uses early and late correlators' output. The latter are obtained by correlating the incoming signal with local code replicas that have been advanced or delayed by $\Delta/2$ chip (where Δ was introduced in Section 4.3.3 as the code discriminator *Early-Late Spacing* (ELS)). After code and carrier wipe-off, the early, prompt and late correlator outputs are passed to a discriminator that estimates the code phase error over the previous integration interval. This estimate is then low-pass filtered and used in a feedback process to drive the local code NCO and local code generation over the next integration interval. It is important to note that since the effects of relative

satellite-receiver motion will affect both carrier and code components of the incoming signal, it is possible to use the carrier tracking loop to aid the code tracking loop. In order to do so, the Doppler frequency estimate derived from the PLL is scaled down (with factor 115) to the chipping rate frequency. In this way, the dynamics and oscillator effects no longer need to be tracked by the DLL which is therefore only affected by noise and code-carrier ionosphere divergence effects.
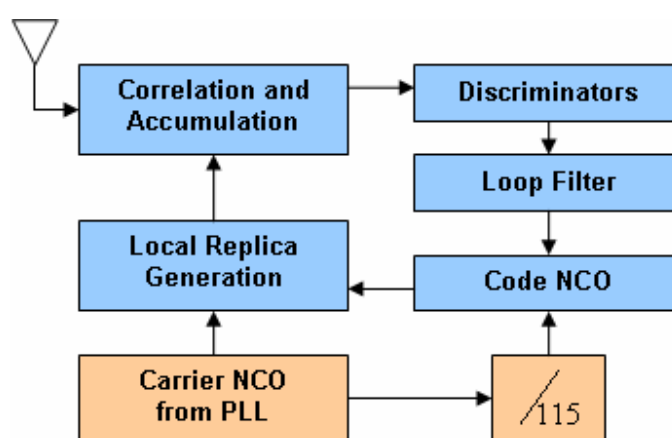
Figure 5-13 – Schematic DLL Architecture

Similarly to the carrier tracking loops, the code tracking loop performance is critically influenced by the coherent integration time, the discriminator and the loop filter. However, the distinction between data and pilot discriminators no longer need to be made in the context of code tracking since the presence of unknown symbol bit transition does not affect the DLL discriminators. The advantage of pilot tracking then primarily resides in the potential use of long coherent integration times. The most important parameter in designing a code discriminator is the choice of an appropriate ELS. Indeed, as shown by Van Dierendonck et al (1992), the *Narrow Correlator*[TM] technology (NC[TM]) that implements narrow early-late spacing can improve the discriminator resistance to noise

and multipath. However, due to the frontend filtering limitations discussed in Section 3.3.2, spacing narrower than one chip cannot be implemented on L5. A one-chip spacing is therefore used herein. Several discriminators and normalizations were investigated; in order to enhance the code tracking loop inherent resistance to noise a *Dot-Product* (DP) discriminator with an Early-plus-Late normalization is implemented herein. Considering that in the presence of carrier aiding the main objective of the code tracking loop filter is to mitigate noise effects, a first-order loop filter with 1-Hz one-sided bandwidth (B_L) is used. Finally, in order to be consistent with the carrier tracking loop update rate, the coherent integration time is set to 10 ms.

The (DP) discriminator is given as (Ward et al 2006)

$$D_{DP} = (I_E - I_L)I_P + (Q_E - Q_L)Q_P. \tag{5-18}$$

From the correlation model in Section 3.3.2, and assuming no external disturbances, it equals

$$D_{DP} = \frac{P}{4}\left(\tilde{R}\left(\delta\tau - \frac{\Delta}{2} \right) - \tilde{R}\left(\delta\tau + \frac{\Delta}{2} \right) \right)\tilde{R}(\delta\tau). \tag{5-19}$$

In essence, code tracking is based on the measure of the difference between the early and late correlation values that are meant to be situated on each side of the correlation peak. Accordingly, to derive the discriminator output values, the two following assumptions must be made: 1) the code phase error is less than half of the early-late spacing, and 2) the early and late correlator values belong to the auto-correlation function main peak.

Under these assumptions and supposing that an infinite frontend filter is used (or, equivalently, that the auto-correlation function main peak is a perfect triangle), Equation 5.19 can be approximated as (Ray 2005)

$$D_{DP} \approx \frac{P}{2}\left(1 - |\delta\tau|\right)\delta\tau ,$$ **(5-20)**

which shows that the DP discriminator's output depends on both incoming signal power and input error. To eliminate these dependencies, an early-plus-late normalization is used

$$N = \left(I_E + I_L\right)I_P + \left(Q_E + Q_L\right)Q_P \approx \frac{P}{4}\left(2 - \Delta\right)\left(1 - |\delta\tau|\right),$$ **(5-21)**

which gives the following expression for the normalized discriminator $\overline{D}_{DP}$

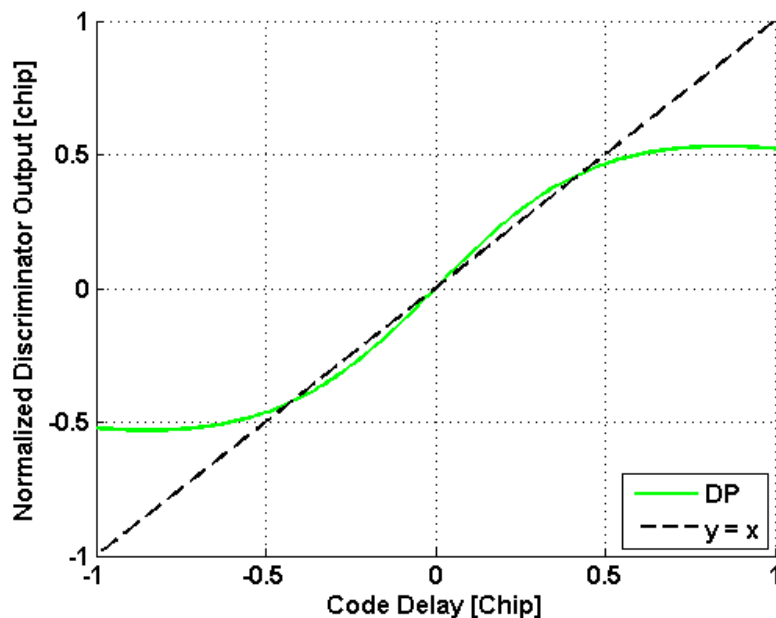$$\overline{D}_{DP} = \frac{(2 - \Delta)D_{DP}}{2N} = \delta\tau$$ **(5-22)**

Figure 5-14 – Normalized DP discriminator Output Using a One Chip ELS

This normalized discriminator is shown in Figure 5-14, and can be seen to be the exact unbiased estimate of the code delay input error over ± 0.5 chips.

Outside this region, this discriminator offers a less favourable behaviour as it tends to always underestimate the code tracking error. This can make tracking perilous as it implies that the receiver will be unable to correct a growing error. However, the use of a wide ELS and of a very precise carrier aiding should help reduce the impact of dynamics on code tracking and limit the occurrence of such problems.

5.4.2 Code Tracking Error Sources and Sensitivity

Considering that the dynamic stress and oscillator errors are absorbed by the carrier aiding, the most important errors affecting the DLL are thermal noise (with standard deviation $\sigma_{DLL,noise}$) and multipath. It is important to note, however, that the tracking error introduced by multipath does not directly affect the code tracking sensitivity. In fact, multipath-induced tracking errors can be seen as biases that will shift the DLL discriminator stable lock point away from where it should be; however, they do not increase the tracking jitter. Considering this, the total DLL jitter and its rule-of thumb tracking threshold can be expressed as (Ward et al 2006)

$$3\sigma_{DLL} = 3\sigma_{DLL,noise} \leq \frac{\Delta}{2}. \tag{5-23}$$

Now that the generic code tracking has been presented, it is interesting to study its performance in the presence of noise and multipath.

5.5 L5 Code Tracking in the Presence of Noise

In order to assess the impact of white noise on code tracking, the approach followed herein is both theoretical and empirical.

5.5.1 Impact on Overall Code Tracking Accuracy

Accounting for frontend filtering effects, the theoretical DLL tracking error variance due to Gaussian noise when using a DP discriminator (assuming perfect normalization and perfect carrier tracking) is given, in seconds squared, as (Julien 2005)

$$\sigma^2_{DLL,DP} = \frac{B_L.\left(1-\frac{1}{2}.B_L.T_I\right).\int_{-B}^{B}G_{L5}(f)\sin^2(\pi.f.\Delta)df}{\frac{C}{N_0}.\left(2\pi.\int_{-B}^{B}f.G_{L5}(f)\sin(\pi.f.\Delta)df\right)^2}.\left(1+\frac{1}{\frac{P}{N_0}.T_I.\int_{-B}^{B}G_{L5}(f).df}\right). \quad \textbf{(5-24)}$$

Equation 5.24 shows that the code tracking error variance depends on the five following parameters: 1) the shape of the spreading sequence PSD, 2) the frontend filter bandwidth, 3) the early-late spacing, 4) the incoming signal C/N_0, and 5) the coherent integration time. It can be seen that spreading sequences with wider PSD (or, equivalently, with sharper and narrower correlation peak) will tend to enable more accurate code tracking. Similarly, for a given spreading sequence, longer coherent integration time, wider frontend filtering and narrower ELS will produce a smaller code tracking error.

The standard deviation of the code delay estimation in white noise derived from Equations 5.24 for a DP discriminator and a 1 Hz one-sided loop filter bandwidth is shown in Figure 5-15 for various coherent integration times. It is expected that the use of longer coherent integration times will help reduce the code tracking error variance. To this end, the presence of a dataless channel is of major interest since it implies that the

only mechanism that limits the duration of the coherent integration is the power degradation due to frequency errors.
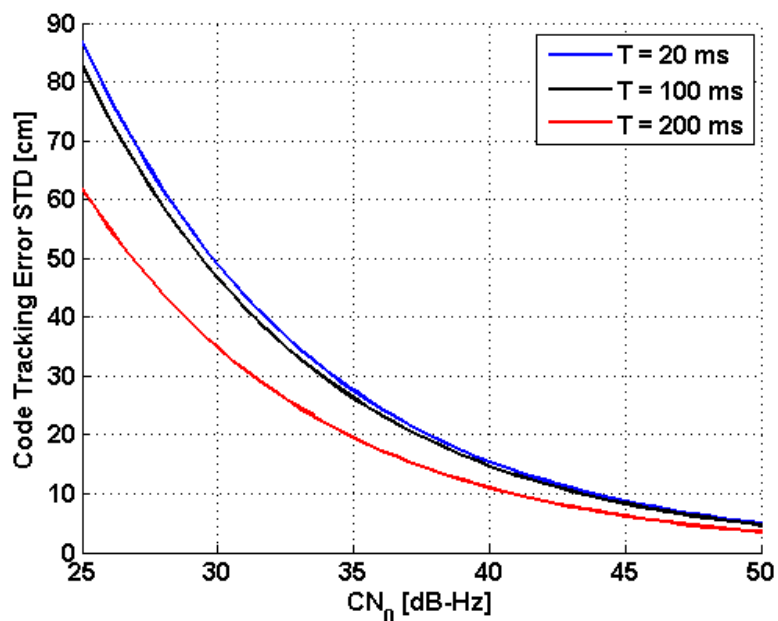
Figure 5-15 – Code Tracking Error in White Noise

The easiest way to constrain these frequency errors is to use shorter coherent integration times on the carrier tracking loop. Mismatched code and carrier tracking loop update rates can easily be implemented as long as the code update rate is an integer multiple of the carrier update rate. Besides, it is important to bear in mind that if carrier aiding of the code tracking loop is implemented, an update of the carrier tracking loop will also result in some code NCO adjustments.

To confirm these theoretical results, Figure 5-16 shows the estimated STD of the pseudorange measurements obtained for various coherent integration times.
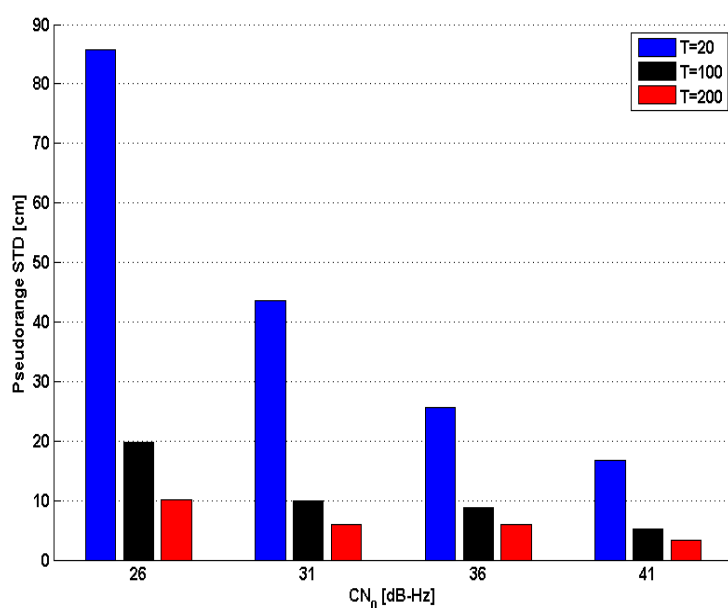
Figure 5-16 - Estimated Pseudorange STD versus C/N$_0$ for Various Code Coherent Integration Time

The effects of satellite and receiver clock errors have been removed from the pseudoranges' STD shown in Figure 5-16. As expected, the pseudoranges get more accurate when longer coherent integration times are used. The STD values obtained using a 20 ms coherent integration time closely follow those predicted by the theory. However, for longer coherent integration time, the empirical STD values shown tend to become overly optimistic, especially at low C/N$_0$.

5.6 L5 Code Tracking in the Presence of Multipath

Insightful multipath environments being extremely hard to simulate, the approach taken here to assess the effect of multipath on code tracking accuracy is purely theoretical. To this end, the impact of multipath on code tracking is often represented as an error

envelope representing the maximum error resulting from a single multipath with a certain phase, delay and amplitude. In order to define the error induced by a given multipath, the common approach is to find the discriminator stability point (that is, the point where the discriminator output crosses the origin) in the presence of this multipath.

Figure 5-17 shows the L5 code error tracking using a DP discriminator, and assuming two different values of *Signal-to-Multipath Ratio* (SMR)
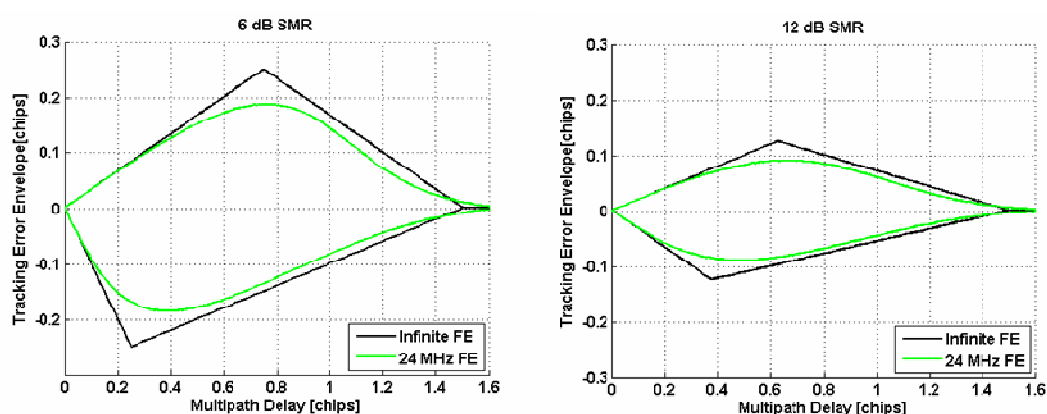
Figure 5-17 – Code Tracking Error Envelope for a 1 chip ELS and Assuming a Single Multipath with an SMR of a 6 (Left) and 12 dB (Right)

As anticipated, the L5 code is insensitive to multipath with delays longer than 1.6 chips (or, equivalently, 45 m). This tremendous improvement, compared to the C/A code is a direct consequence of the fast chipping rate used on L5. However, it is important to note this improvement is limited by the necessary use of code discriminators with wide early-late spacing that have poorer inherent multipath mitigation capacities than narrow ELS. When compared to the thermal noise impact on code tracking studied in Section 5.5, and illustrated in Figure 5-15, it can be seen that specular multipath is a very serious source of code tracking error.

5.7 Data/Pilot Combining

Sections 5.2 and 5.5 above demonstrated that in terms of both carrier and code tracking, the use of a dataless channel could bring significant improvements in terms of accuracy and sensitivity. It would however be possible to further improve the overall L5 tracking accuracy by implementing a data/pilot combined tracking. This was done, at the PRN-only tracking stage, using a weighted sum of the data and pilot discriminator outputs. However, once the NH alignment has been performed, data/pilot combining must be performed with care so as to jointly benefit from the reliability of pure pilot tracking, and the accuracy of combined tracking. To this end, Julien (2005) introduced several discriminator combinations. These combinations, however, provided a diminishing return with decreasing C/N_0 (i.e. when they were the most needed). Because of such restrictions, Ries et al (2002) and Bastide (2004) recommended pure pilot tracking. This approach, however, reduces the available power by 3 dB. In light of the above, a better combining strategy is desired. As mentioned by Yang et al (2004) and Mongrédien et al (2006), in tracking mode the data and pilot channels can be combined at three different stages to drive a single carrier NCO: at the discriminator output, at the loop filter output or at the correlator output. The latter approach is expected to provide the best noise mitigation performance since it recombines the independent data and pilot noise components prior to any non-linear operations and is therefore implemented herein. The concept of coherent correlator level data/pilot combining was already introduced in Section 4.2.2 for signal acquisition purposes. For clarity, Figure 5-18 illustrates it in the context of signal tracking. After Doppler removal and spreading code wipe-off, the data and pilot correlator outputs are either aligned (Figure 5-18a) or in phase opposition (Figure 5-18b).

It is then possible to recombine them according to either scenario and select the one with the highest amplitude. The correlators thus obtained are hereinafter referred to as combined correlators.
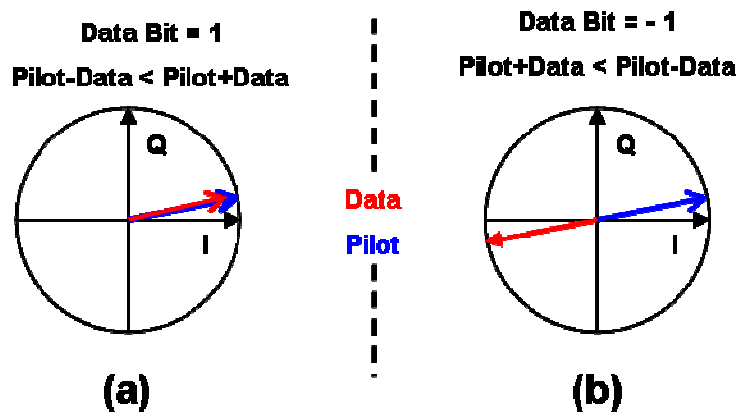
Figure 5-18 – Data/Pilot Coherent Combining

Equivalently, they can be expressed as

$$\Psi_{Comb} = \Psi_{Pilot} + sign(D_d).\Psi_{Data} \tag{5-25}$$

where Ψ is the correlator output (in-phase or quadra-phase) of the subscripted quantity.

It is important to note that this procedure is equivalent to estimating the sign of the symbol bit and removing its effect on the data correlators. The combined correlators thus obtained recombine the full signal power and can be considered free of symbol bit transitions. The risk of selecting the wrong data/pilot coherent combination (or, equivalently, the wrong symbol bit sign) is low for common values of C/N_0. Besides, this approach can help reduce the complexity of the L5 tracking loop as a single discriminator and a single loop filter will be required to process the data and pilot correlator outputs in the code and carrier tracking loops.

Now that the coherent correlator combining strategy has been reviewed, it is interesting to assess its performance in terms of code and carrier tracking accuracy and sensitivity.

5.7.1 Data/Pilot Combined Tracking Accuracy

In order to evaluate the code and carrier tracking accuracy of the proposed data/pilot combined tracking in static mode, the signal power profile shown in Figure 5-4 is used. To provide a fair comparison of the data only, pilot only and data/pilot tracking implementations, the coherent integration time is set to 10 ms for all strategies. Figure 5-19 shows the estimated pseudoranges and Doppler STD derived from single and combined channel tracking strategies. As expected, combined tracking outperforms single channel tracking in terms of pseudorange and Doppler measurement accuracy for the entire range of C/N_0 values investigated. It is important to note that the data-only tracking implementation loses lock at approximately 26 dB-Hz. This explains why the Doppler and pseudorange STDs are unavailable for data tracking at this C/N_0 value.
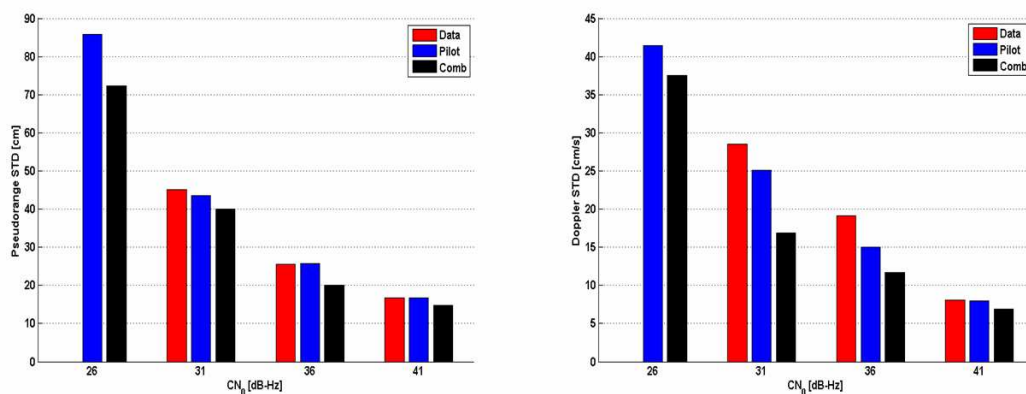
Figure 5-19 - Estimated Pseudorange (Left) and Doppler (Right) STD versus C/N_0 for Various Channel Tracking Implementations

In terms of single channel tracking performance, pilot-only tracking provides more accurate Doppler and pseudorange measurements than data-only tracking, even though the improvement is rather marginal in terms of pseudoranges. As previously explained, in the context of code tracking accuracy, the main advantage of pilot tracking resides in the use of longer coherent integration times, which is not done here.

5.7.2 Data/Pilot Combined Tracking Sensitivity

To illustrate the sensitivity of the proposed data/pilot combined tracking, Figure 5-20 shows the estimated Doppler frequency derived, in static mode, from single and combined carrier tracking strategies.
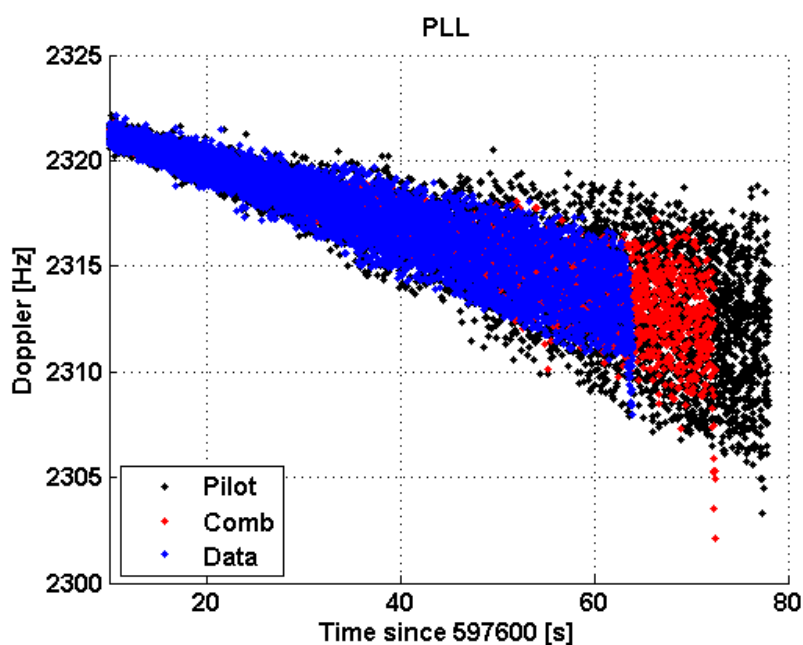
Figure 5-20 - Estimated Doppler for the Data Only, Pilot Only and Data/Pilot Combined Carrier Tracking Loop

Comparing the signal power profile shown in Figure 5-4 with the estimated Doppler frequencies shown in Figure 5-20, it can be inferred that, for this data set, the tracking

sensitivity of the data/ pilot combined PLL is approximately 23 dB-Hz. When expressed with respect to the full signal power, the tracking sensitivity of the data and pilot only PLLs are to 26 and 21 dB-Hz respectively.

It is important to note that, for low C/N_0 values, symbol bit recovery becomes unreliable, which explains why the data/pilot combined tracking threshold falls between those of the data and pilot channels. The results shown in Figure 5-19 and Figure 5-20 illustrate the trade-off that has to be drawn between reliability and accuracy when the L5 data and pilot channels are coherently recombined at the correlator level.

CHAPTER SIX: GPS L5 KALMAN FILTER-BASED TRACKING

This chapter presents a discussion on the advantages of *Kalman filter*-based (KF) tracking applied to the GPS L5 signal. KF tracking was originally introduced to overcome some of the GPS C/A signal limitations in terms of acquisition and tracking sensitivity, and to enable GPS receiver operations in environments where previously impossible (Psiaki & Jung 2002, Humphreys et al 2005, Yu et al 2006). Later research also demonstrated the ability of KF tracking to produce high quality carrier phase measurements at the L1 frequency (Petovello & Lachapelle 2006), and therefore, established its interest for high-accuracy applications. However, to date, no attempts have been made, in the context of high-accuracy, to apply KF tracking to the L5 signal. In light of the above, this chapter intends to assess the advantages of the KF implementation applied to the L5 signal in terms of tracking accuracy and sensitivity. After a thorough description of its theoretical basis, the performance of KF tracking is discussed in terms of code and carrier tracking. Finally the advantages of KF tracking are confirmed at the position level, which is one of the main contributions of this dissertation.

6.1 Kalman Filter Overview

Section 3.3.3 reviewed the basic concepts of the *Least Squares Adjustment* (LSA) process for use in parametric estimation. This approach is limited to estimating the unknown parameters based on measurements only. However, when some knowledge of the system behaviour over time is available, a better estimate of the unknown parameters can be obtained.

6.1.1 Estimation of Dynamic Systems

Specifically, if the state vector x is known to relate to the observation vector z through

$$z_k = H_k x_k + v_k \tag{6-1}$$

and to behave as

$$\dot{x}(t) = F(t)x(t) + G(t)w(t) \tag{6-2}$$

where the dot represents a time derivative, t is the time variable, F is the dynamics matrix which describes the dynamics of the system, G is the shaping matrix which shapes the white input noise, and w is a vector of zero-mean white noise with Gaussian distribution, then a Kalman filter can be used to optimally estimate the desired parameters using both available measurements and assumed system dynamics.

The Kalman filtering process is a recursive algorithm that uses a series of measurement and prediction steps to obtain an optimal estimate of the state vector. It is a commonly used technique that is widely discussed in the literature (Gelb 1974, Brown & Hwang 1992). The following discussion, based on Gelb (1974), reviews the final form of the discrete-time algorithm. Using the measurement model in Equation 6.1 and under the additional assumption that v_k is a zero-mean white noise with Gaussian distribution, an updated estimate of the state vector and its covariance can be obtained as

$$\hat{x}_k^+ = x_k^- + K_k v_k \tag{6-3}$$

$$C_{xk}^+ = \left(I - K_k H_k \right) C_{xk}^- \tag{6-4}$$

where the superscript "-" and "+" indicate a quantity before and after measurement update respectively, K is the Kalman gain matrix given by

$$K_k = C_{xk}^- H_k^T \left(H_k C_{xk}^- H_k^T + C_{zk} \right)^{-1} \tag{6-5}$$

and v is the innovation sequence given by

$$v_k = z_k - H_k x_k^-. \tag{6-6}$$

The innovation sequence can be viewed as the amount of new information brought into the system by the measurements. The Kalman gain can be interpreted as a weighing factor that compares the quality of the measurements against that of the current state estimate and then determines the amount of new information that should be accepted by the system.

The prediction of the state vector and its covariance can then be performed using

$$\hat{x}_{k+1}^- = \Phi_{k,k+1} \hat{x}_{k1}^+ \tag{6-7}$$

$$C_{xk+1}^- = \Phi_{k,k+1} C_{xk}^+ \Phi_{k,k+1}^T + Q_k \tag{6-8}$$

where $\Phi_{k,k+1}$ is the transition matrix from epoch k to epoch $k+1$, and Q_k is the discrete-time process noise matrix.

Assuming that the dynamics matrix is time invariant over the prediction interval Δt, the transition matrix and the discrete-time process noise matrix can be obtained, respectively, as the solutions of

$$\Phi_{k,k+1} = \exp(F\Delta t) \tag{6-9}$$

$$Q_k = \int_k^{k+1} \Phi_c(t, t+\tau) G(\tau) Q_c(\tau) G^T(\tau) \Phi_c^T(t, t+\tau) d\tau \tag{6-10}$$

where $\Phi_c(t_m, t_n)$ is the continuous-time transition matrix between times t_m and t_n, and $Q_c(t)$ is the continuous-time spectral density matrix of the input noise vector w.

Now that the theoretical concepts of discrete-time Kalman filtering have been reviewed, the following subsections discuss how this technique can be applied to GPS L5 signal tracking.

6.2 Kalman Filter Based Tracking

The KF tracking implementation used herein is illustrated in Figure 6-1, and closely follows that proposed in Petovello & Lachapelle (2006) and Mongrédien et al (2007b).
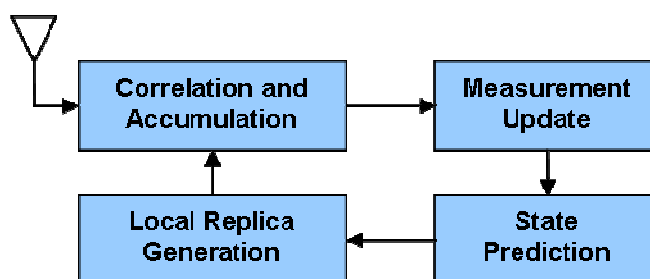
Figure 6-1 – Schematic Kalman Filter Based Tracking Loop

The signal enters the tracking loop after down-conversion, filtering, sampling and acquisition. Similar to CB tracking, the samples are first passed to a correlation function where carrier and code wipe-off are performed. After accumulation, however, the correlator outputs are no longer passed to individual code and carrier discriminators but rather to a unique Kalman filter that tries to jointly estimate the errors in the code and carrier phase and frequency alignment. These estimates are then used, in a feedback loop, to update the code and carrier NCO and drive the local signal generation for the next

epoch. The measurement and dynamic models used in this filter are discussed in the following subsections.

6.2.1 Measurement Model

The two KF measurement models considered herein are derived from the expression of the pilot and coherently combined data/pilot correlator outputs given in Equations 3.12, 3.13 and 5.25, respectively. Their expressions are repeated here for convenience. Assuming a correlator offset of $\Delta/2$ (e.g. half the CB early-late spacing), the in-phase and quadra-phase pilot correlator outputs are given by

$$I_{Pilot} = A\tilde{R}(\delta\tau - \Delta/2)\sin(\delta\phi) \tag{6-11}$$

$$Q_{Pilot} = A\tilde{R}(\delta\tau - \Delta/2)\cos(\delta\phi) \tag{6-12}$$

where $A = \dfrac{\sqrt{P}}{2}\dfrac{\sin(\pi\delta f T_I)}{\pi\delta f T_I}$ corresponds to the effective amplitude of the correlator outputs

when accounting for the power degradation due to the frequency inaccuracies, and the average phase error is expanded as

$$\delta\phi = \delta\phi_0 + \delta f_0\frac{T_I}{2} + \delta\alpha_0\frac{T_I^2}{6} \tag{6-13}$$

where the "0" subscript indicates a value at the beginning of the integration period and $\delta\alpha$ is the phase acceleration.

Similarly, the in-phase and quadra-phase combined correlator outputs are given by

$$I_{Comb} = I_{Pilot} + sign(D_d)I_{Data} \tag{6-14}$$

$$Q_{Comb} = Q_{Pilot} + sign(D_d)Q_{Data} \tag{6-15}$$

The reason for combining the amplitude and frequency error terms is that the attenuation due to frequency errors is very difficult to separate from the variations in amplitude. This implies that the frequency error can only be observed through the expanded phase error. When considering this measurement model, three particular aspects need to be further discussed. First, as illustrated in Figure 6-2, the frontend filtered correlation function is modelled herein using a fourth order polynomial.
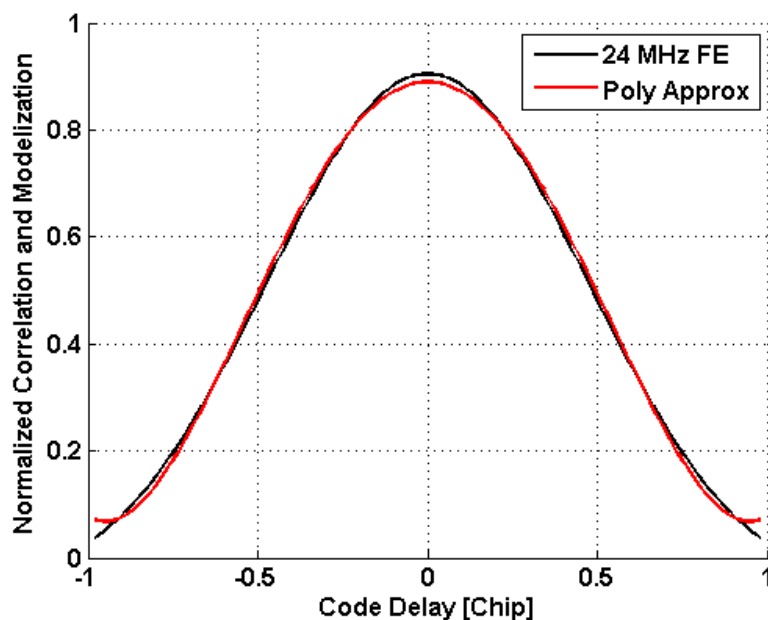

Figure 6-2 - Fourth order Polynomial Approximation of the Filtered L5 Correlation Function

In addition to accurately modelling the frontend filtering effects, this approach alleviates issues related to the presence of slope discontinuities in the triangular auto-correlation function model, and ensures the numerical stability of the filter.

Second, the covariance matrix of the observations is computed as a function of the estimated signal C/N$_0$. Specifically, the diagonal elements of this matrix are given as (Van Dierendonck 1997)

$$\sigma_I^2 = \sigma_Q^2 = \frac{1}{2.10^{0.1C/N_0}T_I} \tag{6-16}$$

and the off-diagonal elements (corresponding to the covariance between two correlator outputs separated by a $\Delta/2$ spacing) as

$$\text{cov}[I, I(\Delta/2)] = \text{cov}[Q, Q(\Delta/2)] = \frac{\tilde{R}(\Delta/2)}{2.10^{0.1C/N_0}T_I}. \tag{6-17}$$

Finally, a hard symbol bit sign decision is implied through the use of the combined correlator outputs. It is important to bear in mind that bit sign errors will degrade the correlator outputs and may trigger loss of lock at low signal power. To alleviate this problem, Psiaki & Jung (2002) and Yu et al (2006) introduce a soft data bit decision algorithm. This algorithm uses a weighted sum to recombine the outputs of the two separate filters running both bit sign hypotheses in parallel. This approach was shown to provide interesting sensitivity gain improvements at low signal power but has the drawback of degrading accuracy at high signal power. While it would be feasible to apply a similar strategy to the L5 case, this is not done herein; rather, the focus is put on comparing the performance of the pilot and combined measurement update strategies.

Now that the measurement models have been defined, a description of the dynamic model is presented.

6.2.2 Dynamic Model

The filter implemented herein directly uses the early, prompt and late correlator outputs to estimate the amplitude, code phase error, initial carrier phase error, initial carrier frequency error and initial carrier acceleration error. This translates into the following state model:

$$
\frac{d}{dt}\begin{pmatrix} A \\ \delta\tau \\ \delta\varphi_0 \\ \delta f_0 \\ \delta\alpha_0 \end{pmatrix} = \begin{pmatrix} 0 & 0 & 0 & 0 & 0 \\ 0 & 0 & 0 & \beta & 0 \\ 0 & 0 & 0 & 1 & 0 \\ 0 & 0 & 0 & 0 & 1 \\ 0 & 0 & 0 & 0 & 0 \end{pmatrix}\begin{pmatrix} A \\ \delta\tau \\ \delta\varphi_0 \\ \delta f_0 \\ \delta\alpha_0 \end{pmatrix} + \begin{pmatrix} 1 & 0 & 0 & 0 & 0 \\ 0 & 1 & \beta & 0 & 0 \\ 0 & 0 & 1 & 0 & 0 \\ 0 & 0 & 0 & 1 & 0 \\ 0 & 0 & 0 & 0 & 1 \end{pmatrix}\begin{pmatrix} w_A \\ w_\tau \\ w_\phi \\ w_f \\ w_\alpha \end{pmatrix} \qquad \textbf{(6-18)}
$$

where β converts units of radians into units of chips and w is the process noise of the subscripted quantity.

In essence, this model uses the carrier frequency and acceleration errors to propagate the code and carrier phase errors. The amplitude and code phase process noise are expected to account for signal level variations and code-carrier ionospheric divergence, respectively. The carrier phase and carrier frequency process noise are expected to account for the oscillator jitter effects. Similar to (Brown & Hwang 1992), the oscillator frequency noise is modelled through two components, namely white noise and random walk. Finally, the carrier acceleration process noise is expected to account for the receiver-satellite LOS dynamics.

For computing the noise value that drives the amplitude estimate, some consideration is given to the expected amplitude variations due to 1) changes in the true satellite-receiver range, and 2) attenuation due to frequency inaccuracies. Although no ionospheric errors are simulated, the noise value that drives the code error is obtained by estimating the

expected code-carrier ionospheric divergence variations due to changes in satellite elevation. The noise values that drive the oscillator phase and frequency errors follow the model described by Brown & Hwang (1992). It is important to note, however, that these values do not follow the elevated frequency noise model proposed in (ibid). This model was built to approximate the clock frequency noise in the flicker region. This flat region of the oscillator frequency noise is extremely hard to model and corresponds to time intervals of approximately 1 s. When considering the common 1-Hz navigation solution update rate, modeling the clock frequency noise behaviour in the flicker region is of critical importance. However, in the context of tracking loop updates, where the typical update rate is on the order of a few tens of milliseconds or less, it is more relevant to accurately model the white frequency noise. Finally the noise value that drives the acceleration error is obtained by examining the expected acceleration variations along the satellite orbital trajectory. The final values are shown in Table 6.1.

Table 6.1 – State Spectral Density

State	Process Noise
Amplitude	$1e^{-6}$/Hz
Average Code Phase Error	$1e^{-5} chip^{-2}/s^2$/Hz
Initial Carrier Phase Error	$\pi.f^2.h_0$ rad^2/Hz
Initial Frequency Error	$4\pi^3.f^2.h_{-2}$ rad$^2/s^2$/Hz
Initial Acceleration Error	5 rad$^4/s^4$/Hz
where h_{-2} and h_0 are the random walk components of the oscillator frequency noise given in Table 3.1	

Now that the KF models have been discussed, the expected benefits of KF tracking are reviewed.

6.2.3 Expected Advantages of Kalman Filter Tracking

The expected benefit of KF tracking is three-fold. First, by weighting the quality of the prediction against that of the measurements before each tracking loop update, the Kalman gain effectively provides adaptive bandwidth filtering. This should therefore minimize the need for long coherent integration times and improve tracking sensitivity. Second, the dynamic and measurement models offer a unique opportunity to utilize any prior information about the operating environment of the receiver (e.g. oscillator used, expected level of receiver dynamics, or frontend filtering). This implies that the KF implementation can provide more consistent tracking performance over a wider range of tracking conditions. Finally, and in contrast with CB tracking, the KF implementation enables code and carrier NCO updates not only in frequency but also in phase. This, in turn, should allow for a more accurate alignment of the local code and carrier replica or, equivalently, for more accurate code and carrier tracking.

Prior to evaluating the actual performance of KF tracking, it is important to ensure that the filter can accurately track signals at high C/N_0.

6.2.4 Kalman filter Based Implementation Validation

Figure 6-3 shows the estimated Doppler derived from CB and KF tracking. It shows that the KF implementation can track the Doppler frequency of PRN 10 more precisely than the CB implementation. The results shown for PRN 10 are representative of all the simulated satellites.
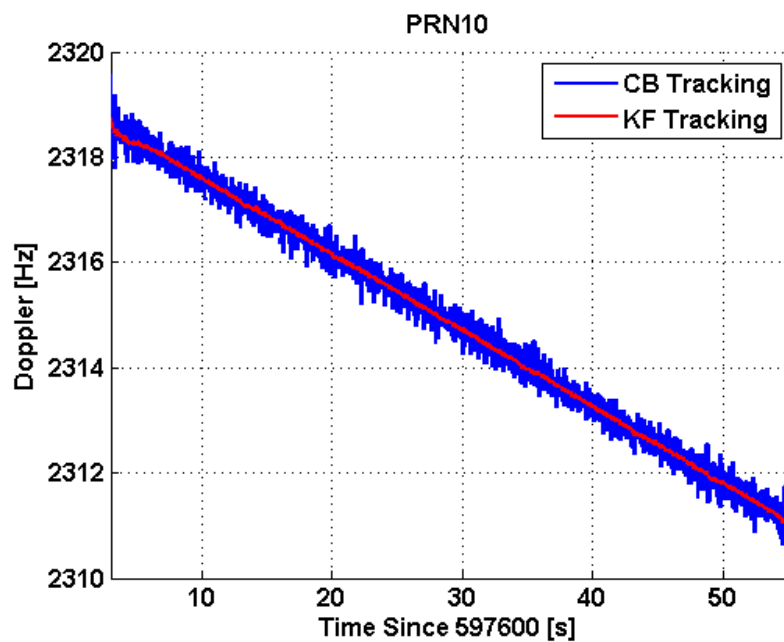
Figure 6-3 – Estimated Doppler for PRN 15 Using CB and KF Tracking

Now that the ability of the KF implementation to accurately track the incoming signals has been demonstrated, it is important to compare its performance with that of the CB implementation. This is done hereinafter in the presence of noise, oscillator phase noise and receiver dynamics.

6.3 KF Tracking in the Presence of Noise

KF and CB tracking performance for pilot-only and data/pilot combined measurement models are compared in terms of accuracy and sensitivity. To this end, the power profile shown in Figure 5.4 is used. In addition, the coherent integration time is set to 10 ms, and the CB tracking is implemented with the parameters discussed in Sections 5.1 and 5.4. It should be noted that these CB parameters were selected to accommodate a wide range of

tracking conditions and to illustrate the general trends observed for CB code and carrier tracking.

6.3.1 Tracking Accuracy

Figure 6-4 shows the estimated Doppler and pseudorange measurement error STD derived from various CB and KF tracking implementations. It appears that in terms of frequency tracking the KF implementation outperforms its CB counterpart by approximately one order of magnitude for all the C/N_0 values investigated. In terms of code tracking, the improvements brought by the KF implementation are not as significant, especially for high C/N_0 values. Interestingly, the accuracy of the frequency and time estimates obtained from KF tracking shows very little susceptibility to C/N_0 variations. This is a consequence of the adaptive noise filtering that is provided by the Kalman filter. However, it should be noted that the CB tracking accuracy could be improved by narrowing the loop filter bandwidth as it would enable better white noise mitigation.
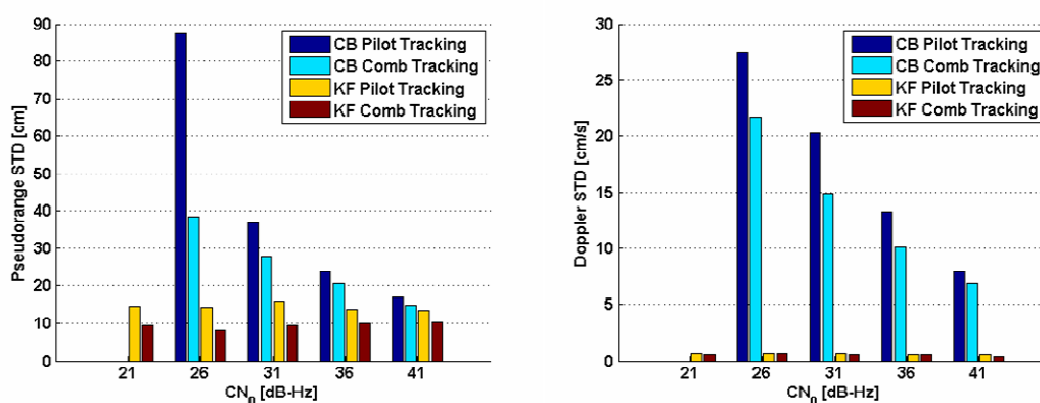
Figure 6-4 – Estimated Pseudorange (Left) and Doppler (Right) Error STD using CB and KF Pilot and Combined Tracking Implementations for Various C/N$_0$

To further investigate the impact of signal power variations on KF tracking accuracy, Figure 6-5 shows the estimated Doppler and pseudorange measurement error STD derived from KF tracking implementations only.
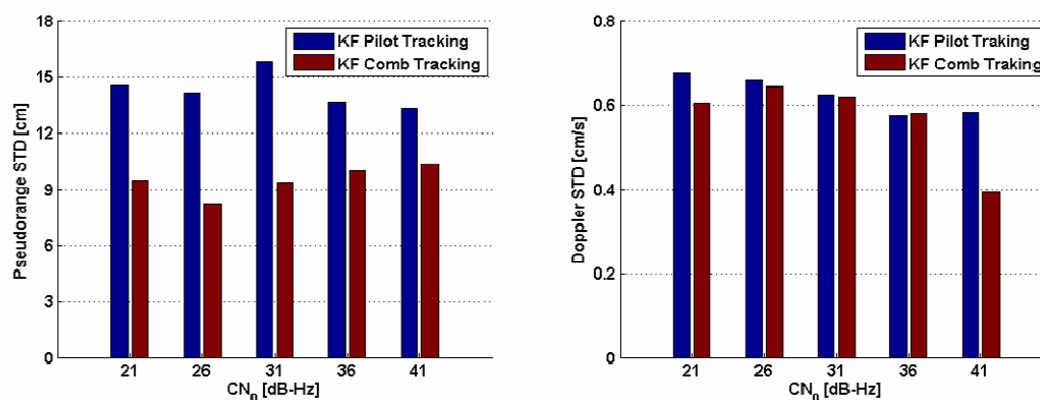
Figure 6-5 - Estimated Doppler (Left) and Pseudorange (Right) Error STD using KF Pilot and Combined Tracking for Various C/N$_0$

Examining Figure 6-5 it can be seen that the KF tracking accuracy is not greatly affected by incoming signal power variations. In terms of carrier tracking the variations observed are on the order of a few millimetres per second at most. Accordingly, the benefits of using combined rather than pilot-only correlator outputs are marginal. The trends observed in terms of code tracking are slightly different. While the accuracy of the time estimates derived from pilot-only tracking appears to be fairly constant across the range of C/N$_0$ values investigated, there seem to be a non-negligible improvement to be obtained by using the data/pilot combined rather than the pilot-only correlator outputs. While these trends seem contradictory at first instance, it is important to bear in mind that the various C/N$_0$ values are obtained by slowly decreasing the power of PRN 15. This implies that as the time increases (and the C/N$_0$ decreases), the Kalman Filter can

progressively decrease the weight it gives to the measurements and increase the trust it places in the predicted estimates. In contrast, the 3 dB gain in equivalent C/N_0 enabled by the use of combined correlator outputs intervenes at the beginning of the data set and can therefore help increase the accuracy of the time estimates.

Now that the code and carrier accuracy gain enabled by KF tracking have been assessed, it is of major interest to investigate the advantages of the KF implementation in terms of tracking sensitivity.

6.3.2 Tracking Sensitivity

To illustrate the sensitivity of the proposed KF tracking implementation, Figure 6-6 shows the estimated Doppler frequency derived from the combined CB and KF tracking implementations. The KF implementation is able to track the signal until the end of the data set which, according to the power profile shown in Figure 5.4, corresponds to a C/N_0 value of approximately 20 dB-Hz. The CB implementation, on the other hand, loses lock at approximately 23 dB-Hz. This result demonstrates that the KF implementation can also bring significant improvements in terms of tracking sensitivity. It is important, however, to bear in mind that the very stable operating conditions of the receiver (and therefore of its tracking loops) enable the Kalman Filter to rely more on its dynamics model than on the measurements it gets from the correlators. In rapidly changing environments, where the Kalman Filter would need to accept more information from the correlator outputs, this sensitivity value would likely change. Furthermore, it should be noted that the CB tracking threshold could be lowered by narrowing the loop filter bandwidth as it would enable better white noise mitigation.
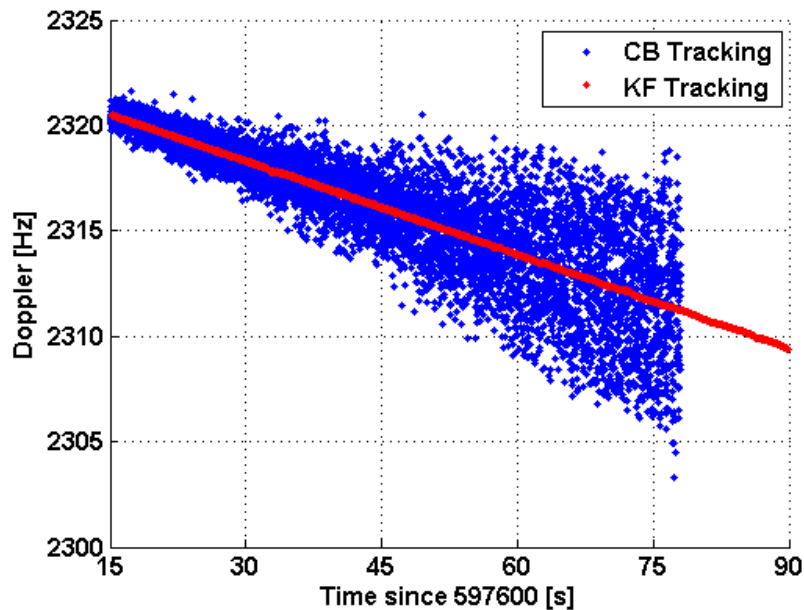
Figure 6-6 - Estimated Doppler using the Data/Pilot Combined CB and KF Tracking Implementations

Now that the KF tracking accuracy and sensitivity has been assessed in the presence of white noise, it is of major interest to evaluate its modelling capacities in terms of oscillator frequency noise.

6.4 KF Tracking in the presence Oscillator Frequency Noise

The impact of oscillator frequency noise on CB phase tracking has been assessed in Section 5.3. It was shown that the resulting phase jitter in the PLL was a function of the oscillator and loop filter bandwidth used. For a given oscillator, the use of wider loop filter bandwidth could help reduce the impact of the oscillator frequency noise but would, at the same time, increase the impact of white noise. The ideal solution would then be to use an adaptive PLL that would narrow its loop filter bandwidth at low C/N_0 (when the

thermal noise dominates the error budget) and widen it at high C/N_0 (to better track the signal variations due to oscillator frequency noise). This is exactly what is intended in the KF implementation through the continuous update of the Kalman gain.

6.4.1 Carrier Tracking Accuracy

To illustrate the accuracy of the oscillator frequency noise modelling in the KF implementation Figure 6-7 shows the estimated Doppler measurement STD derived at various C/N_0 from the pilot-only and data/pilot combined CB and KF implementations when data sets are collected using the following external FTS reference: 1) an OCXO, 2) a TCXO or 3) a Rubidium. As discussed in Section 5.3, the oscillator that offers the highest CB phase tracking accuracy is the OCXO, followed by the TCXO and Rubidium oscillator. In contrast, it appears the KF implementation provides similar performance whether the external oscillator used is a Rubidium or an OCXO. Since these oscillators possess very different noise parameters, this result would seem to indicate that the KF appropriately weighs the measurements and predicted estimates in its Kalman gain computations. However, this conclusion does not seem to hold for the case of the TCXO oscillator since it provides significantly worse phase tracking accuracy than the other oscillators. This also could imply that the parameters used to model the TCXO oscillator do not match its actual performance.
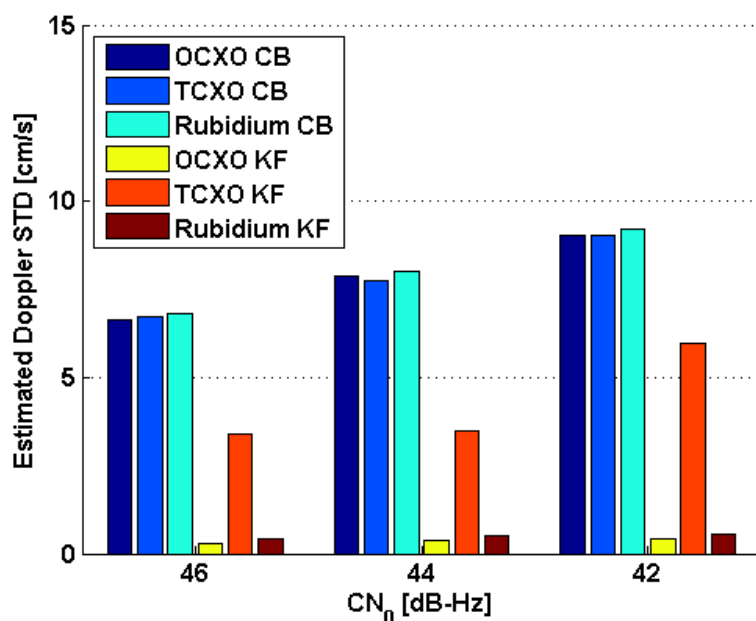
Figure 6-7 - Estimated Doppler Error STD for Various External Oscillator References using CB and KF Combined Tracking for various C/N$_0$

To further illustrate the importance of oscillator modelling in KF tracking, Figure 6-8 shows the Doppler measurement error STD obtained when the OCXO, TCXO and Rubidium oscillator parameters are used to process the data set collected with the Rubidium oscillator. As expected, the oscillator parameters that offer the highest accuracy are the Rubidium ones followed by the OCXO and TCXO parameters. Examining Figure 6-7 and Figure 6-8, it appears that the values used to model the TCXO frequency noise might be overly optimistic. This would imply that the filter relies too heavily on the dynamic model to estimate the carrier phase and frequency error at the beginning of the integration interval and treats as noise some signal variations that are in fact due to oscillator variations.
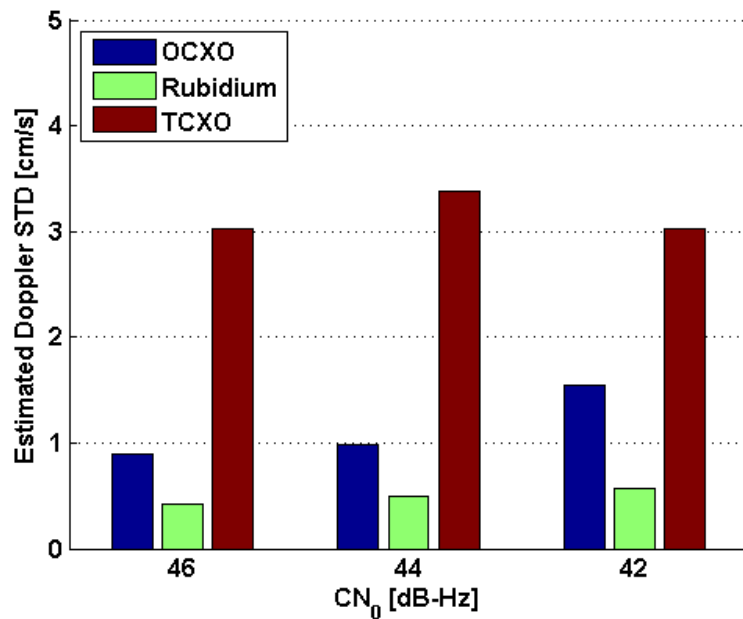
Figure 6-8 - Estimated Doppler Error STD obtained by Processing the Rubidium Data Set using Different Clock Parameters in the KF Tracking

The other error source that the filter tries to account for in his update of the Kalman gain matrix is receiver dynamics. The next section evaluates the modelling capacities of the Kalman Filter in terms of receiver dynamics.

6.5 Performance in the Presence of Dynamics

The motion profile introduced in Section 5.3, which includes both constant acceleration and constant velocity periods, is used here to analyse the ability of the filter to model receiver dynamics. Figure 6-9 shows the estimated three-dimensional velocity STD obtained when CB and KF tracking implementations are used to process the static and kinematic data sets. As expected from the Doppler measurement accuracy shown in

Section 6.3.1, the velocity estimates derived from KF tracking are significantly more accurate than those obtained from CB tracking.
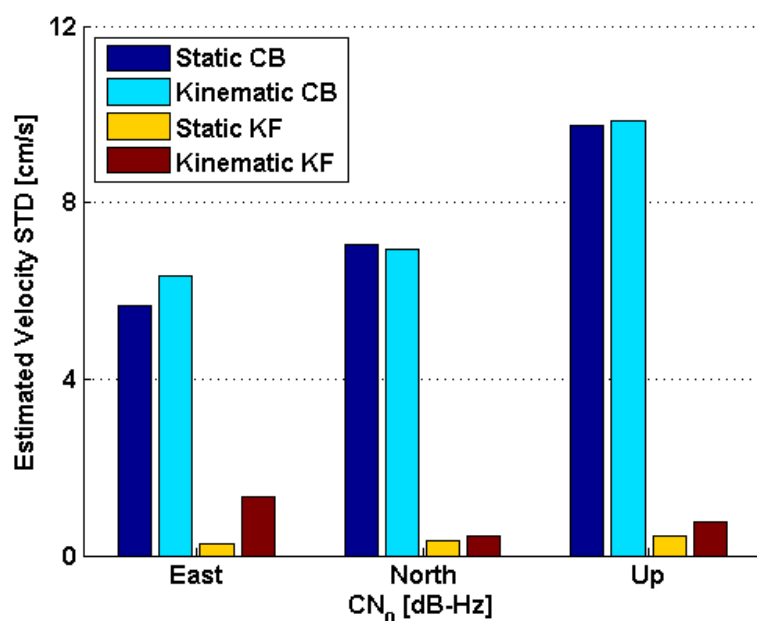
Figure 6-9 – Estimated Three-Dimensional Velocity STD for Static and Kinematic Receivers using CB and KF Tracking Implementations

It is interesting to note, however, that the east velocity estimate is slightly noisier than its north and up counterparts. This is due to the fact that at the end of the constant acceleration period, the Kalman Filter relies too heavily on the predicted estimate and therefore overestimates the east velocity. It would be possible to reduce this effect by increasing the acceleration process noise but this would increase the impact of measurement noise and would likely degrade the overall accuracy of the three-dimensional velocity estimation.

Sections 6.3, 6.4 and 6.5 above showed the advantage of the KF implementation in terms of tracking accuracy, tracking sensitivity and oscillator modelling. It is then of major

interest to assess how these tracking improvements translate in terms of *Position, Velocity and Time* (PVT) solution.

6.6 PVT Accuracy

The pseudorange and Doppler measurements obtained from the receiver tracking loops are passed to the navigation filter which uses them to estimate the receiver position and velocity. As previously mentioned, the navigation filter implemented herein is an LSA; this implies that the position and velocity estimates are obtained independently from the pseudoranges and Doppler measurements, respectively. Besides, no carrier smoothing of the pseudorange measurement is implemented. This epoch-by-epoch approach was selected to better illustrate the impact of code and carrier tracking accuracy at the position and velocity levels.

6.6.1 Estimated Position Accuracy

Figure 6-10 shows the horizontal position errors obtained when using the pseudorange measurements derived from the CB and KF tracking implementations respectively. The position accuracies obtained when using pseudorange measurements from ten satellites broadcast with an estimated C/N_0 of 44 dB-Hz are at the decimetre level for both tracking implementations.
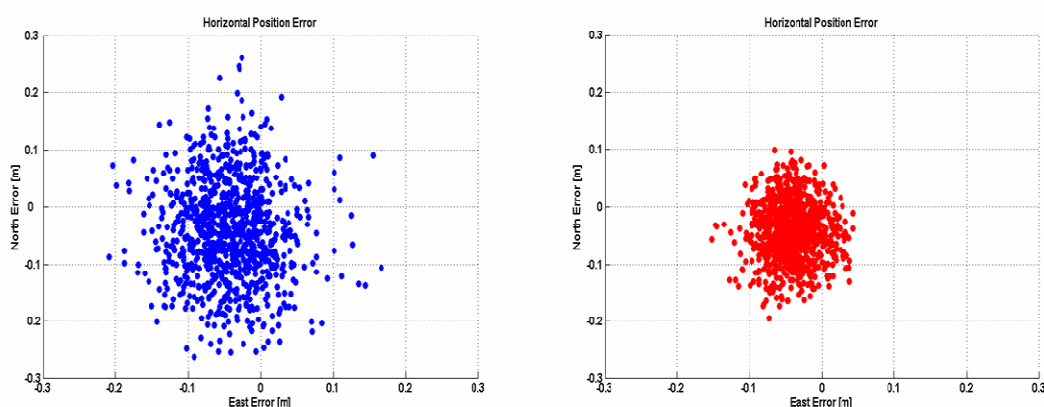
Figure 6-10 – Horizontal Position Errors using the CB (Left) and KF (Right) Tracking Implementations

However, as confirmed by the position error STD values shown in Table 6.2, the improvements brought by the KF implementation in terms of code tracking can be seen to translate into more accurate receiver position estimates.

Table 6.2 – Position Error STD

Direction	Mean Position Error [cm]		Position Error STD [cm]	
	CB	KF	CB	KF
East	- 4.1	- 4.2	5.2	3.0
North	- 4.2	- 4.2	8.6	5.0
Up	-10.0	-10.1	19.4	12.6

As expected from the satellite constellation configuration the position estimation is noisier in the up direction.

It can also be seen that there is a bias is the position estimation derived from both KF and CB tracking implementations which is likely a consequence of the short duration of the data set used to generate these results.

6.6.2 Estimated Velocity Accuracy

Figure 6-11 and Figure 6-12 show the three-dimensional velocity errors obtained when using the Doppler measurements derived from the CB and KF tracking implementations, respectively. These velocity errors are obtained when using Doppler measurements from ten satellites broadcast with an estimated C/N_0 of 44 dB-Hz. Note that the scale of the y-axis is different in the two figures.
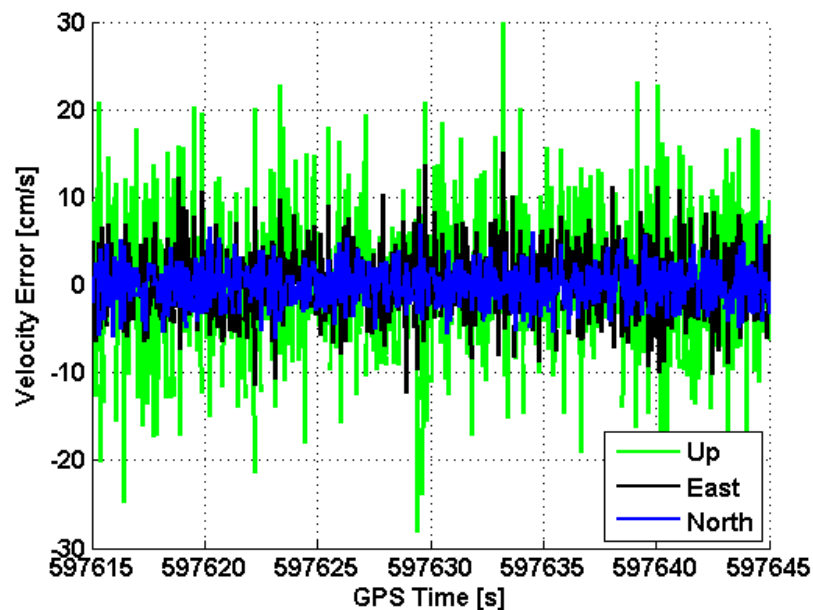
Figure 6-11 – Three-Dimensional Velocity Errors using the CB Tracking Implementation
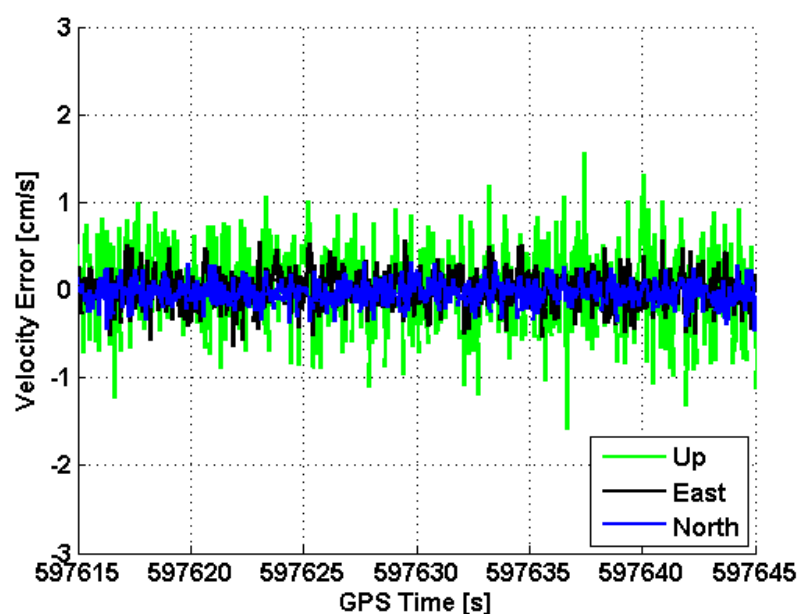
Figure 6-12 - Three-Dimensional Velocity Errors Using the KF Tracking Implementation

In contrast with the results shown in the position domain the velocity accuracies obtained when using the Doppler measurements derived from CB and KF tracking do not have the same order of magnitude. In fact, while the velocity estimates derived from CB tracking are affected by decimetre level errors, those obtained from KF tracking show error variations at the centimetre level. These results, confirmed by the velocity error STD values shown in Table 6.3, are consistent with the trends observed at the measurement level since the KF implementation was shown to provide significant accuracy improvements in terms of carrier tracking. As in the position domain, the velocity estimation is always less accurate in the up direction.

Table 6.3 - Velocity Error STD

Direction	Mean Velocity Error [cm/s]		Velocity Error STD [cm/s]	
	CB	KF	CB	KF
East	- 0.1	0.0	2.3	0.1
North	0.3	0.0	4.1	0.2
Up	0.4	0.0	8.7	0.5

It is interesting to note that the velocity error standard deviations shown in Table 6.3 are lower than those shown in Figure 6-9, even for the static receiver. This derives from the fact that the results shown in Figure 6-9 are obtained using a four-satellite navigation solution. In the absence of redundancy, the effect of Doppler measurement noise is expected to be magnified in the velocity domain.

6.7 Conclusion on GPS L5 Kalman Filter-Based Tracking

Despite all the improvements that are enabled by the L5 pilot channel in terms of CB tracking, it has been shown herein that the KF implementation can provide some additional gains in terms of tracking accuracy and sensitivity. These improvements are fairly marginal in terms of code tracking accuracy but reach approximately one order of magnitude in terms of carrier tracking accuracy. Besides, a 3 dB gain was observed in terms of tracking sensitivity.

The modelling capabilities of the Kalman Filter were demonstrated in terms of oscillator frequency noise and receiver dynamics.

 The tracking improvements enabled by the KF implementation were also shown to translate into better positioning accuracy. Similar behaviour can therefore be anticipated for very precise double difference carrier phase positioning.

The impact of satellite geometry on the accuracy of the position and velocity was also illustrated. Specifically, it was shown that the position and velocity estimate are noisier in the up direction. Additionally, the benefits of measurement redundancy were highlighted.

CHAPTER SEVEN: CONCLUSIONS AND RECOMMENDATIONS

A thorough assessment of the performance of the GPS L5 signal was successfully completed herein. Several acquisition and tracking strategies were proposed and their relative performance assessed. The simulated L5 IF samples used to conduct this evaluation were obtained using a Spirent GSS 7700 hardware simulator and a NovAtel L5 frontend. An L5 software receiver was developed as part of this thesis and used to produce the results presented in previous chapters.

The following sections summarize the major findings of this work and make recommendation for potential improvements.

7.1 Conclusions

The purpose was to investigate and assess, from a signal processing point-of-view, the impact of the future L5 signal structure on GPS receiver operations from acquisition and tracking to measurements formation and navigation solution derivation. The major conclusions of this work are as follows:

Acquisition Performance

In order to alleviate the high computational load associated with combined algorithms, the acquisition of the PRN and NH codes was performed sequentially.

1. The implementation of the L5 coarse acquisition step is affected by the potential occurrence of unknown NH bit sign transitions. This requires the implementation of zero-padding strategies and constrains the coherent integration time to exactly 1 ms

which, in turns, limits the achievable correlation gain and affects the L5 coarse acquisition sensitivity. To increase the equivalent C/N_0 (and, therefore, enhance detection performance) several data/pilot combining algorithms were proposed and compared. The coherent combining method that makes use of the synchronicity and orthogonality of the data and pilot channels was shown to provide the best theoretical detection performance, followed by the differential and non-coherent combining strategies.

2. The L5 fine acquisition involves the introduction of an intermediate tracking step. This 1-ms FLL-based tracking strategy reduces the frequency uncertainty after coarse acquisition and enables reliable acquisition of the received NH code delay. The NH code delay acquisition is performed using the pilot channel only; this strategy combines robustness with simplicity, and benefits from the superior NH_{20} correlation properties.

Constant Bandwidth Tracking Performance

The improvements brought by the L5 pilot channel were confirmed in terms of carrier and code tracking.

1. The main asset, for a carrier tracking loop running on a pilot channel, resides in the use of more efficient discriminators. Since they do not need to address the unknown data bit transition issue, the pilot discriminators used for phase and frequency tracking can provide significant gain in terms of frequency tracking accuracy and sensitivity. These improvements mostly derive from the fact that the pilot discriminators possess extended stability and linear tracking domains. The sensitivity

gain enabled by the pilot discriminators was shown to be approximately 6 dB for both PLL and FLL. From a phase tracking stand-point, the use of a pure PLL discriminator also ensures better resistance to dynamics and oscillator errors, and therefore limits the occurrence of cycle slips. This is of particular interest for carrier smoothing of the pseudoranges and/or carrier ambiguity resolution for double difference carrier phase positioning.

2. Phase tracking and frequency tracking were compared in terms of accuracy and sensitivity. As expected, phase tracking was shown to be the most accurate. Similarly, phase tracking was found to provide higher tracking sensitivity.

3. The pilot channel also allows the use of long coherent integration times. The use of long coherent integration times on the carrier tracking loop is limited by both the quality of the receiver FTS and the expected receiver dynamics. In contrast, the use of long coherent integration times on the code tracking loop is enabled by the carrier aiding that absorbs the effects of oscillator frequency noise and receiver dynamics. This was shown to provide significant accuracy gain, especially at low C/N_0.

4. From the above conclusions it would seem reasonable to perform the GPS L5 tracking on the pilot channel. Combined with a single prompt in-phase correlator on the data channel (to enable subframe synchronization and navigation message decoding), this pilot-only tracking strategy would combine robustness and low computational burden. This approach, however, does not make use of all the available power which, in turns, can reduce measurements accuracy. To circumvent this problem a coherent data/pilot combining at the correlator level was introduced. It was shown to provide significant gains in terms of code and carrier tracking accuracy. Its

performance, in terms of tracking sensitivity, was shown to fall halfway between those of the data and pilot channel implementations.

Kalman Filter Based Tracking Performance

The benefits of Kalman filter-based tracking were demonstrated in terms of code and carrier tracking sensitivity and accuracy.

1. The foremost benefit of the KF tracking implementation resides in its modeling capacities. Specifically, the opportunity to include the effects of frontend filtering, oscillator phase noise or dynamics in the measurement and dynamic models effectively provides adaptive bandwidth filtering and reduces the impact of noise on the code and carrier tracking loops.

2. The accuracy improvements are more significant in terms of carrier tracking since the Doppler estimates derived from the KF tracking loop are about one order of magnitude less noisy than those derived from the CB tracking loop. This is of particular interest since it is the carrier tracking loops that show the lowest performance when CB tracking is used.

3. In terms of sensitivity, KF tracking was shown to outperform its CB counterpart by approximately 3 dB when the receiver operates in stable conditions.

4. The performance of Kalman filter-based tracking was also shown to be less dependent on the incoming signal C/N_0 than its constant bandwidth counterpart. However, some accuracy improvements were still observed when the data and pilot channel were coherently combined at the correlator level.

PVT Solution

Using an epoch-by-epoch LSA, the impact of code and carrier tracking accuracy was illustrated at the position and velocity levels.

1. As expected, the advantages of the Kalman Filter-based tracking were confirmed in the position domain. In particular, the accuracy of the velocity estimates obtained when using KF tracking were shown to be approximately one order of magnitude better than those derived from CB tracking. In terms of position accuracy, the improvement was shown to be at the centimetre level.

2. The impact of satellite geometry on the accuracy of the position and velocity estimates was briefly introduced. Specifically, the position and velocity estimate were shown to be noisier in the up direction. Besides, measurement redundancy was shown to enable some accuracy gain in terms of velocity estimation.

7.2 Recommendations for Future Work

Following these conclusions, it is necessary to identify the limitations of the research presented herein and, accordingly, to formulate the following recommendations for future work:

1. An investigation of L5 multipath mitigation in the presence of more diverse multipath types is required. Due to the difficulty to simulate an insightful multipath environment, only specular multipath was considered herein. It would be valuable to assess the effect of diffuse multipath as well.

2. Assess the tracking performance in the presence of higher order dynamics. The results shown herein were limited to acceleration dynamics which are more

representative of vehicle navigation. By investigating the performance of the CB and KF tracking in the presence of higher order dynamics, a better overall assessment would be obtained.

3. Investigate tracking performance in the presence of higher oscillator frequency noise. The results shown herein were obtained using high quality oscillators. It would be valuable to assess the performance degradations that would ensue if low-end quartz oscillators were used as the external FTS.

4. Investigate the accuracy/sensitivity trade-off that would result from the use of a soft symbol bit decision in the Kalman Filter-based tracking implementation.

5. Conduct some L5 performance analysis in the presence of interference, and specifically of the aeronautical interferences present in this frequency band.

6. Consolidate the L5 performance analysis at the position level. In particular, it would be interesting to further investigate the accuracy of the L5 carrier phase measurements and, therefore, to assess the potential of the L5 signal for double difference carrier phase positioning and attitude determination.

7. Evaluate the performance of a dual L1/L5 frequency receiver. Specifically the interest of the frequency diversity should be investigated, at the position level, in terms of ionospheric mitigation capacities and resistance to interference and jamming. Furthermore, at the measurement level, it would be of major interest to assess the accuracy, reliability and sensitivity gains that might be achieved through the implementation of an L5-aided tracking of the L1 C/A signal.

8. Finally, although the simulation tools used in this dissertation were chosen to provide L5 IF samples that were as close as possible to what will be transmitted by the GPS

satellites, it would be valuable to test the algorithms proposed on real data. The first GPS satellite to transmit the L5 signal is schedule for launch in June this year, which will provide an excellent opportunity to confirm some of the results presented in this dissertation.

REFERENCES

Allan, D.W., N. Ashby and C.C. Hodge (1997), *The Science of Time Keeping,* Application Note 1289, Hewlett Packard.

Axelrad, P. and R.G. Brown (1997), *GPS Navigation Algorithms* in *Global Positioning System: Theory and Applications Volume I,* Progress in Astronautics and Aeronautics Volume 164, AIAA, pp. 409-434.

Bastide, F. (2004), *Analysis of the Feasibility and Interests of Galileo E5a/E5b and GPS L5 Signals for Use With Civil Aviation*, PhD Thesis, Institut National Polytechnique de Toulouse.

Betz, J.W. (2002), *Binary Offset Carrier Modulation for Radionavigation*, Navigation: Journal of the U.S. Institute of Navigation, Vol.48, No. 4.

Betz, J.W. and R. Kolodzieski (2000), *Extended Theory of Early-Late Code Tracking for a Bandlimited GPS Receiver*, Navigation: Journal of the U.S. Institute of Navigation, Vol. 47, No. 3.

Blanchard, A. (1975), *Technique des boucles d' asservissement de phase,* Lecture Notes, Ecole Supérieure d'electricité

Borio, D. (2007), *Combining Techniques for the Acquisition of the New Composite GNSS Signals*, PLAN internal report.

Borio, D., L. Camoriano and L. Lo Presti (2006), *Impact of the Acquisition Search Strategy on the Detection and False Alarm Probabilities in a CDMA Receiver*, Proceedings of the IEEE/ION PLANS 2006.

Braasch, M. (1997), *Multipath Effects* in *Global Positioning System: Theory and Applications Volume I*, Progress in Astronautics and Aeronautics Volume 164, AIAA, pp. 547-568.

Brenner, M., R. Reuters and B. Schipper (1998), *GPS Landing System Multipath Evaluation Techniques and Results,* Proceeding of the U.S. Institute of Navigation GPS 1998

Brown, R.G. and P.Y.C. Hwang (1992), *Introduction to Random Signals and Applied Kalman Filtering,* John Wiley & Sons, Inc., second edition

Cannon, M.E. (2004), *Satellite Positioning*, ENGO 561 Lecture Notes, Department of Geomatics Engineering, The University of Calgary.

Conley, R., R. Cosentino, C. Hegarty, E.D. Kaplan, J.L. Leva, M. Ujit de Haag and K. Van Dyke (2006), *Performance of Stand-Alone GPS* in *Understanding GPS Principles and Applications,* Artech House Inc

Dottling, M., A. Jahn, D. Didascalou and W. Wiesbeck (2001), *Two- and Three-Dimensional Ray Tracing Applied to the Land Mobile Satellite (LMS) Propagation Channel,* IEEE Antenna and Propagation Magazine, Vol. 43, No. 6.

Fontana, R.D., W. Cheung, P.M. Novak, and T. Stansell (2001), *The New L2 Civil Signal*, Proceedings of the US Institute of Navigation GNSS 2001.

Fornay, G.D. (1973), *The Viterbi Algorithm,* Proceedings of the IEEE Transaction, Vol. 60, No. 3.

Gernot, C., S.K. Shanmungam, K. O'Keefe and G. Lachapelle (2007), *A Novel L1 and L2C Combined Detection Scheme for Enhanced GPS Acquisition,* Proceedings of the U.S. Institute of Navigation GNSS 2007.

Gold, R. (1967), *Optimal Binary Sequences for Spread Spectrum Multiplexing,* IEEE Transactions on Information Theory, Vol. 13, Issue 4, Oct., pp. 619-621.

GPS World (2008), *L5 Demo Satellite Schedule for Launch in June*, 30 January 2008.

Hegarty, C. (1999), *Evaluation of the Proposed Signal Structure for the New Civil GPS Signal at 1176.45 MHz*, WN99W0000034, The MITRE Corporation.

Hegarty, C. (2006), *Optimal and Near-Optimal Detectors for Acquisition of the GPS L5 Signal,* Proceedings of the U.S. Institute of Navigation NTM 2006.

Hegarty, C., T. Kim, S. Ericson, P. Reddan, T. Morrissey, and A.J. Van Dierendonck (1999), *Methodology for Determining Compatibility of GPS L5 with Existing Systems and Preliminary Results*, Proceedings of the US Institute of Navigation AM 1999.

Hegarty, C., M. Tran, and J.W. Betz (2004a), *Multipath Performance of the New GNSS Signals*, Proceedings of the US Institute of Navigation NTM 2004.

Hegarty, C., M. Tran, and A.J. Van Dierendonck (2004b), *Acquisition Algorithms for the GPS L5 Signal*, Proceedings of the US Institute of Navigation GNSS 2004.

Hu, T., G. Lachapelle and R. Klukas (2007), *Controlled GPS Signal Simulation for the Indoor,* Navigation: Journal of the U.S. Institute of Navigation, Vol.60, No. 2.

Hudnut, K., B. Titus, J. Taylor and T. Stansell (2004), *Improving the L1 Signal – GPS III Offers the Opportunity,* Presentation by U.S. Geological Survey, Inter-Agency GPS Executive Board and U.S. Air Force.

Humphreys T.E., M.L. Psiaki, P.M. Kintner Jr. and B.M. Ledvina (2005), *GPS Carrier Tracking Loop in The Presence of Ionospheric Scintillations,* Proceedings of the U.S. Institute of Navigation GNSS 2005.

Irsigler, M. and B. Eissfeller (2002), *PLL Tracking in the Presence of Oscillator Phase Noise*, GPS Solutions, Vol. 5, No. 4

IS-GPS-705 (2005), *GPS L5 Interface Control Document – Navstar GPS Space Segment / User Interfaces*, September 2005.

IS-GPS-200D (2004), *Interface Control Document – Navstar GPS Space Segment / User Segment L5 Interfaces*, ARINC Incorporated, December 2004.

Jahn, A., H. Bischl and G. Heiss (1996), *Channel Characterization for Spread Spectrum Satellite Communications,* Proceedings of the IEEE 4th International Symposium on Spread Spectrum Techniques and Applications, Vol.3.

Julien, O. (2005), *Design of Galileo L1F Receiver Tracking Loops*, PhD Thesis, UCGE Report #20227, Department of Geomatics Engineering, The University of Calgary.

Kaplan, E.D., J.L. Leva, D. Milbert and M.S. Pavloff (2006), *Fundamentals of Satellite Navigation* in *Understanding GPS Principles and Applications,* Artech House Inc

Kay, S.M. (1993), *Fundamentals of Statistical Signal Procession Volume II: Detection Theory*, Prentice Hall Inc.

Klobuchar, J.A. (1997), *Ionospheric Effects on GPS* in *Global Positioning System: Theory and Applications Volume I,* Progress in Astronautics and Aeronautics Volume 164, AIAA, pp. 485-516.

Klukas, R., G. Lachapelle, C. Ma and G. Jee (2003), *GPS Signal Fading Model for Urban Centers,* IEEE Microwave, Antenna and Propagation Magazine, Vol. 150, No. 4.

Lachapelle, G. (2004), *Advanced GPS Theory and Applications*, ENGO 625 Lecture Notes, Department of Geomatics Engineering, The University of Calgary.

Lachapelle, G., M.E. Cannon, R. Klukas, S. Singh, R. Watson, P. Boulton, A. Read and K. Jones (2004), *Hardware Simulator Models and Methodologies for Indoor Performance Assessments of High-Sensitivity Receivers,* Canadian Aeronautics and Space Journal, Vol. 50, No 3.

Ma, C., G. Lachapelle, and M.E. Cannon (2004), *Implementation of a Software GPS Receiver*, Proceedings of the US Institute of Navigation GNSS 2004.

Macabiau, C. (2003), *Communications par Spectre Etalé,* Lecture Note, ENAC.

Macabiau, C., L. Ries, F. Bastide, and J-L Issler (2003), *GPS L5 Receiver Implementation Issues*, Proceedings of the U.S. Institute of Navigation GNSS 2003.

MacGougan, G.D. (2003), *High Sensitivity GPS Performance Analysis in Degraded Signal Environment*, Master's Thesis, UCGE Report #20176, Department of Geomatics Engineering, The University of Calgary

Marcum, J.I. (1960), *A Statistical Detection Theory of Pulsed Radar*, IRE Transaction on Information Theory, Vol. 6.

McGraw, G. and M. Braasch (1999), *GNSS Multipath Mitigation Using Gated and High Resolution Correlator Concept*, Proceedings of the US Institute of Navigation NTM 1999.

Misra, P. and P. Enge (2006), *Global Positioning System: Signals, Measurements, and Performance,* Ganga-Jamuna Press.

Mongrédien, C., G. Lachapelle and M.E. Cannon (2006), *Testing GPS L5 Acquisition and Tracking Algorithms using a Hardware Simulator,* Proceedings of the U.S. Institute of Navigation GNSS 2006

Mongrédien, C., G. Lachapelle and M.E. Cannon (2007a), *Performance Evaluation of a GPS L5 Software Receiver using a Hardware Simulator*, Proceedings of the European Navigation Conference 2006.

Mongrédien, C., G. Lachapelle and M.E. Cannon (2007a), *Performance Evaluation of a Kalman Filter Based Tracking for the New GPS L5 Signal*, Proceedings of the U.S. Institute of Navigation GNSS 2007.

Muthuraman, K., S.K. Shanmungam and G. Lachapelle (2007), *Evaluation of Data/Pilot Tracking Algorithms for GPS L2C Signals Using Software Receiver,* Proceedings of the U.S. Institute of Navigation GNSS 2007.

O'Driscoll, C. (2007), *Performance Analysis of the Parallel Acquisition of Weak GPS Signals,* PhD Thesis, The National University of Ireland.

Parkinson, B.W. (1997a), *Introduction and Heritage of NAVSTAR, the Global Positioning System* in *Global Positioning System: Theory and Applications Volume I,* Progress in Astronautics and Aeronautics Volume 164 AIAA, pp.3-28

Parkinson, B.W. (1997b), *GPS Error Analysis* in *Global Positioning System: Theory and Applications Volume I,* Progress in Astronautics and Aeronautics Volume 164 AIAA, pp.469-484

Petovello, M.G. and G. Lachapelle (2000), *Estimation of Clock Stability Using GPS,* GPS Solution, Vol. 3, No. 4

Petovello, M.G. and G. Lachapelle (2006), *Comparison of Vector-Based software Receiver Implementations With Application to Ultra-Tight GPS/INS Integration,* Proceedings of the U.S. Institute of Navigation GNSS 2006.

Petovello, M.G., C. O'Driscoll and G. Lachapelle (2007), *Ultra-Tight GPS/INS Integration for Carrier Phase Positioning in Weak Signal Environments,* NATO RTO-SET-104 Symposium on Military Capabilities Enabled by Advances in Navigation Sensor, Antalya, Turkey.

Proakis, J. (2000), *Digital Communications, 4th Edition*, McGraw-Hill Science/Engineering/Math.

Psiaki, M.L. and H. Jung (2002), *Extended Kalman Filter Methods for Tracking Weak GPS Signals,* Proceedings of the US Institute of Navigation GNSS 2002.

Psiaki, M.L., T.E. Humphreys, A.P. Cerruti, S.P. Powell and P.M. Kintner, *Tracking L1 C/A and L2C Signals through Ionospheric Scintillations,* Proceedings of the U.S. Institute of Navigation GNSS 2007.

Raquet, J.F. (2004), *GPS Receiver Deign*, PhD ENGO 699.10, Department of Geomatics Engineering, the University of Calgary.

Ray, J.K. (1998), *Mitigation of GPS Code and Carrier Multipath Effects using a Multi-Antenna System,* PhD Thesis, UGCE Report #20136, Department of Geomatics Engineering, The University of Calgary

Ray, J.K. (2005), *Advanced Receiver Design*, ENGO 699.73 Lecture Notes, Department of Geomatics Engineering, The University of Calgary.

Ries, L., C. Macabiau, O. Nouvel, Q. Jeandel, W. Vigneau, V. Calmettes, and J-L Issler (2002), *A Software Receiver for GPS-IIF L5 Signal*, Proceedings of the U.S. Institute of Navigation GNSS 2002.

Shanmugam, S.K. (2008), *New High-Sensitivity Detection Techniques for GPS L1 C/A and Modernized Signals Acquisition,* PhD Thesis, UGCE Report #20264, Department of Geomatics Engineering, The University of Calgary.

Shanmugam, S.K., R. Watson, J. Nielsen, and G. Lachapelle (2005), *Differential Signal Processing Schemes for Enhanced GPS Acquisition*, Proceedings of the US Institute of Navigation GNSS 2005.

Skone, S. (2005), *Atmospheric Effects on Satellite Navigation Systems,* ENGO 633 Lecture Notes, Department of Geomatics Engineering, The University of Calgary.

Snellius, W. (1621), *Cyclometria sive de circuli dimensione.*

Spilker, J.J. (1977), *Digital Communications by Satellite,* Prentice-Hall, Englewood Cliffs, NJ.

Spilker, J.J. (1997a), *GPS Navigation Data* in *Global Positioning System: Theory and Applications Volume I,* Progress in Astronautics and Aeronautics Volume 164, AIAA, pp. 121-176.

Spilker, J.J. (1997b), *GPS Signal Structure and Theoretical Performance* in *Global Positioning System: Theory and Applications Volume I,* Progress in Astronautics and Aeronautics Volume 164, AIAA, pp. 57-120.

Spilker, J.J. (1997c), *Satellite Constellation and Geometric Dilution of Precision* in *Global Positioning System: Theory and Applications Volume I,* Progress in Astronautics and Aeronautics Volume 164, AIAA, pp. 177-208.

Spilker, J.J. and A.J. Van Dierendonck (2001), *Proposed New L5 Civil GPS Codes*, Navigation: Journal of the Institute of Navigation, Vol. 48, No. 3, Fall 2001.

Tran, M. (2004), *Performance Evaluation of the New GPS L5 and L2 Civil (L2C) Signals*, Navigation: Journal of the U.S. Institute of Navigation, Vol. 51, No. 3

Tran, M. and C. Hegarty (2002), *Receiver Algorithms for the New Civil GPS Signals*, Proceedings of the US Institute of Navigation NTM 2002

Van Dierendonck, A.J. (1997), *GPS Receivers* in *Global Positioning System: Theory and Application Volume I*, Progress in Astronautics and Aeronautics Volume 164, AIAA, pp. 329-408.

Van Dierendonck, A.J., P. Fenton, and T. Ford (1992), *Theory and Performance of Narrow Correlator Spacing in GPS Receiver*, Navigation: Journal of the U.S. Institute of Navigation, Vol. 39, No. 3.

Walpole, R.E., R.H. Myers and S.H. Myers (1998), *Probability and Statistics for Engineers and Scientist, 6th Edition,* Prentice Hall

Ward, P., J. Betz and C. Hegarty (2006), *Satellite Signal Acquisition, Tracking and Data Demodulation* in *Understanding GPS Principles and Applications,* Artech House Inc

Watson, R. (2005), *High-Sensitivity GPS L1 Signal Analysis for Indoor Channel Modeling,* Mater's Thesis, UGCE Report #20216, Department of Geomatics Engineering, The University of Calgary.

Winkel, J.O. (2003), *Modeling and Simulating GNSS Signals Structure and Receivers,* PhD Thesis, University FAF Munich.

Yang, C. (2000), GPS *Code Correlation with FFT under Pseudo-Quadrature Sampling*, Proceedings of the U.S. Institute of Navigation NTM 2000

Yang, C., C. Hegarty, and M. Tran (2004), *Acquisition of the GPS L5 Signal Using Coherent Combining of the I5 and Q5*, Proceedings of the US Institute of Navigation GNSS 2004.

Yu, W. (2007), *Selected GPS Receiver Enhancements for Weak Signal Acquisition and Tracking,* Master Thesis, UGCE Report #20249, Department of Geomatics Engineering, The University of Calgary.

Yu, W., S. Skone and G. Lachapelle (2006), *PLL Performance for Signals in the Presence of Thermal Noise, Phase Noise and Ionospheric Scintillations,* Proceedings of the U.S. Institute of Navigation GNSS 2006.

Zheng, B. and G. Lachapelle (2004), *Acquisition Schemes for a GPS L5 Software Receiver,* Proceedings of the U.S. Institute of Navigation GNSS (2004).

Ziedan (2005), *Extended Kalman Filter Tracking and Navigation Message Decoding of Weak GPS L2C and L5 Signals* (2005), Proceedings of the U.S. Institute of Navigation GNSS 2005.

APPENDIX A: LOCK DETECTORS

When a satellite is being tracked, it is important to know how well it is being tracked to ensure that the pseudorange, Doppler and carrier phase measurements passed to the navigation filter are reliable and accurate. This function is performed by the so-called lock detectors. This appendix describes the lock detectors implemented herein for the DLL, PLL and FLL.

A.1. Code Lock and C/N$_0$ Estimation

Code lock detection is frequently assimilated to C/N$_0$ estimation since a good code lock is required to achieve good C/N$_0$ (Van Dierendonck 1997). The comparison of the total signal-plus-noise power observed in two different noise bandwidths can be used to observe the C/N$_0$. To this end, the total signal-plus-noise powers observed in wide and narrow noise bandwidths are given, respectively, by

$$WBP_k = \left(\sum_{i=1}^{M} \left(I_{P,i}^2 + Q_{P,i}^2 \right) \right)_k \tag{A. 1}$$

$$NBP_k = \left(\sum_{i=1}^{M} \left(I_{P,i} \right) \right)_k^2 + \left(\sum_{i=1}^{M} \left(Q_{P,i} \right) \right)_k^2 \tag{A. 2}$$

where the coherent integration time T used to obtain the normalized in-phase and quadra-phase correlator outputs $I_{P,i}$ and $Q_{P,i}$ is set to 1 ms, and M is an integer number chosen to ensure that the correlation performed over time interval MT_I does not straddle a symbol bit boundary.

Using the known distribution of the normalized correlator outputs and the statistical properties of a random variable defined as the ratio of two random variables, Van Dierendonck (1997) shows that the normalized power defined as

$$NP_k = \frac{WBP_k}{NBP_k}$$
(A. 3)

gives statistics that provide monotonic functions of C/N$_0$.

The C/N$_0$ estimator can then be written as

$$\frac{\hat{C}}{N_0} = \frac{1}{T_I} \frac{\hat{\mu}_{NP} - 1}{M - \hat{\mu}_{NP}}$$
(A. 4)

where the normalized power is averaged over 1 s using

$$\hat{\mu}_{NP} = \frac{1}{K} \sum_{k=1}^{K} \mu_{NP}$$
(A. 5)

which reduces its variance by a factor $\sqrt{K}$.

The C/N$_0$ estimator implemented herein uses $M = 10$ and $K = 100$ on both data and pilot channels.

A.2. Carrier Phase Lock and Estimation

Phase lock detection is frequently used to confirm frequency and phase lock, and can be performed using the normalized estimate of the cosine of twice the carrier phase error given by (Van Dierendonck 1997)

$$C2\Phi_k = \frac{NBD_k}{NBP_k}$$
(A. 6)

where $NBD_k = \left(\sum\limits_{i=1}^{M} (IP_i)^2 \right)_k - \left(\sum\limits_{i=1}^{M} (QP_i)^2 \right)_k$.

Van Dierendonck (1997) shows that Equation A.6 can be approximated as

$$C2\Phi_k \approx \cos(2\delta\phi) \tag{A. 7}$$

The value of this phase lock detector will converge toward 1 when the phase error tends toward 0. To reduce its variance, the PLL lock detector output is also averaged over 1 s.

A.3. Carrier Frequency Lock and Estimation

It is important, when the carrier tracking purely relies on an FLL, to ensure that the signal is effectively being tracked. To this end, the following FLL detector is used

$$C2f = \frac{dot^2 - cross^2}{dot^2 + cross^2} \tag{A. 8}$$

where the dot and cross products are given, respectively, by

$$dot = I_{P,k-1}Q_{P,k} - I_{P,k}Q_{P,k-1} \tag{A. 9}$$

$$cross = I_{P,k-1}I_{P,k} + Q_{P,k-1}Q_{P,k} \tag{A. 10}$$

From the correlation model developed in Section 3.3.2, and assuming that 1) the code tracking is perfect and 2) the frequency error can only be observed through the expanded phase error, the dot and cross products can be approximated as

$$dot = \frac{P}{4} D_{NH}^2 \sin(\delta\phi_k - \delta\phi_{k-1}) \tag{A. 11}$$

$$cross = \frac{P}{4} D_{NH}^2 \cos(\delta\phi_k - \delta\phi_{k-1}) \tag{A. 12}$$

where D_{NH}^2 is the product of the successive NH bit signs, and the average phase estimation error is expanded as

$$\delta\phi_k = \delta\phi_{k-1} + \delta f_k T_I \qquad\qquad \textbf{(A. 13)}$$

Finally, using Equations A. 8, A.11 and A.12, the FLL lock detector can be approximated as

$$C2f = \cos(4\pi\delta f_k T_I). \qquad\qquad \textbf{(A-14)}$$

The value of this frequency lock detector will converge toward 1 when the frequency error tends toward 0. To reduce its variance, the FLL lock detector output is also averaged over 1 s.

APPENDIX B: MEASUREMENT FORMATION

The natural measurements of a receiver tracking loops are not the pseudoranges or Doppler measurements used in the navigation filter but rather the local code and carrier replicas used in the correlation function. This appendix describes how the former can be obtained from the latter.

B.1. Pseudorange

The basic measurement derived from the code tracking loop of the receiver is the apparent transmit time of the signal from the satellite to the receiver. It is defined as the difference between signal reception time, as determined by the receiver clock, and the transmission time, as marked on the signal (and determined by the satellite clock). The satellite and receiver rely on independent FTS to maintain GPS time and, therefore, are not synchronous. As a result, the measurement of the apparent the propagation time is biased (hence its name, pseudorange). The measured range P, determined from the apparent transit time, is given as (Misra and Enge 2006)

$$P(t) = c\left[T_R(t) - T^S(t - \tau)\right] \tag{B. 1}$$

where τ is the true code transmit time, t is the true GPS reception, $t - \tau$ is the true GPS transmission time, $T_R(t)$ is the reception time measured by the receiver and $T^S(t - \tau)$ the transmission time measured by the satellite. The receiver and satellite time scale can be related to the GPS time scale using, respectively,

$$T_R(t) = t + \delta t_R(t) \tag{B. 1}$$

$$T^S(t-\tau) = (t-\tau) + \delta t^S(t-\tau) \qquad \textbf{(B. 3)}$$

where $\delta t_R(t)$ and $\delta t^S(t)$ are the time varying receiver and satellite clock biases, respectively. While it is possible to correct for the satellite clock bias using the satellite clock parameters broadcasted in the navigation message, the receiver clock bias, is common between all the pseudoranges, must be estimated as part of the navigation solution.

Now that the generic pseudorange formation has been discussed, it is interesting to assess how the FEC encoding applied to the L5 navigation message affects the formation of the L5 pseudoranges.

B.1.1. L5 Pseudorange

To decode the L5 navigation message, a Viterbi decoder must be used. However, this decoding algorithm introduces a delay that is function of the constrain length it uses. The Viterbi decoder implemented in the frame of this dissertation uses a constraint length of 5. This results in a 68-symbol bit delay that needs to be accounted for. To this end, the receive time, is kept common for all satellites, and the transmit time is modified to account for the decoding delay. The L5 pseudoranges can therefore be calculated as follows:

$$P_{L5}(t) = c\left[T_R(t) - T^S(t-\tau-T_D)\right] \qquad \textbf{(B. 4)}$$

where T_D is the time delay introduced by the Viterbi decoder, and $T^S(t-\tau-T_D)$ is the modified transmit time.

Accordingly, the satellite computations (e.g. position, velocity and clock error) must be referenced to the modified transmit time.

B.2. Carrier Phase Measurement

The carrier phase measurement can be defined as the difference between the phases of incoming signal carrier at transmit time and the local carrier replica at receive time, where the phase of the local carrier replica is measured in number of cycles generated since an arbitrary starting time. The carrier phase measurement is therefore composed of a fixed unknown number of whole cycles (due to the arbitrary starting time) and a varying fractional number of cycles (due to the relative receiver-satellite motion). Consequently, the carrier phase measurement can be written, in cycles, as (Misra & Enge 2006)

$$\Phi(t) = \Phi_R(t) - \Phi^S(t - \tau) + N \qquad \textbf{(B. 5)}$$

where τ is the true carrier transmit time, $\Phi_R(t)$ is the phase of the local carrier replica at the true GPS reception time t, $\Phi^S(t - \tau)$ is the phase of the received signal carrier at the true GPS transmit time $t - \tau$, and N is the integer ambiguity.

It is important to note that, due to the integer ambiguity, it is not possible to directly use carrier phase measurements for single point positioning. However, provided no cycle slips occur, this integer ambiguity will cancel out in the differentiation process, enabling the use of carrier smoothing techniques (Cannon 2004). These techniques merge the absolute pseudorange and relative carrier phase capabilities by progressively increasing their reliance on carrier phase based pseudorange rates to monitor the satellite-receiver range variations.

B.3. Doppler Measurement

The receiver-satellite Doppler measurement is derived from the receiver carrier tracking loop and can be defined, in cycle per second, as (Misra & Enge 2006)

$$\dot{\Phi}(t) = \frac{\Phi(t + \delta t) - \Phi(t)}{\delta t} \qquad \textbf{(B. 6)}$$

It is important to note that the Doppler measurement is affected by the time varying receiver and satellite clock drifts where the satellite clock drift can be corrected using the broadcasted satellite clock drift correction, and the receiver clock drift can be estimated as part of the navigation solution.